Particles with Tunable Functionality by a Nonaqueous Emulsion Polymerization Approach

Dissertation

zur Erlangung des Grades

„Doktor der Naturwissenschaften“

im Promotionsfach Chemie

am Fachbereich Chemie, Pharmazie und Geowissenschaften
der Johannes-Gutenberg Universität
in Mainz

Robert Dorresteijn
geboren in Köln

Mainz im Jahr 2014

Dekan: Prof. Dr. [redacted]

1. Berichterstatter: Prof. Dr. [redacted]

2. Berichterstatter: Prof. Dr. [redacted]

Tag der mündlichen Prüfung: 19.06.2015

D77 (Dissertation Universität Mainz)

Die vorliegende Arbeit wurde in der Zeit von November 2011 bis September 2014 am Max-Planck-Institut für Polymerforschung in Mainz unter Betreuung von Prof. Dr. [redacted] durchgeführt.

Herrn Prof. Dr. [redacted] möchte ich sehr herzlich für die gezielte, großartige Unterstützung und die stetige Diskussionsbereitschaft bezüglich der Bearbeitung dieses interessanten Themas danken.

Meinen Eltern

Table of Contents

Index of Abbreviations I

1 Abstract 1

2 Introduction 4

2.1 Emulsions 5

2.2 Nonaqueous Emulsions 8

2.3 Nanoparticles in Cancer Therapy 13

3 Motivation and Objectives 15

4 Results and Discussion 19

4.1 Poly(L-lactide) Nanoparticles via Ring-Opening Polymerization (ROP) in Non-Aqueous Emulsion 19

4.2 Biocompatible Polylactide-*block*-Polypeptide-*block*-Polylactide Nanocarrier 36

4.3 Polylactide-*block*-Polypeptide-*block*-Polylactide Copolymer Nanoparticles with Tunable Cleavage and Controlled Drug Release 51

4.4 Polarity Reversal of Nanoparticle Surfaces by the Use of UV-Sensitive Polymeric Emulsifiers 74

4.5 Metallocene Supported on Porous and Nonporous Polyurethane Particles for Ethylene Polymerization 89

5 Annotations / Unpublished Results 114

5.1 Reproducible Synthesis of Poly(L-Lactide) Nanoparticles 114

5.2 Reproducible Synthesis of Poly(Urethane) Particles 115

6 Summary and Outlook 123

7 Supporting Information 127

7.1 To 4.2: Biocompatible Polylactide-block-Polypeptide-block-Polylactide Nanocarrier 128

7.2 To 4.3: Polylactide-*block*-Polypeptide-*block*-Polylactide Copolymer Nanoparticles with Tunable Cleavage and Controlled Drug Release 139

7.3 To 4.4: Polarity Reversal of Nanoparticle Surfaces by the Use of UV-Sensitive Emulsifiers 142

8 References 148

9 List of Figures 158

10 List of Tables 164

11 List of Publications 165

12 Acknowledgments 167

Index of Abbreviations

b	*block*
BDMAEE	bis(2-dimethylaminoethyl)ether
δ	chemical shift
d	diameter
DBTDA	dibutyltin diacetate
DLS	dynamic-light-scattering
DMF	*N,N'*-dimethylformamide
DMSO	dimethyl sulfoxide
DP	degree of polymerization
DSC	differential scanning calorimetry
Fig.	figure
GPC	gel permeation chromatography
HPLC	high-performance liquid chromatography
IMes	1,3-bis(2,4,6-trimethylphenyl)-imidazole-2-ylidene
NHC	*N*-heterocyclic carbene
O/W	oil-in-water
PDI	polydispersity index
PE	poly(ethylene)
PEG	poly(ethylene glycol)
PEO	poly(ethylene oxide)
PGlu	poly(glutamate)
PGlu(Pyr)	poly(1-pyrenyl methyl glutamate)
PI	poly(isoprene)
PLLA	poly(L-lactide)
PMMA	poly(methyl methacrylate)
PU	poly(urethane)
ROP	ring-opening polymerization
rt	room temperature

sec-BuLi	secondary butyl lithium
SDS	sodium dodecyl sulfate
SEM	scanning electron microscopy
SIMes	1,3-bis(2,4,6-trimethylphenyl)-4,5-dihydroimidazole-2-ylidene
TEDA	triethylene diamine
T_g	glass transition temperature
US	ultrasonication
W	Tryptophan
W/O	water-in-oil

1 Abstract

This dissertation focused on application-driven projects that all utilized nonaqueous emulsion polymerization techniques. The nonaqueous emulsion polymerization employs two organic solvents, which are immiscible due to different polarities. To emulsify the organic solvent-solvent interface, an amphiphilic block copolymer, such as a poly(isoprene)-*block*-poly(methyl methacrylate) copolymer or poly(isoprene)-*block*-poly(ethylene oxide) copolymer, is applied. The polymerization in the dispersed phase finally results in the formation of a polymer particle. In contrast to common aqueous emulsion polymerizations that are limited to radical-based polymerizations, the nonaqueous counterpart affords the use of a much broader portfolio of components and polymerization techniques: the absence of water allows for the utilization of water-sensitive compounds (acid chlorides, isocyanates e.g.) and polymerization techniques such as the polycondensation reaction, where water shifts the reaction equilibrium to the monomer side.

Chapter 4.1 presents a successful method for the generation of well-defined poly(L-lactide) (PLLA) nanoparticles in a single step by a moisture-sensitive polymerization of L-lactide in nonaqueous emulsion. The PLLA nanoparticles had diameters of roughly 70 nm and contained PLLA polymer chains with molecular weights that were readily altered by varying the monomer consumption to initiator concentration. Based on the success of this polymerization method and PLLA's biocompatibility, the upcoming drug delivery systems consistently were prepared in nonaqueous emulsion and contained PLLA as structural basis.

Chapter 4.2 shows a model reaction in which a peptide was successfully incorporated into the polymer of a PLLA nanoparticle. The peptide consisted of tryptophan spacer groups and two functional groups on each side of the peptide (two terminal hydroxyl groups). Owing to the

bifunctionality, initiation of the lactide polymerization by this peptide gave a PLLA-*block*-peptide-*block*-PLLA triblock copolymer with the peptide in the centered position. Performing this reaction in nonaqueous emulsion resulted in the formation of well-defined nanoparticles, consisting of this triblock copolymer. The non-cytotoxicity of such particles, when incubated with HeLa cells, proved the biocompatibility of the particle dispersion. The success of peptide incorporation into PLLA nanoparticles paved the way toward the use of bioresponsive peptides, in order to impart a stimulus to the particle.

In **Chapter 4.3**, the synthesis of a drug-carrying nanoparticle is described, which showed drug release and associated cytotoxicity selectively in tumor tissue, owing to stimuli-responsive polymer particles. By analogy with the polymer of Chapter 4.2, the polymer consisted of a PLLA-*block*-peptide-*block*-PLLA triblock copolymer, but this time with a peptide that is bioresponsive: the recognition site in the peptide (PLGLAG) is selectively cleaved by tumor-associated enzymes. Since the peptide was located in the middle of the polymer, cleavage caused drastic reduction of the polymer's molecular weight. The resulting physicochemical changes (higher mobility of the polymer fragments) most likely enabled drug release, caused cell-death, and hampered mitosis when incubated with tumor cells. A comparison of cellular effects with particles that had a scrambled peptide sequence, demonstrated the selectivity of drug release: the particles with the scrambled sequence were proven to be non-cytotoxic.

Chapter 4.4 deals with a common obstacle of particle dispersions that have been manufactured in nonaqueous systems - their transfer into water for their final purpose. Typically, a second surfactant layer is applied, which, however, might cause aggregation and different behavior in the desired application[1-2]. Therefore, a poly(ethylene glycol)-*block*-poly(1-pyrenyl methyl glutamate) copolymer was synthesized, which at first was amphiphilic and, therefore, stabilized PLLA particles in a nonpolar organic

solvent. Thereby, the nonpolar poly(1-pyrenyl methyl glutmate)-block oriented toward the nonpolar organic phase. Upon UV-irradiation, the pyrenyl methyl units were cleaved from the polar poly(glutamic acid)-block, resulting in polarity reversal of the particle surface from hydrophobic (nonpolar) to hydrophilic (polar). In this way, transfer of PLLA nanoparticles from nonpolar organic solvent into water without aggregation or the addition of further surfactant layers was finally feasible.

In **Chapter 4.5**, the synthesis and the use of porous poly(urethane) (PU) particles as a support for an olefin polymerization are described. The production of poly(ethylene) particles with PU as a support was conducted by [redacted] and [redacted]. PU particles have previously been generated in nonaqueous emulsion[3]. However, to use such a particle more efficiently as a support for olefin polymerizations, porosity was needed in order to have a larger surface area for catalyst immobilization and to ensure fragmentation of the structure during polymerization, which is important for high monomer consumption and for the transparency of the final product. Porosity was achieved by adding defined amounts of water to a nonaqueous emulsion: the water reacted with diisocyanate molecules, resulting in a release of carbon dioxide and formation of pores. The degree of porosity (proportional to the surface area) was dependent on the amount of applied water, which consequently gave control over the amount of immobilized catalyst on the support. Laser scanning confocal fluorescence microscopy (LSCFM) images of poly(ethylene) particles demonstrated complete fragmentation of the PU support during polymerization.

2 Introduction

Dispersed polymer nanoparticles find use in a variety of materials such as toners, column packing materials, pharmaceutics, coatings and adhesives[4-5]. Owing to the *nanometer size* (diameters of 1-100 nm) and the corresponding large ratio of surface area to volume, nanoparticles possess unique physicochemical properties[6-7]. Compared to a bulk material of the same composition, nanomaterials perform exceptional feats of reactivity, conductivity and optical sensitivity[6-7]. The synthesis of polymer nanoparticles is commonly conducted in emulsion polymerization. This method goes back to the second world war, where efficient alternatives for latex rubber were needed[8]. The great control of the product's property and its versatility are responsible for its industrial success later on[8-9].

The resulting latex product is called polymer dispersion, respectively, polymer emulsion, depending on the aggregation state of the dispersed species. Exact assignment to either of those denotations is often difficult, since the polymer's glass transition temperature, its molecular weight and its chain length strongly influence the aggregation state of the dispersed polymer[8]. Compared to homogeneous methods, the advantage of this heterogenic process is the avoidance of the Trommsdorff-Norrish Effect (Autoacceleration) during polymerization, which might occur in bulk polymerization. This term describes the observed increase of viscosity during radical polymerization that hampers chain termination and, therefore, results in overheating of the reaction mixture[10]. In a heterogenic process, the viscosity remains approximately the same owing to the presence of a continuous phase, where occurring heat of reaction can easily dissipate. This contributes to the use of the emulsion polymerization process in industrial plants.

2.1 Emulsions

Emulsions contain at least two immiscible solvents. A biphasic system, for example, consists of one continuous phase and one dispersed phase (Figure 2.1.1).

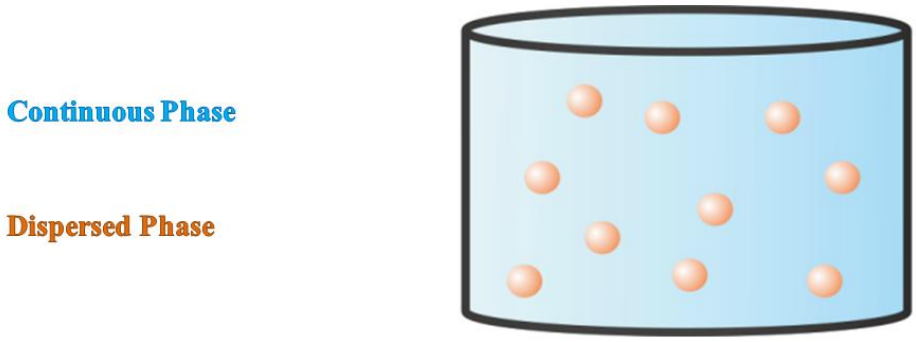

Figure 2.1.1. Scheme of biphasic emulsion.

In case of an oil-in-water emulsion (O/W-emulsion), a nonpolar oil is dispersed in the continuous phase water (polar). An example from everyday life is milk, where nonpolar milk fat is dispersed in water. Contrary, biphasic emulsions in which water is the dispersed phase and the nonpolar oil is the continuous phase are called water-in-oil emulsion (W/O-emulsion). This is the case for butter or mayonnaise, for example. The interfacial tension of two immiscible solvents determines the size of the dispersed droplets in the continuous phase. In order to obtain smaller dispersed droplets, application of energy through stirring or sonication is needed. This has to do with the increasing surface-to-volume ratio when the droplet size is decreased. To stabilize the larger interface, an emulsifier can be added. The emulsifier reduces the solvent interaction (cohesion) and reduces the interfacial tension[11]. Since power equals the product of the interfacial tension and the interface, addition of emulsifier leads to a larger interface and, therefore, smaller dispersed droplets[11-12].

Emulsifiers are of amphiphilic nature. They consist of a polar (hydrophilic) group and a nonpolar (hydrophobic) group. The polar unit can be anionic, cationic, amphoteric or nonionic. The nonpolar group usually consists of a nonpolar hydrocarbon chain.

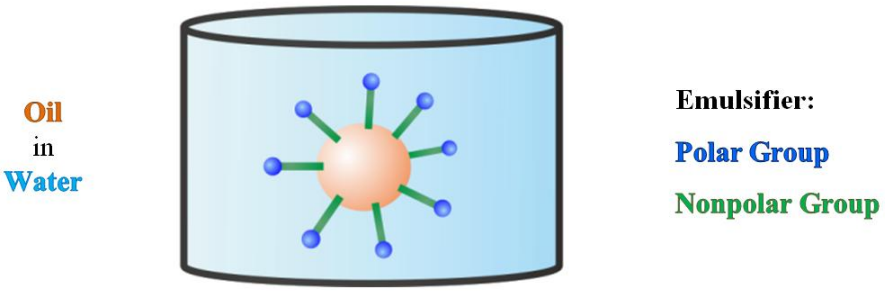

Figure 2.1.2. Scheme of a surfactant-stabilized O/W-emulsion.

In an O/W-emulsion, the polar group of the emulsifier faces the aqueous phase, where its nonpolar group reaches into the lipid phase (Figure 2.1.2). In case of ionic headgroups, electrostatic interactions between the polar groups of the emulsifier molecules result in stably dispersed droplets[13]. In the reverse case (in W/O-emulsions), stabilization of the interface is achieved by steric repulsion of the nonpolar chain segments of the emulsifier[13].

In emulsions, two kinds of aging processes occur that lead to inhomogeneity: coalescence and Ostwald ripening. Coalescence describes fusion of droplets with time (Figure 2.1.3, top). This phenomenon can be hampered by the addition of an emulsifier to the solvent mixture and the corresponding reduction of interfacial tension and solvent interaction[14]. Ostwald ripening describes diffusion of components through the continuous phase from smaller droplets into larger ones (Figure 2.1.3, bottom)[15-16].

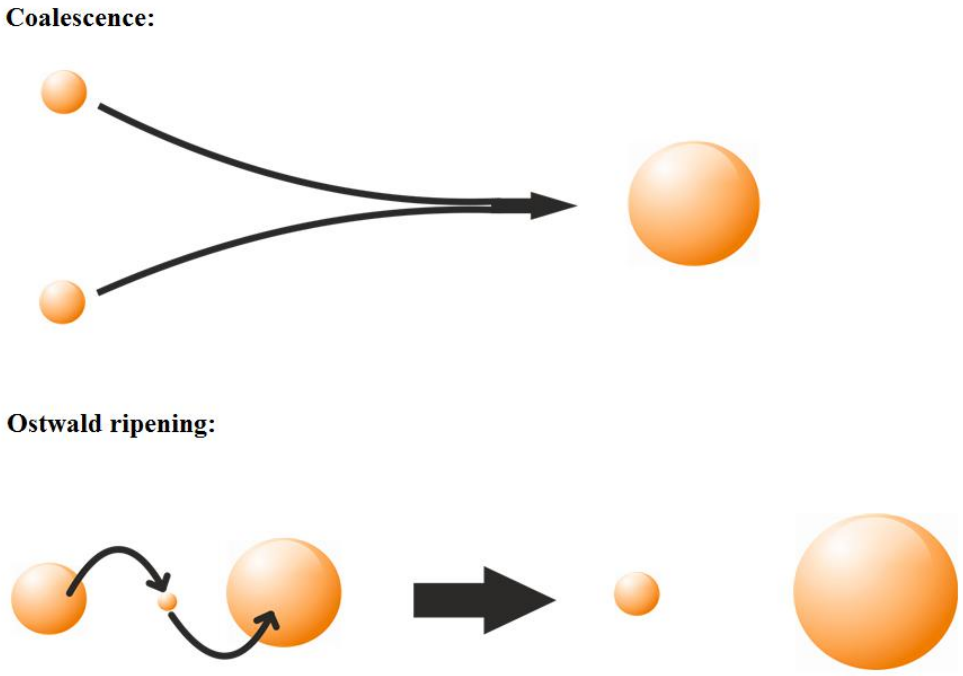

Figure 2.1.3. Schematic representation of coalescence and Ostwald ripening.

In contrast to coalescence, Ostwald ripening is a migratory process that cannot be hampered by the addition of an emulsifier. It reduces the *Laplace pressure* between the continuous phase and the dispersed phase[16]. This kind of pressure is proportional to the ratio of surface area to volume. Therefore, smaller droplets possess higher Laplace pressures than larger ones and accordingly disappear first[16]. Ostwald ripening can be slowed down by adding a hydrophobe to an O/W-emulsion (or lipophobe in case of W/O-emulsions). The hydrophobe creates an osmotic pressure inside of the droplet that counteracts the Laplace pressure[16-17].

The rate of Ostwald ripening is linearly dependent on the droplet concentration[16]. Contrary, the rate of coalescence depends on the squared droplet concentration, which is why the Ostwald ripening takes an inferior position in the aging process[16].

2.2 Nonaqueous Emulsions

A dispersed droplet in an emulsion can be used as a small reaction chamber for polymerization reactions in order to generate polymer particle dispersions. In Chapter 2.1 emulsions were described that contain water either as continuous or dispersed phase. The presence of water, however, is a limiting factor regarding choice of component and polymerization technique. Water-sensitive molecules (acid chlorides, isocyanates, water-sensitive catalysts e.g.) and reactions (polyaddition, polycondensation e.g.) cannot be used, respectively, performed decently. A nonaqueous emulsion, based on exclusively organic solvents, should overcome this limitation and allow the generation of dispersed polymer particles that have not been accessible in a single step.

A nonaqueous emulsion consists of two organic solvents that have different polarity and are, therefore, immiscible. Accordingly to the aqueous emulsion (Chapter 2.1), one solvent serves as continuous phase and the other one as dispersed phase, depending on the volume ratio. Addition of an emulsifier reduces the interfacial tension. First approaches in generating nonaqueous emulsions go back to the works of Riess et al. from the 60s and 70s[18-22]. Therein, emulsions were generated consisting of either *N*,*N*-dimethylformamide (DMF) and *n*-hexane or acetonitrile and cyclohexane[18]. Cameron et al. and Imhof et al. expanded the choice of solvents for a nonaqueous emulsion. Emulsions of either petrol ether, decane or silicon oils and polar DMF or dimethyl sulfoxide (DMSO) were successfully generated[23-24]. First polymerization attempts in a water-free emulsion were conducted by Antonietti et al.[25]. The used monomer was soluble in the dispersed polar organic phase, but insoluble in the continuous phase (nonpolar organic solvent)[25]. As a result, particles were obtained. They were, however, inhomogeneous regarding particle morphology due to the use of low molecular weight surfactants (sodium dodecyl sulfate (SDS))[13, 25]. While in aqueous emulsions the polarity difference between

water and organic solvent is large, this difference between two immiscible organic solvents is not so severe. Therefore, a low molecular weight surfactant does not suffice to stabilize such an interface[13, 26-28]. Efficient stabilization of an immiscible organic solvent mixture can be achieved by high molecular weight block copolymers. In contrast to low molecular weight surfactants that reach the thermodynamic equilibrium, block copolymers rapidly assemble to aggregates which are kinetically hampered to reach thermodynamic equilibrium[29]. Therefore, those polymers can sterically shield the droplets and form kinetically frozen aggregates[13, 29].

In order to stabilize two immiscible organic solvents, the block copolymer must possess two blocks having different polarity (A-*block*-B copolymer). For example, block A has to be selectively soluble in the dispersed phase, while block B must be exclusively soluble in the continuous phase (Figure 2.2.1)[18, 28]. In that way, stabilization of a large interface can be achieved[18, 28].

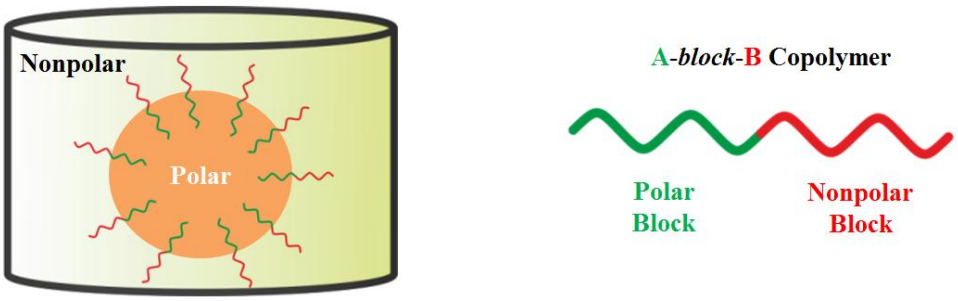

Figure 2.2.1. Schematic representation of a nonaqueous emulsion with an amphiphilic block copolymer as emulsifier.

Müller et al. developed a Poly(isoprene)-*block*-Poly(methyl methacrylate) (PI-*b*-PMMA) copolymer that was proven to stabilize a nonaqueous emulsion with a polar dispersed phase, wherein various polymerizations such as polyaddition[3], polycondensation[30] or oxidative polymerization[31] were successfully performed. While the nonpolar PI block stabilized either cyclohexane or *n*-hexane, the polar PMMA block stabilized either DMF or

acetonitrile. To ensure selective solubility of each block in a distinctive solvent, the copolymer was designed according to the concept of the Hansen solubility parameter[32]. When a polymer and a solvent have the same solubility parameter, the polymer should theoretically be well-soluble in the solvent.

The Hansen solubility parameter (δ) consists of three major types of interactions:

- Dispersion interaction parameter (δ_D)
- Permanent dipole-permanent dipole interaction parameter (δ_P)
- Hydrogen bonding interaction parameter (δ_H)

The following equation shows how those interactions contribute to δ:

$$\delta^2 = \delta_D^2 + \delta_P^2 + \delta_H^2$$

Hence, δ can be derived from the square root of the sum of each squared parameter[32]. In Figure 2.2.2, δ of nonpolar and polar organic solvents as well as δ of polymers that have been used in nonaqueous emulsion are shown.

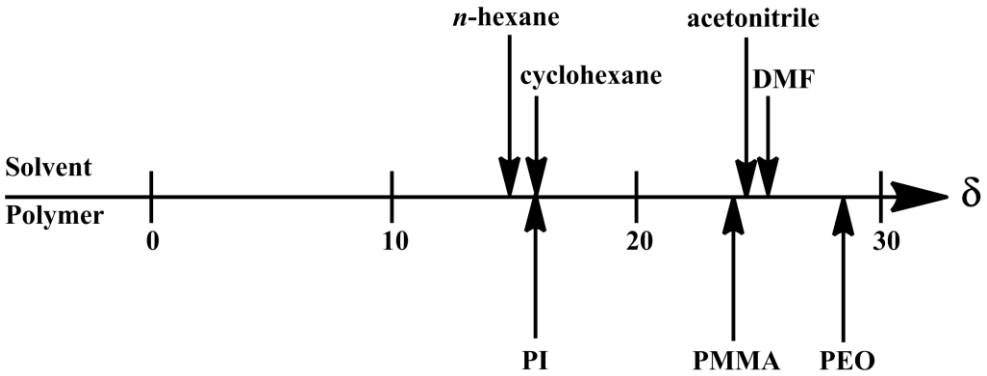

Figure 2.2.2. Hansen solubility parameters of certain organic solvents and polymers.

Similar δ of PI and either *n*-hexane or cyclohexane as well as of PMMA and either acetonitrile or DMF strongly suggest high stability of an emulsion consisting of the PI-*b*-PMMA copolymer as emulsifier of two immiscible organic solvents (*n*-hexane or cyclohexane and DMF or acetonitrile). This was experimentally corroborated by Müller et al.[33].

To exert this stable nonaqueous emulsion for particle generation, the polymerization must exclusively occur in the dispersed droplets. Therefore, at least one component (monomer, comonomor, catalyst or initiator) must be selectively soluble in the dispersed phase and should be present before the polymerization starts[13, 30, 33-35]. Figure 2.2.3 visualizes a common nonaqueous emulsion polymerization. The spherical structures of the last two cylinders are 3D-cuts of micelles to visualize their content.

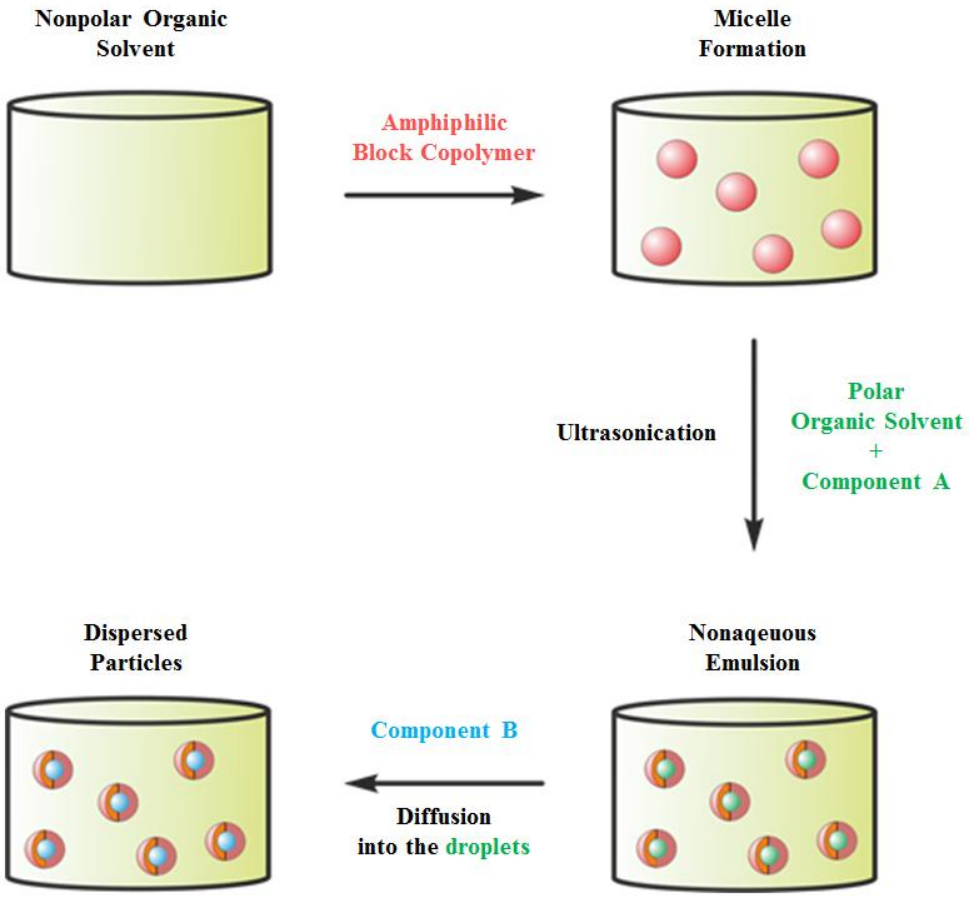

Figure 2.2.3. Schematic representation of a nonaqueous emulsion polymerization.

First, an amphiphilic block copolymer is added to a nonpolar organic solvent. Due to the amphiphilicity of the copolymer, micelles are being formed. Hereby, the nonpolar block faces the solvent, while the polar block is shielded from it. Subsequently, component A (monomer e.g.) is dissolved in a polar organic solvent and added to the micellar system. Final addition of a component B solution (initiator e.g.) results in polymerization after its diffusion into the dispersed phase, since all necessary polymerization components are present in one reaction chamber. After complete monomer consumption, the final polymer nanoparticle dispersion is obtained.

Figure 2.2.3 shows the use of ultrasonication after formation of the nonaqueous emulsion. It leads to homogenization of the dispersed droplets: the high energy of ultrasonication results in shearing of the droplets into smaller uniform droplets, which after droplet collision are monomodally distributed in the continuous phase[36] (Figure 2.2.4).

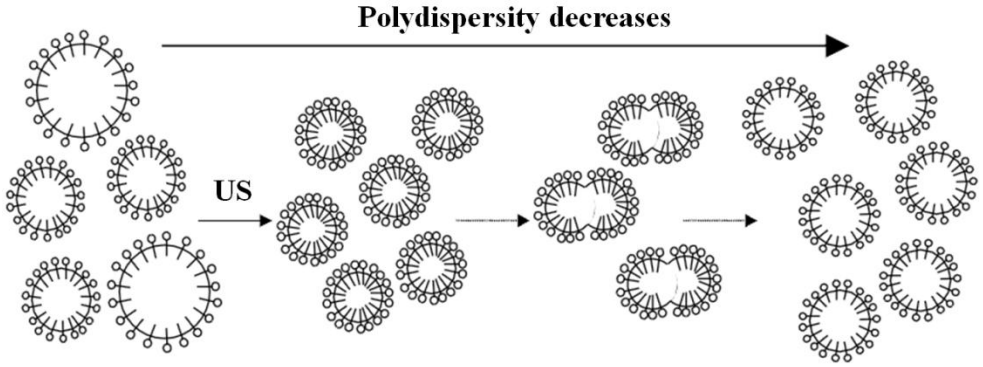

Figure 2.2.4. Schematic representation of homogenization by ultrasonication[36].

As the shape of the droplet determines the shape of the dispersed particle, a homogeneous emulsion gives a homogeneous particle dispersion[13, 36]. Furthermore, ultrasonication of the emulsion ensures equal amount of polymerization components in the droplets, which is of importance for polymerizations where exact stoichiometry is mandatory (step-growth reaction).

2.3 Nanoparticles in Cancer Therapy

Nanomedicine has become an emerging field over the past decades owing to the unique physicochemical properties of nanomaterials. Numerous biocompatible drug delivery systems based on inorganic nanoparticles[37-38][39-41], and organic nanoparticles[42-43] have had an impact on various branches of medicine including cardiology, oncology, pulmonology, and immunology[38]. The global revenue for advanced drug delivery systems was estimated to $151.3 billion in 2013[44], with targeted drug delivery as largest segment[44].

But what are the benefits of materials being *nano*? Specifically in cancer therapy, the size of a delivery system plays a crucial role regarding efficient drug delivery: the rapid formation of new tumor vessels leads to abnormal architectures with an endothelium having wide fenestrations[45]. While a small-sized drug molecule can readily diffuse out of tumor tissues, nanosized particles that once diffused into a tumor tissue remain in there due to the high pressure of interstitial fluid[46]. Such properties are exploited to accumulate nanocarriers in tumor vessels (the so-called Enhanced Permeability and Retention Effect)[45]. In other words, a certain selectivity of drug transport is exclusively achieved by the *nanosize* of the carrier (passive targeting).

When the dysfunctional tissue is reached, nanoparticles have the advantage to strongly interact with cell lipids[47]. Compared to bulk material, nanoparticles possess a larger ratio of surface to volume, resulting in an overall higher surface reactivity[47]. Consequently, they cause disruption of the cell membrane by formation of nanoscale holes, and membrane thinning[48]. However, this effect decreases again going from nanoparticles to single drug molecules[49]. The greater van der Waals interaction and the corresponding stronger adhesive force of nanoparticles are suggested to be responsible for this observation[49] – they dominate the elastic energy and

cohesion of molecules[49]. As a result, the membrane molecules are displaced and enclose the nanoparticle, causing particle uptake by the cell (phagocytosis)[49].

Besides passive targeting (size and corresponding surface reactivity), a more targeted delivery to a particular cell type can be ensured by addressing the metabolic changes in cancer cells: specific receptors on cell membranes and specific enzymes/proteins are overexpressed in the tumor tissue[50-54]. Therefore, antibodies[55], oligosaccharides[56] or peptides[45] are attached to the particle surface either by covalent linkage to functional groups or intermolecular interactions (electrostatic interaction e.g.)[40, 42, 57]. Those groups perform the task to target a particular cell and to bind the carrier/therapeutic to the cancer cell[38, 58-59]. As a result, the drug is selectively released in dysfunctional environment.

Besides targeting function, such ligands can also act as therapeutic themselves: for example the monoclonal antibody Trastuzumab not only targets HER2/neu receptors that are overexpressed on breast cancer cells, but even hampers cancer cell proliferation[60].

A combination of active targeting and the abovementioned passive targeting is of particular interest. The benefits are obvious: lower drug concentrations and a lower number of dosages are required, which reduce the side effects that are caused by chemotherapy in a significant way[38]. This might finally result in an improved patient compliance[38].

3 Motivation and Objectives

The use of the nonaqueous emulsion as a platform for the synthesis of particle dispersions containing polymers that arise from moisture-sensitive reactions were first introduced in the [redacted] group by [redacted][33]. Successful polycondensation reactions of acid chlorides and alcohols[30], as well as polyaddition reactions[3], and oxidative polymerizations[61] were carried out in nonaqueous emulsions and demonstrated the ease of this one pot method for particle generation. My predecessor [redacted] extended the portfolio of applicable polymerization techniques in nonaqueous emulsion by performing ring-opening metathesis polymerizations (ROMP) of norbornene derivatives[34] and free radical polymerizations[62]. By sequential polymerization, he even succeeded in generating hybrid structured nanoparticles having core-shell morphologies[35, 63]. Those experiments proved that the nonaqueous system is a very versatile platform for the formation of various polymer particles, yet the particles were not designed for a specific use. Therefore, the objective of this work is to synthesize functional particles in nonaqueous emulsion that are tailored for desired applications.

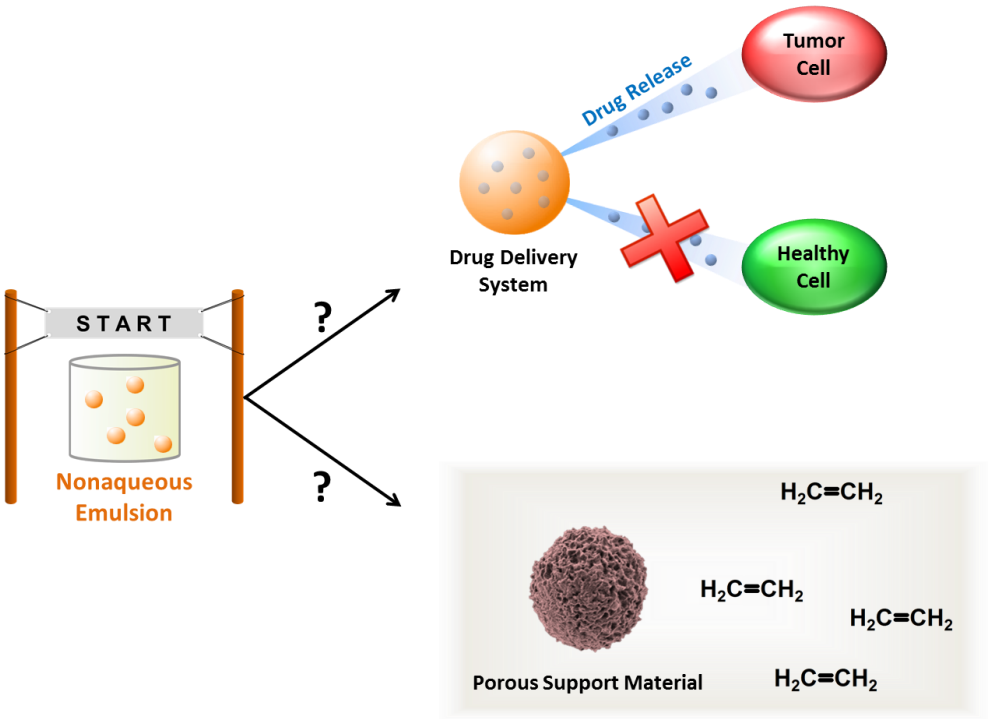

Figure 2.3.1. Schematic illustration of the use of a nonaqeous emulsion as starting point for the design of functional particles for specific applications.

The first project deals with the synthesis of drug-carrying nanoparticles for cancer therapy. The required carrier characteristics for efficient drug delivery are, however, hard to combine in one system:

- the carrier must be biocompatible
- the carrier size in blood must be within 50 and 250 nm
- the drug must be stably encapsulated in the carrier (non-leaking)
- the drug must be selectively released in tumor tissue

It shall be investigated whether the nonaqueous emulsion can be used as starting point for the synthesis of a drug delivery system that fulfills the above-mentioned requirements.

Biocompatibility is likely achieved through the appropriate choice of polymer. Poly(L-lactide) (PLLA) is biocompatible, biodegradable and has, therefore, been used frequently as a bioresorbable material for biomedical

applications[64-65]. Yet its synthesis in a nonaqueous emulsion has previously not been carried out, and thus is tested in an effort to form particles in a single step. The resulting PLLA nanoparticles shall then be investigated regarding morphology control and tunability of polymer properties.

The ideal carrier size should be achieved simply through the parameters of the nonaqueous emulsion polymerization technique, which typically forms particles with diameters of ~ 50-100 nm. Nonetheless, a huge challenge involves the subsequent transfer of such particles from organic solvent into water (aqueous dispersions are needed for biomedical applications), since aggregation could lead to carrier sizes that are far beyond the ideal size.

Further investigations focus on the loading of PLLA particles with drug molecules. Does the rigidity of PLLA suffice to stably encapsulate the drug and to prevent its leakage from the carrier? If so, can it be selectively released in a dysfunctional environment? Therefore, a specific stimulus is needed. Peptides have proven to respond to external stimuli such as pH[66], or enzyme overexpression[2] with change of their secondary structure[67], their polarity[68] or even their chemical structure[69]. Based on such properties, they shall be studied for incorporation into PLLA nanoparticles in order to give bioresponsivity to the system. Thereby, the impact of peptide response on the physicochemical property of the carrier system is a key factor: it determines whether drug release occurs and if so, how selective it occurs. This study should additionally give insights into the cargo-mediating mechanism.

The next project copes with the aforementioned issues of particle transfer. For hydrophobic particles that need to be transferred into water for their final application, hydrophilization of the particle surface must occur. Commonly, a second amphiphile is added. However, this step usually results in aggregation[2], potentially hampering its usability for the final application. Therefore, the goal of this project is the synthesis of an

emulsifier (amphiphilic block copolymer) that stabilizes particles in nonpolar solvents and in water without adding further surfactants. Consequently, the polymer block, which faces the continuous phase, must be forced to change its polarity from hydrophobic to hydrophilic at a desired stage. It shall be investigated whether a chemistry of protective groups can fulfill this demand of polarity reversal.

The last project deals with the formation of a new support material for the polymerization of olefins. Currently, the common support material is silica particles, which are non-spherical and broad in their size distribution. This is an issue regarding product quality and processability. The size and the morphology of the support dictate that of the polyolefin product. As a result, polymer particles formed from these silica-based supports are typically neither uniform nor spherical in shape, and are difficult to process. Therefore, the goal of this project is the synthesis of a support material that is uniform in size, that is spherical and possesses a large surface area for catalyst immobilization. This shall be accomplished with spherical, porous poly(urethane) (PU) particles that are synthesized in an uncommon nonaqueous emulsion. PU is generated by reacting diisocyanates with diols. Presence of water during polymerization leads to the coexisting formation of poly(urea) and carbon dioxide. In a nonaqueous emulsion, the amount of water can be precisely adjusted and should, therefore, influence the porosity. It shall be investigated whether porosity, the corresponding surface area, and, thus, the activity toward polymerization can be controlled by the emulsion system itself. This necessitates plenty of optimization regarding reaction conditions and component choices (monomers, catalysts).

4 Results and Discussion

4.1 Poly(L-lactide) Nanoparticles via Ring-Opening Polymerization (ROP) in Non-Aqueous Emulsion

Authors:

Robert Dorresteijn, Robert Haschick, Markus Klapper, Klaus Müllen

ToC:

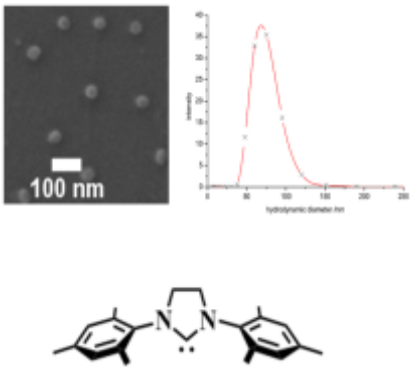

Cover Page:

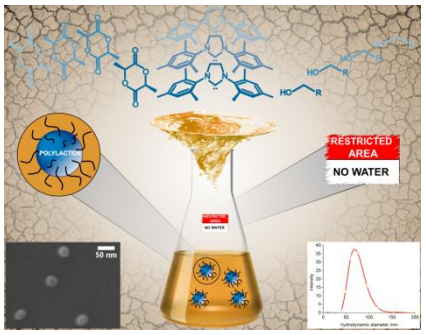

Published in:

Macromolecular Chemistry and Physics

(Reprinted with permission from (*Macromol. Chem. Phys.*, **2012**, *213*, 1996-2002.).

Abstract

The preparation of poly(L-lactide) nanoparticles via ring-opening polymerization (ROP) of L-lactide is conducted in non-aqueous emulsion. In this process acetonitrile is dispersed in either cyclohexane or *n*-hexane as the continuous phase. Stabilization of this system is achieved through the use of a PI-*b*-PEO respectively a PI-*b*-PS copolymer as emulsifier. The air and moisture sensitive *N*-heterocyclic carbene 1,3-bis(2,4,6-trimethylphenyl)-2-ididazolidinylidene (SIMes) catalyzes the polymerization of L-lactide at ambient temperatures. Hence, spherical poly(L-lactide) nanoparticles with an average diameter of 70 nm are obtained under very mild conditions. The molecular weight of poly(L-lactide) in the PI-*b*-PEO stabilized system always correlates with the theoretical results and therefore indicates a low occurrence of side-reactions in this system. Thus, the non-aqueous emulsion technique demonstrates its good applicability towards the generation of well-defined poly(L-lactide) nanoparticles.

Introduction

Aliphatic polyesters are widely applied in biological fields due to their biodegradability and biocompatibility.[70] One frequently investigated example of aliphatic polyesters is polylactide. It possesses good mechanical properties in addition to its biodegradability and biocompatibility, which makes it interesting for biomedical applications.[71] Polylactide can be obtained either by polycondensation of lactic acid, a step-growth polymerization, or ring-opening polymerization (ROP) of lactide, a chain-growth polymerization. A variety of metal catalysts, tin-octanoate[72] e.g., catalyze the ROP of lactide, leading to polylactide with a high molecular weight and a high monomer conversion. Nevertheless, we were interested in a metal-free approach to generate completely organic polylactide. The ROP

of lactide can be catalyzed by organo-catalysts, like an *N*-heterocyclic carbene (NHC) for example.[73-74] This approach poses an attractive alternative to metal catalysts in obtaining polylactide for biomedical and electronic applications.[75-76]

Concerning biomedical applications, dispersions of polylactide nanoparticles are mainly of interest. So far, polylactide nanoparticles are obtained in two steps. After the polylactide formation, the polylactide nanoparticles are obtained in a second step through nanoprecipitation or the high pressure emulsification and solvent evaporation method.[77-80] Aqueous emulsion polymerization, as the almost exclusively used method to prepare polymer dispersions, is however not applicable in this case. The major drawback in this traditional emulsion polymerization lies within the existence of water. Due to water in this system neither the polycondensation reaction nor the ROP are satisfactorily feasible to obtain polylactide nanoparticles. The polycondensation reaction of lactic acid in aqueous emulsion polymerization would lead to polymers with low molecular weights, as water shifts the equilibrium towards the monomer side. The ROP of lactide, normally leading to polylactide with high molecular weight and low polydispersity, fails completely in aqueous emulsion due to the high air and moisture sensitivity of the catalysts used for a ROP of lactide under mild conditions. The polymerization of lactide must therefore be carried out under inert atmosphere, where the absence of water is ensured. Thus there is a strong need for a suitable technique to generate well-defined polylactide nanoparticles in a controlled manner, concerning the desired molecular weight and its molecular weight distribution. Our main focus lies on the solution of this challenge and to generate polylactide nanoparticles under mild conditions in a non-aqueous one-step procedure, without the need of secondary dispersion of previously generated polylactide. The recently developed non-aqueous emulsion polymerization[61] could be predestinated for the polylactide case. This method has proven to be a

versatile technique for obtaining polymer nanoparticles by polymerizing a variety of sensitive monomers, e.g. diisocyanates or diacid chlorides.[3, 30] Such a non-aqueous emulsion consists of two immiscible inert organic solvents. The interfacial tension between two organic solvents is lower, compared to oil-in-water systems. Nevertheless, stabilization can be achieved through the use of an amphipolar block copolymer. Whereas low-molecular-weight surfactants, which are used as stabilizing agents in aqueous emulsion polymerizations, reach the thermodynamic equilibrium rapidly, block copolymers in many cases do not.[29] Therefore the exchange rate between unimeric and aggregated block copolymers is very low and allows the formation of stable micelles in selective solvents.[29] For example poly(isoprene)-*block*-poly(methylmethacrylate) (PI-*b*-PMMA), poly(isoprene)-*block*-poly(ethylene oxide) (PI-*b*-PEO) and poly(isoprene)-*block*-poly(styrene) (PI-*b*-PS) copolymers are capable of emulsifying solvent mixtures containing *N,N'*-dimethylformamide (DMF) or acetonitrile and *n*-hexane respectively cyclohexane for days.[3, 20, 30-31, 35, 61-63, 81] This system, as it contains neither protic solvents nor reactive functional groups, will be applied for the ROP of lactide, catalyzed by the air and moisture sensitive *N*-heterocyclic carbene 1,3-bis(2,4,6-trimethylphenyl)-2-ididazolidinylidene (SIMes). It will be demonstrated that spherical monodisperse poly(L-lactide) nanoparticles can be obtained under very mild conditions.

Experimental Section

General Remarks

All solvents and reagents were purchased from Sigma Aldrich. The PI-*b*-PS copolymer, the PI-*b*-PMMA copolymer and the PI-*b*-PEO copolymer were prepared using a sequential anionic polymerization technique.[82] L-lactide was washed with diethyl ether in order to remove lactic acid, dried under

vacuum afterwards and stored in the glovebox at -5 °C. 1,3-bis(2,4,6-trimethylphenyl)-2-imidazolidinylidene (SIMes) was used as received and stored under inert atmosphere at -20 °C. 1-Pyrenebutanol was stored under inert atmosphere at room temperature and was used as received. To determine the molecular weight distribution (MWD) of polylactide a gel permeation chromatography (GPC) was carried out at 30 °C using MZ-Gel SDplus 10E6, 10E4 and 500 columns in tetrahydrofuran (THF) as the eluent vs. polystyrene standards. The detector was an ERC RI-101 differential refractometer. The degree of polymerization (DP) of the polylactide nanoparticles and the composition of the block copolymers were determined by ^{1}H-NMR spectroscopy in dichloromethane (DCM) as the solvent via end-group analysis respectively peak analysis, using a Bruker Avance spectrometer operating at 300 MHz. Scanning electron microscopy (SEM) images were taken using a Zeiss Gemini 912 microscope. The SEM sample preparation proceeded the following way: the nanoparticles were dispersed in cyclohexane respectively *n*-hexane and drop casted on a silica wafer. The average diameters of the particles visualized in SEM images were determined by diameter measurements of 100 randomly chosen particles. Dynamic Light Scattering (DLS) was used to determine the droplet size of the investigated emulsions and the size of generated polylactide nanoparticles. The measurements were performed on a Malvern Zetasizer 3000 with a fixed scattering angle of 90° and on an ALV/LSE-5004-correlator using a He/Ne-laser operating at 632.8 nm.

Typical preparation of Poly(L-lactide) Nanoparticles

PI-*b*-PEO copolymer (0.050 g) was magnetically stirred in cyclohexane (14.4 g, 171 mmol) at room temperature. L-lactide (0.076 g, 0.53 mmol) was dissolved in acetonitrile (0.230 g, 5.59 mmol) and then added dropwise to the cyclohexane/PI-*b*-PEO dispersion. The emulsion was formed by treatment with sonication for 15 min using a Bandelin Sonorex RK255H

ultrasonic bath operating at 640 W. SIMes (4.68 mg, 15.3 µmol) and 1-pyrenebutanol (4.20 mg, 15.3 µmol) were dissolved in acetonitrile (0.176 g, 4.29 mmol) and added dropwise to the emulsion under inert atmosphere. The emulsion was stirred for 15 min at room temperature to produce poly(L-lactide) nanoparticles. A sample was taken out of the emulsion in order to analyze the particle size and morphology via DLS and SEM. The particles of the remaining emulsion were precipitated in methanol and separated by centrifugation to form 0.26 g of a white solid. The emulsifier was washed out by repeated centrifugation, redispersion in pure cyclohexane and washing with methanol afterwards. The DP and the MWD were determined via ^{1}H-NMR spectroscopy respectively GPC after drying the solid under vacuum.

Results and Discussion

For the ROP of L-lactide, in order to obtain poly(L-lactide) nanoparticles, a stable non-aqueous emulsion system is introduced, as this system has already proven to be applicable to water-sensitive polymerizations.[3, 30, 35, 61, 81] Non-aqueous emulsions are prepared by combination of two immiscible organic solvents and by stabilization of this mixture with an emulsifying agent. In previous investigations of immiscible organic solvent mixtures we have concluded that a DMF/*n*-hexane and an acetonitrile/cyclohexane mixture, stabilized by a PI-*b*-PMMA copolymer, are the most promising systems for these kind of reactions as they are long-term stable.[35] The combination of solvents and block copolymer leads to the formation of inert dispersed ‘nanoreactors’, wherein sensitive polymerizations can occur due to the absence of any protic groups, as they exist neither in the emulsifier nor in the solvents. Therefore this system should also allow the use of catalysts suitable for the ROP of L-lactide under mild conditions in non-aqueous emulsion, as they are all highly air and moisture sensitive.

However, the catalysts must fulfill two requirements in order to be applicable to a non-aqueous emulsion. First of all the catalyst must be highly active below the boiling temperatures of the continuous and the dispersed phase. Secondly the polymerization must be completed before Ostwald ripening and cohesion causes inhomogeneous droplet sizes. A rapid polymerization procedure ensures the formation of particles with a monomodal particle size distribution. The ROP of L-lactide catalyzed by 4-dimethylaminopyridine (DMAP)[76], triazol-carbenes[83] and thiourea-amine derivatives[84] at ambient temperatures leads to polylactide with high monomer conversions, yet only after very long reaction times (4 h – 306 h). Due to their long reaction times, these catalysts are not ideal. In contrast to that, *N*-heterocyclic carbenes (NHCs), like 1,3-bis(2,4,6-trimethylphenyl)imidazole-2-ylidene (IMes) or 1,3-bis(2,4,6-trimethylphenyl)-2-ididazolidinylidene (SIMes), are able of catalyzing the polymerization of cyclic esters to polyesters at room temperature within 1 hour.[73-74] Thus, these cheap catalysts are highly reactive towards the ROP of lactide and in addition lead to polylactide with a highly controllable molecular weight, low polydispersity and a high monomer conversion.[73, 85-86] Nevertheless the NHCs lack an inert atmosphere, due to the high air and moisture sensitivity mentioned above. To utilize the good catalytic properties towards the ROP of L-lactide in order to generate poly(L-lactide) nanoparticles, a non-aqueous emulsion system under inert atmosphere is needed.

Before the heterogeneous polymerizations were performed a homogeneous polymerization of L-lactide, catalyzed by SIMes and initiated by 1-pyrenebutanol, in acetonitrile and DMF was investigated in order to choose the more appropriate solvent as dispersed phase for the ROP of L-lactide in non-aqueous emulsion. The polymerization in DMF generated poly(L-lactide) with a lower molecular weight, compared to the expected molecular weight derived from the ratio of monomer consumption versus catalyst and initiator concentration, and a broad MWD (dispersity 2.79). In contrast to

the result in DMF, the polymerization performed in acetonitrile led to polymers with the expected molecular weight and lower polydispersity (dispersity 1.40). This suggested that the polymerization of L-lactide performed in DMF, in comparison to the polymerization in acetonitrile, gave an increased amount of side-reactions, like transesterifications.[74, 87] In addition, the solubility of polyesters in acetonitrile is better than in DMF. This is why acetonitrile was chosen as the dispersed phase in non-aqueous emulsion for the ROP of L-lactide.

Emulsifiers for Non-Aqueous Emulsion Polymerization of L-lactide

We had used PI-*b*-PMMA copolymers as emulsifiers for non-aqueous emulsions to obtain a variety of different polymer nanoparticles.[3, 30-31, 35, 61-63, 81] Unfortunately, the attempt of polymerizing L-lactide in non-aqueous emulsion, emulsified by this copolymer, did not result in dispersed poly(L-lactide) nanoparticles. A strong interaction of the electron-rich carbene group of the catalyst SIMes and the electrophilic ester group of the PMMA block was believed to be the reason for the unsuccessful polymerization attempt. Nevertheless, we want the catalyst to strongly interact with an ester group, since L-lactide also possesses ester groups. Therefore new emulsifiers had to be applied for the existing system. It was demonstrated that PI-*b*-PS copolymers are capable of emulsifying DMF/*n*-hexane mixtures.[20] Maximum emulsifying efficiency was achieved with copolymers of a molecular weight from 30000 – 40000 $g \cdot mol^{-1}$ and a PI-to-PS ratio of 1:1.[20] In general high molecular weights of block copolymers as emulsifying agents are essential, since low interfacial tensions reign between two organic solvents in an oil-in-oil emulsion (O/O emulsion). As the polymerization of L-lactide in DMF didn't lead to well-defined poly(L-lactide), an *n*-hexane/acetonitrile mixture, emulsified by a PI-*b*-PS copolymer, was investigated. Therefore DLS measurements of emulsions with various block copolymer amounts were conducted in order to determine the size of the 'nanoreactors', wherein the polymerization takes

place. The PI-*b*-PS copolymer has a number average molecular weight of 35000 g·mol^{-1} (dispersity 1.04) and a molar block composition of 50% PI and 50% PS (DP_{PI} = 198, DP_{PS} = 199). All DLS measurement of a *n*-hexane/acetonitrile mixture stabilized with different amounts of the PI-*b*-PS copolymer (0.8 – 3.2 wt-%) showed an existence of acetonitrile 'nanoreactors' with an average diameter of 36 nm in the continuous phase *n*-hexane. A stabilization of an alternative cyclohexane/acetonitrile mixture with the PI-*b*-PS copolymer, in order to avoid n-hexane and its canceroganic, mutagenic and toxic to reproduction (CMR) properties, could not be achieved as polystyrene is soluble in both cyclohexane and acetonitrile. Therefore we synthesized a PI-*b*-PEO copolymer. This block copolymer allowed us to perform the lactide polymerization also in a cyclohexane/acetonitrile mixture as poly(ethylene oxide) is more polar than polystyrene and therefore insoluble in cyclohexane. The generated PI-*b*-PEO copolymer has a number average molecular weight of 45700 g·mol^{-1} (dispersity 1.06) and a molar block composition of 55% PI and 45% PEO (DP_{PI} = 441, DP_{PEO} = 357). In order to perform the polymerization in a non-aqueous emulsion with the lowest possible amount of stabilizing agent, we investigated cyclohexane/acetonitrile mixtures stabilized by various amounts of PI-*b*-PEO copolymer (0.010 – 0.200 g). The mixtures constisted of cyclohexane (14.4 g, 171 mmol), acetonitrile (0.230 g, 5.59 mmol) and were emulsified by stirring and sonication after the addition of emulsifier.

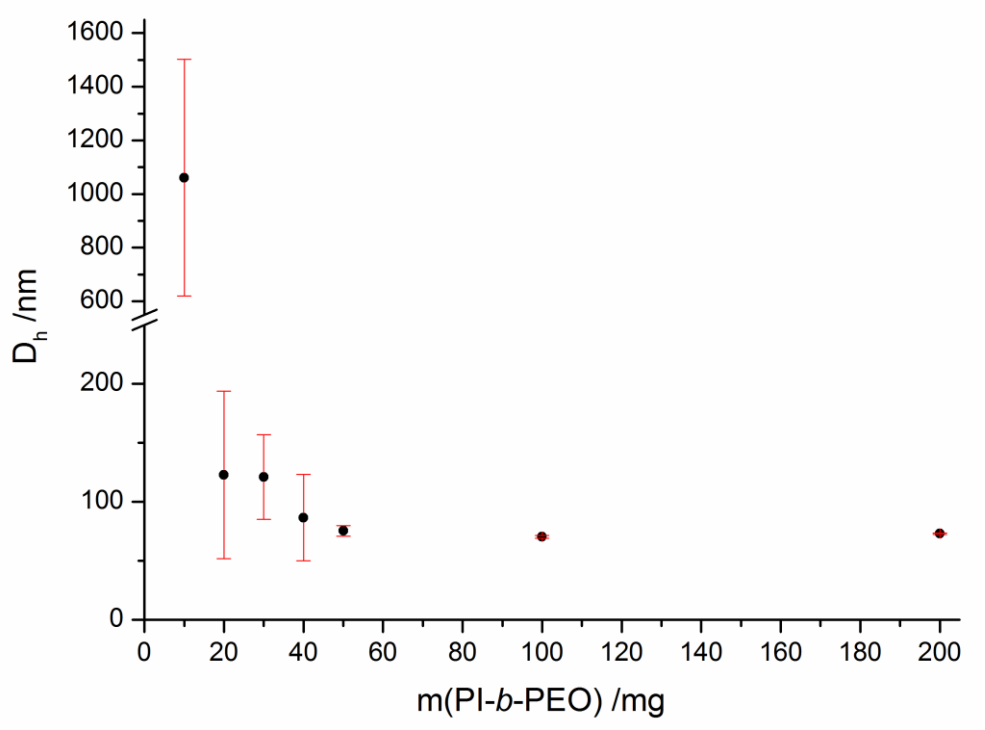

Figure 4.1.1. DLS measurement of 0.406 g acetonitrile dispersed in 14.4 g cyclohexane using a PI-b-PEO copolymer (left to right: 0.010 g, 0.020 g, 0.030 g, 0.040 g, 0.050 g, 0.100 g, 0.200 g) as emulsifier. Stirring and ultrasonification of the mixture led to emulsion.

The results of the DLS measurements proved the formation of stable emulsions with 0.34 wt-% of stabilizing agent or higher (0.050 – 0.200 g of PI-*b*-PEO in our experiments; Figure 4.1.1). The average droplet diameter of the acetonitrile 'nanoreactors' measured 72 nm. A block copolymer amount lower than 0.34 wt-% led to both an increase of the droplet size and an increase of the droplet size distribution (Figure 4.1.1). This fewer amount of block copolymers in the mixture leads to an insufficient stabilization of the interfacial tension between the dispersed droplets with a droplet size of 72 nm. Due to the previously shown DLS results in Figure 4.1.1 a non-aqueous emulsion with 0.34 wt-% of PI-*b*-PEO copolymer was used for the polymerization of L-lactide. This system and the PI-*b*-PS copolymer stabilized system was believed to generate poly(L-lactide) nanoparticles, since SIMes is selectively soluble in the dispersed acetonitrile phase. The

preparation of dispersed poly(L-lactide) nanoparticles in non-aqueous emulsion is shown schematically in Figure 4.1.2 for the PI-*b*-PEO case.

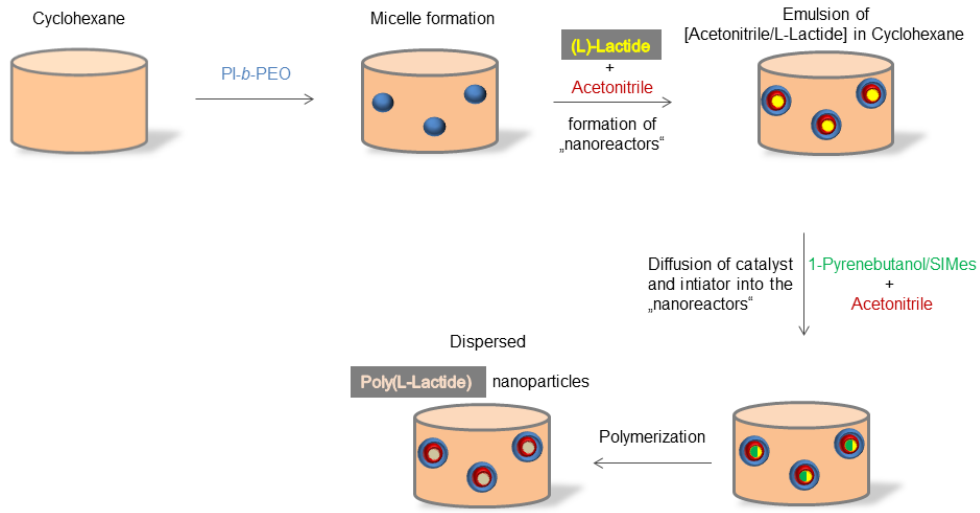

Figure 4.1.2. Preparation of poly(L-lactide) nanoparticles in non-aqueous emulsion.

L-lactide was dissolved in the polar organic solvent (acetonitrile) and emulsified in the nonpolar organic solvent (cyclohexane). The diffusion of SIMes and 1-pyrenebutanol into the dispersed droplets started the polymerization. The obtained poly(L-lactide) nanoparticles were investigated by DLS and SEM measurements. To determine the DP and the MWD by ^{1}H-NMR spectroscopy respectively GPC the particles were finally precipitated in methanol, centrifuged and redissolved in DCM respectively THF. The precipitated poly(L-lactide) nanoparticles were well-redispersable in cyclohexane, since, according to DLS measurements, no aggregation occurred.

Table 4.1.1. Experimental conditions and results of the preparation of poly(L-lactide) in non-aqueous emulsion.

Sample	**M/Cat/I** [a]	**$DP_{(theo)}$** [b]	**$DP_{(exp)}$** [c]	**MWD** [d]	**D_h** [e] **[nm]**	**D_h** [e), f] **[nm]**

1	18:1:1	35	35	1.10	70 ± 6	46 ± 26
2	25:1:1	50	49	1.23	72 ± 2	-
3	35:1:1	70	78	1.11	70 ± 7	53 ± 6
4 [g)]	35:1:1	70	48	1.15	106 ± 3	-
5 [g)]	35:1:1	70	57	1.24	86 ± 11	-
6 [h)]	35:1:1	70	-	-	36	-

Emulsion: Acetonitrile (0.406 g) dispersed in cyclohexane (14.4 g) stabilized by PI-*b*-PEO (0.050 g); Polymerization: L-lactide (0.076 g) + 3-6 mol-% SIMes + 3-6 mol-% 1-pyrenebutanol at ambient temperature for 15 min.

a) Monomer/Catalyst/Initiator ratio (n(L-lactide) / n(SIMes) / n(1-pyrenebutanol));
b) Degree of polymerization; calculated for one end-group per chain;
c) Degree of polymerization; determined by end-group analysis from ^{1}H-NMR spectroscopy;
d) Molecular-weight distribution determined via GPC vs polystyrene standards;
e) Hydrodynamic diameter determined via DLS;
f) Hydrodynamic diameter determined via DLS after removal of the emulsifier;
g) Stabilization of the emulsion by a PI-*b*-PS copolymer (0.200 g) in *n*-hexane as the continuous phase;
h) Stabilization of the emulsion by a PI-*b*-PMMA copolymer (0.200 g) in *n*-hexane as the continuous phase.

As shown in Table 4.1.1, L-lactide was successfully polymerized by non-aqueous ring-opening emulsion polymerization using SIMes as catalyst, 1-pyrenebutanol as initiator, acetonitrile as the dispersed phase, *n*-hexane or cyclohexane as the continuous phase and a PI-*b*-PS respectively PI-*b*-PEO copolymer as emulsifier. The molecular weights of poly(L-lactide) derived from GPC measurements against polystyrene standards correlated with the DPs derived from ^{1}H-NMR spectroscopy taking the Mark-Houwink constants into account.[88-90]

Poly(L-lactide) Nanoparticles Stabilized by PI-b-PS copolymer

The polymerization in non-aqueous emulsion stabilized by a PI-*b*-PS copolymer led to polylactide with a narrow MWD (as low as 1.15), but a DP lower than the one derived from the ratio of the monomer consumption versus catalyst and initiator concentration (Table 4.1.1). ^{1}H-NMR spectroscopy of poly(L-lactide) in the PI-*b*-PS copolymer stabilized emulsion offered a mean monomer conversion of 0.87, what is conform to the resulted DP. Prolonging the reaction time from 15 min to 30 min in order to generate poly(L-lactide) with a DP correlating to the calculated DP and therefore yield a higher monomer conversion wasn't successful, since this catalyst also catalyzes transesterification reactions.[91] The poly(L-lactide) nanoparticles possessed a size of roughly 100 nm, as derived from DLS measurements.

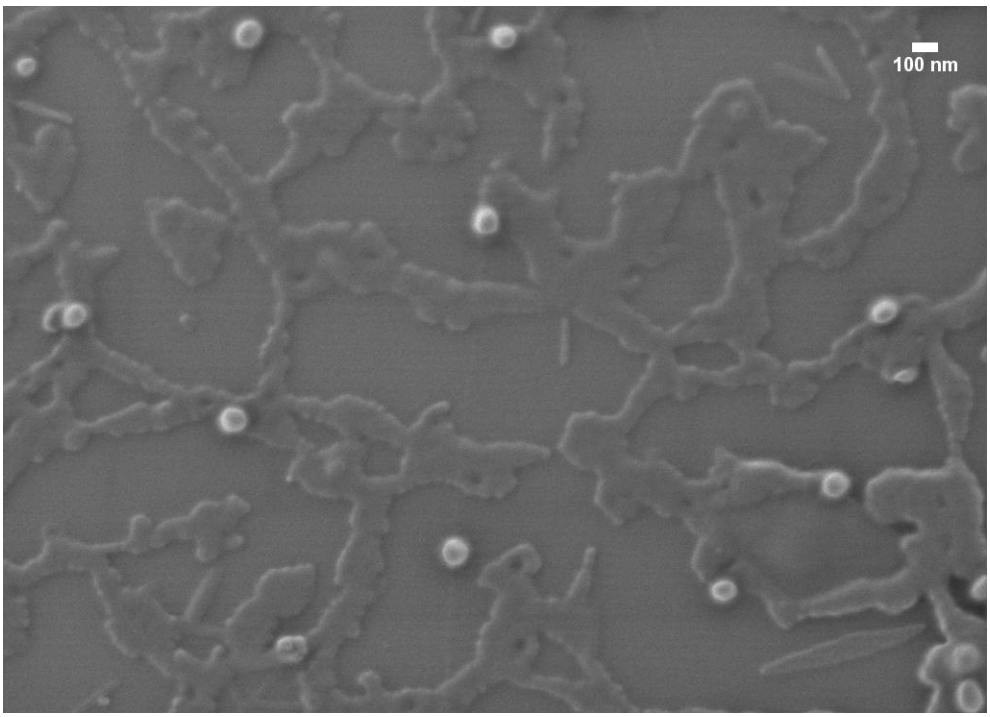

Figure 4.1.3. SEM micrograph of poly(L-lactide) nanoparticles synthesized in non-aqueous emulsion stabilized by a PI-b-PS copolymer; the mean particle size determined by SEM (based on 100 randomly chosen particles) was 100 nm (± 8 nm).

The particle size derived from DLS measurements correlated with the particle size determined from SEM micrographs (Figure 4.1.3). This demonstrates that the poly(L-lactide) nanoparticles are well-dispersed by the PI-*b*-PS copolymer in *n*-hexane and that its possible influence on the measured diameters was to be neglected. As can be seen in Figure 4.1.3, the SEM micrograph showed monomodal spherical particles with a smooth surface. Due to the exclusive solubility of SIMes inside the dispersed acetonitrile 'nanoreactors' a spherical shape of generated poly(L-lactide) resulted. ^{1}H-NMR characterization of the obtained polymers after precipitation confirmed a coating by the PI-*b*-PS copolymer. The emulsifier shell provides the possibility to redisperse the obtained nanoparticles in a nonpolar solvent and therefore assures long-term stability.

Poly(L-lactide) Nanoparticles Stabilized by PI-b-PEO copolymer

The poly(L-lactide), generated by polymerization in non-aqueous emulsion stabilized by a PI-*b*-PEO copolymer, always possessed a DP that correlated with the calculated one. The synthesis of poly(L-lactide) with 35, 50 respectively 70 repeating units of L-lactide was demonstrated in this non-aqueous emulsion system. In order to generate poly(L-lactide) with higher DPs, we performed homopolymerizations of L-lactide. Unfortunately we weren't able to synthesize poly(L-lactide) with a higher DP than 90, which is conform to previous works of other research groups.[91] The monomer conversion in the non-aqueous emulsion polymerization process was almost quantitative (yield = 99%) as derived from ^{1}H-NMR spectroscopy. The achieved conversion is similar to the lactide conversions in catalyst systems known from the literature.[73] The poly(L-lactide) nanoparticles uniformly measured an approximate size of 70 nm, determined from DLS measurements, which in addition was independent from the DP of poly(L-lactide) within the particles.

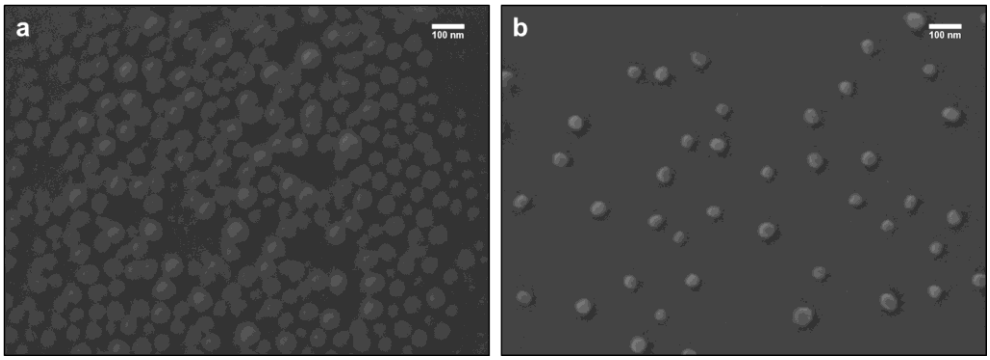

Figure 4.1.4. SEM micrographs of poly(L-lactide) nanoparticles synthesized in non-aqueous emulsion stabilized by a PI-b-PEO copolymer; **a**: SEM micrograph of poly(L-lactide) nanoparticles before washing with a mean particle size of 65 nm (± 5 nm) determined by SEM (based on 100 randomly chosen particles); **b**: SEM micrograph of poly(L-lactide) nanoparticles after washing with a mean particle size of 44 nm (± 6 nm) determined by SEM (based on 100 randomly chosen particles).

The particle morphology could be derived from SEM measurements (Figure 4.1.4). The particle size derived from DLS was similar to the one derived from the SEM micrographs. The slightly smaller value determined from SEM micrographs originated from measuring a hydrodynamic diameter in DLS. This small deviation shows that the poly(L-lactide) nanoparticles are well-dispersed in cyclohexane by the PI-*b*-PEO copolymer. The particles were spherical, possessed a smooth surface and were very monomodal. The spherical shape of the obtained nanoparticles led to the conclusion that the polymerization proceeded exclusively inside the dispersed droplets (Figure 4.1.2). As mentioned in the experimental part, we were able to wash the emulsifier off the particles as confirmed by ^{1}H-NMR spectroscopy. In Figure 4.1.4 the SEM micrographs of the poly(L-lactide) nanoparticles before (a; left) and after (b; right) washing are shown. Due to the washing process the size of the particles, which remained spherical, significantly decreased by roughly 20 nm as confirmed by DLS measurement.

It was demonstrated that with each non-aqueous emulsion system, stabilized by a PI-*b*-PS respectively a PI-*b*-PEO copolymer, spherical poly(L-lactide)

nanoparticles could be generated under very mild conditions. The molecular weight could be altered by varying the ratio of the monomer consumption versus catalyst and initiator concentration. The polydispersity, determined via GPC, was as low as 1.10 as expected from a chain-growth polymerization. This implies a controlled formation of L-lactide particles in non-aqueous emulsion, concerning the well-defined poly(L-lactide) within the obtained monomodal spherical nanoparticles. The spherical shape arises from the selective solubility of SIMes in the dispersed phase, which indicates a miniemulsion mechanism. However, as a diffusion of L-lactide through the continuous phase during the polymerization, which indicates an emulsion polymerization, cannot be excluded, the mechanism cannot be unambiguously assigned to either the one or the other mechanism.

The presented method is the first step in new polylactide chemistry. Concerning biomedical applications, as one potential application, aqueous suspensions of polylactide are needed. Therefore further developments like water-solubilization are necessary. It is conceivable for the already in emulsion existing polylactide nanoparticles to be modified with a hydrophilic shell or targeting functions for specific desired applications in the same pot, since the synthesis of core-shell particles was already demonstrated in previous works.[63] An additional possibility poses the hydrophilization of polylactide particles by embedding them into a shell of charged amphiphilic block copolymers, as described for hydrophobic inorganic particles.[92]

Conclusion

Up to now polylactide nanoparticles have been accessible only by two-steps procedures. After polymer formation, the particles are obtained through nanoprecipitation or the high-pressure emulsification and solvent evaporation method in a separate step.[77-80] Polylactide nanoparticles are

also not accessible through aqueous emulsion polymerization due to the water sensitivity of the required catalysts. The non-aqueous emulsion has already proven its applicability towards many sensitive reactions[3, 30-31, 35, 61-63, 81] and is herein applied for the preparation of poly(L-lactide) nanoparticles by ring-opening polymerization (ROP) in one step. A non-aqueous emulsion system, containing acetonitrile dispersed in either cyclohexane or *n*-hexane, is stabilized by a PI-*b*-PEO respectively a PI-*b*-PS copolymer. Within both systems spherical poly(L-lactide) nanoparticles can be generated by catalyzing and initiating L-lactide with SIMes respectively 1-pyrenebutanol at ambient temperature. In the PI-*b*-PEO copolymer stabilized system well-dispersed spherical particles with an average diameter of 70 nm are generated in one-step. The molecular weight of poly(L-lactide) can be altered by varying the monomer consumption to the catalyst and initiator concentration.

The herein presented method should be suitable for further modifications. A preparation of hybrid nanoparticles by surrounding the particles with a second polymer shell, as already demonstrated for polyurethane particles[18], will be likely achievable in the same pot.

Polylactide is also widely used in pharmaceutical applications due to its biodegradability and biocompatibility mainly as potential drug carrier.[93-94] The mild conditions applied in the non-aqueous emulsion should offer the opportunity to incorporate temperature sensitive drugs already during the formation of the particles. Furthermore, the use of reactive groups either in the emulsifier or in comonomers should be permitted, which will allow the postfunctionalization of the beads by drugs, dyes or peptides. Therefore, we expect that this new approach of producing poly(L-lactide) nanoparticles under water-free and mild conditions expands the portfolio of carrier systems and will have the potential of finding applications in biomedical fields.

4.2 Biocompatible Polylactide-*block*-Polypeptide-*block*-Polylactide Nanocarrier

Authors:

Robert Dorresteijn, Ruben Ragg, Gianluca Rago, Nils Billecke, Mischa Bonn, Sapun H. Parekh, Glauco Battagliarin, Kalina Peneva, Manfred Wagner, Markus Klapper, Klaus Müllen

ToC:

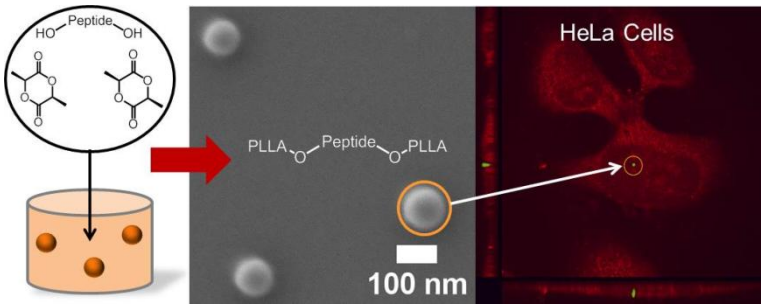

Published in:

Biomacromolecules

(Reprinted with permission from (*Biomacromolecules*, **2013**, *14*, 1572-1577). Copyright (2013) American Chemical Society.)

Abstract

Polypeptides are successfully incorporated into poly(L-lactide) (PLLA) chains in a ring-opening polymerization (ROP) of L-lactide by using them as initiators. The resulting ABA triblock copolymers possess molecular weights up to 11000 $g \cdot mol^{-1}$ and polydispersities as low as 1.13, indicating the living character of the polymerization process. In a non-aqueous emulsion, peptide-initiated polymerization of L-lactide leads to well-defined nanoparticles, consisting of PLLA-*block*-peptide-*block*-PLLA copolymer. These nanoparticles are easily loaded by dye-encapsulation and transferred into aqueous media without aggregation (average diameter of 100 nm) or significant dye leakage. Finally, internalization of PLLA-*block*-peptide-*block*-PLLA nanoparticles by HeLa cells is demonstrated by a combination of coherent anti-Stokes Raman spectroscopy (CARS) and fluorescence microscopy. This demonstrates the promise of their utilization as cargo delivery vehicles.

Introduction

Polymer-based carrier systems have been extensively developed over the past decades. Vehicles having micellar structures are usually generated by immersion and self-assembly of amphiphilic block copolymers in aqueous medium. A drug can be either encapsulated in the micelle or covalently attached to the block copolymer.[58, 95-97] Its release occurs at specific target site owing to environmental effects.[98] Recently, Landfester et al. generated a cargo delivery system based on nanocapsules in an oil-in-oil miniemulsion.[2] There, the polyaddition reaction of toluene diisocyanate and a diamine at the oil droplet interface led to the formation of polyurea nanocapsules, which after transfer into aqueous media measured diameters ranging from 210 nm to 780 nm. The diamine group contains a

glycine/phenylalanine-based (GFF) linker[2], which is cleavable by the proteinase trypsine, found mainly in the human digestive system.

Over the last decade intensive research has been undertaken concerning peptides that are cleavable by proteinases, which are overexpressed at the invasive front of tumor tissues.[69, 99-102] Harris et al. used such a peptide as linker between a hydrophilic polymer and a magnetofluorescent nanoparticle.[101] The hydrophilic polymer veils the cell-internalizing domain of the nanoparticle. Cleavage of the peptide-linker leads to a selective accumulation of the nanoparticle in tumor tissues.[101]

Despite the progress in this field, particularly concerning the versatility of incorporated peptides, challenges remain regarding the stability of encapsulated cargo and particle aggregation. Specifically, incorporation of water-sensitive drugs into micellar vehicles, which originate from self-assembly processes in water, might be detrimental to the drug therefore necessitating non-aqueous processes.[103] Cargo delivery vehicles originating from organic solvents often suffer from aggregation resulting in increased particle sizes after their transfer into water.[2] Aggregation of particles can obstruct their application as drug carrier system since particle sizes near 100 nm are ideal[104-106]: particles larger than 200 nm undergo clearance from the blood stream by Kupffer cells while particles smaller than 100 nm suffer from drainage into blood capillaries and are associated with potential toxicity.[104-106] For delivery systems based on selective accumulation of particles in tumor tissues after cleavage of a peptide sequence, drug-release might be hindered due to complete hydrophobicity of the carriers after peptide-cleavage, resulting in aggregation.[107]

Hence, there is still need for new concepts and processes concerning nanocarrier formation. We explore the use of polypeptide-polylactide latex

particles as carrier system by applying new polylactide chemistry. Bifunctional polypeptides should initiate the lactide polymerization and finally lead to the generation of polylactide-polypeptide-polylactide triblock structures. Poly(L-lactide) (PLLA) is widely applied in biological fields since it is biodegradable, biocompatible and renewable.[64-65, 70, 108] Our non-aqueous emulsion system has previously been shown to be compatible with an air- and moisture-sensitive polymerization of L-lactide, and to lead to well-defined spherical PLLA nanoparticles.[108] As such, the particles are expected to be suitable even for incorporation of water- and temperature-sensitive compounds. Besides incorporation of bifunctional peptide in a biodegradable polymer backbone through a single step polymerization at ambient temperature, additional challenges like preservation of the usual approximate particle size of 100 nm in aqueous media and the observation of complete cell-internalization remain.

Results and Discussion

The ring-opening polymerization (ROP) reactions of L-lactide in the presence of a bifunctional peptide as initiator were at first performed in solution in order to completely characterize the polymer composite. The polymerization was subsequently conducted in non-aqueous emulsion to investigate the morphology of the obtained poly(L-lactide)-*block*-peptide-*block*-poly(L-lactide) (PLLA-*b*-peptide-*b*-PLLA) nanoparticles. Finally the particles were transferred into aqueous media in order to study their internalization in cells, which was followed using the fluorescent marker PMI (9-Bromo-*N*-(2,5,8,11,15,18,21,24-octaoxapentacosan-13-yl)perylene-3,4-dicarboxy monoimide).

So far, incorporation of peptides in polylactide chains has been carried out in three sequential polymerization steps at elevated temperatures.[109] In contrast, the approach presented here permits formation of PLLA-*b*-peptide-*b*-PLLA copolymers at ambient temperature and in a single step. The peptide consists of two serine end groups as initiating groups and tryptophane spacer groups (Ac-SWWWWWS-NH_2). Both serine groups, each bearing one hydroxyl group, should selectively initiate the polymerization of L-lactide, since they are the most nucleophilic groups in the peptide (Scheme 4.2.1). In addition, potential competing indol-units, contained in tryptophane, are proven to not initiate the lactide polymerization.[110-111]

Tryptophane signals in ^{1}HNMR spectroscopy do not superimpose with the serine signals. This simplifies the determination of a successful peptide-incorporation in a polylactide chain.

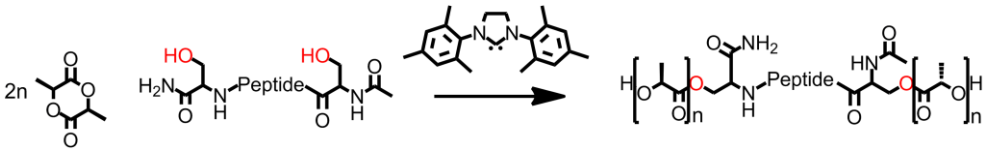

Scheme 4.2.1. Reaction scheme of the peptide initiated L-lactide polymerization.

Homopolymerizations of L-lactide with SIMes as catalyst and Ac-SWWWWWS-NH_2 as initiator were performed. The polymerization conditions and the molecular weight of the obtained polymers are denoted in Table 4.2.1.

Table 4.2.1. Experimental conditions and results of the preparation of PLLA-b-peptide-b-PLLA copolymers in solution (1-2) and in non-aqueous emulsion (3-4).

Sample	M/Cat/I [a]	$Mn_{(theo)}$ [b]	$Mn_{(exp)}$ [c]	MWD [d]	D_h [e] (DLS) [nm]	D [f] (SEM) [nm]	ee [g] [%]
1	35:2:1	5000	5500	1.38	-	-	-

2	70:2:1	10000	11000	1.25	-	-	-
3[j)]	35:2:1	5000	6400	1.31	75 ± 2	76 ± 14	99
3a[j) h)]			6300	1.29	104 ± 20	103 ± 8	-
4[k)]	35:2:1	5000	5500	1.41	79 ± 10	79 ± 10	92
4a[k) i)]			6600	1.13	135 ± 40	121 ± 14	-
4b[k) h)]			7500	1.14	98 ± 15	89 ± 8	-

Homopolymerization: L-lactide (0.076 g) + 3-6 mol-% SIMes + 0.7-3 mol-% Ac-SWWWWWS-NH_2 were dissolved in acetonitrile (0.406 g) and stirred at ambient temperature for 15 min.
Emulsion: Acetonitrile (0.406 g) dispersed in cyclohexane (14.4 g) stabilized by PI-*b*-PEO (0.050 g); Polymerization: L-lactide (0.076 g) + 6 mol-% SIMes + 3 mol-% Ac-SWWWWWS-NH_2 + $8.10 \cdot 10^{-3}$ – $4.44 \cdot 10^{-2}$ mol-% PMI at ambient temperature for 15 min.

a) monomer/catalyst/initiator ratio (n(L-lactide) / n(SIMes) / n(peptide));
b) theoretical molecular weight calculated from the ratio of monomer to initiator;
c) number-averaged molecular weight determined via GPC vs polystyrene standards;
d) molecular weight distribution determined via GPC vs polystyrene standards;
e) hydrodynamic diameter determined via DLS;
f) particle diameter determined by measurement of 100 randomly chosen particles in SEM micrographs;
g) encapsulation efficiency determined via HPLC;
h) particles dispersed in 0.2-wt% Lutensol AP 20 solution;
i) particles dispersed in 0.05-wt% Lutensol AP 20 solution;
j) polymerization conducted in the prior presence of $8.10 \cdot 10^{-3}$ mol-% PMI;
k) polymerization conducted in the prior presence of $4.44 \cdot 10^{-2}$ mol-% PMI.

According to the data shown in Table 4.2.1, the polymerization of L-lactide with Ac-SWWWWWS-NH_2 as initiator was successful with an overall monomer conversion of 99%, as derived from ^{1}HNMR spectroscopy. The molecular weights derived from gel permeation chromatography (GPC) measurements against polystyrene standards always conformed to the expected molecular weight taking the Mark-Houwink constants into account.[88-90] Sample 2 possessed a molecular weight of 11000 g·mol^{-1}. This represents a degree of polymerization (DP) of 160, suggesting approximately 80 repeating units per hydroxyl group. The overall molecular weight of sample 2 exceeds the reported maximum for polylactide

originating from polymerizations with monofunctional initiators and SIMes catalyst (DP ≤ 100, molecular weight of 7200 g·mol^{-1}).[91, 108] Hence, higher molecular weights were achieved owing to the bifunctional structure of the initiating peptide.

The GPC always showed low polydispersity and a monomodal peak without any shoulder indicating initiation of the polymerization by both hydroxyl groups contained in the peptide. To further corroborate the centered position of the peptide in the chain ^{1}HNMR and diffusion ordered spectroscopy (DOSY) measurements were performed. DOSY proved the covalent attachment of the peptide to the polymer. Investigations of the peptide before and after the polymerization by ^{1}HNMR spectroscopy indicated a significant chemical downfield shift of the signals of the methylene groups in both serine units. Taken together, these results demonstrate the reaction of both serines in the lactide polymerization and strongly suggest incorporation of the peptide as the linker between two PLLA chains.

After the successful homopolymerization and structural analysis of the resulting polymer in solution, L-lactide was polymerized in non-aqueous emulsion (Samples 3 and 4 in Table 4.2.1), according to Scheme 4.2.2. The non-aqueous emulsion consisted of acetonitrile dispersed in cyclohexane. Stabilization was achieved by the addition of a PI-*b*-PEO copolymer as emulsifier with a number-average molecular weight of 45700 g·mol^{-1} (dispersity 1.06) and a molar block composition of 55% PI and 45% PEO (DP_{PI} = 441, DP_{PEO} = 357).

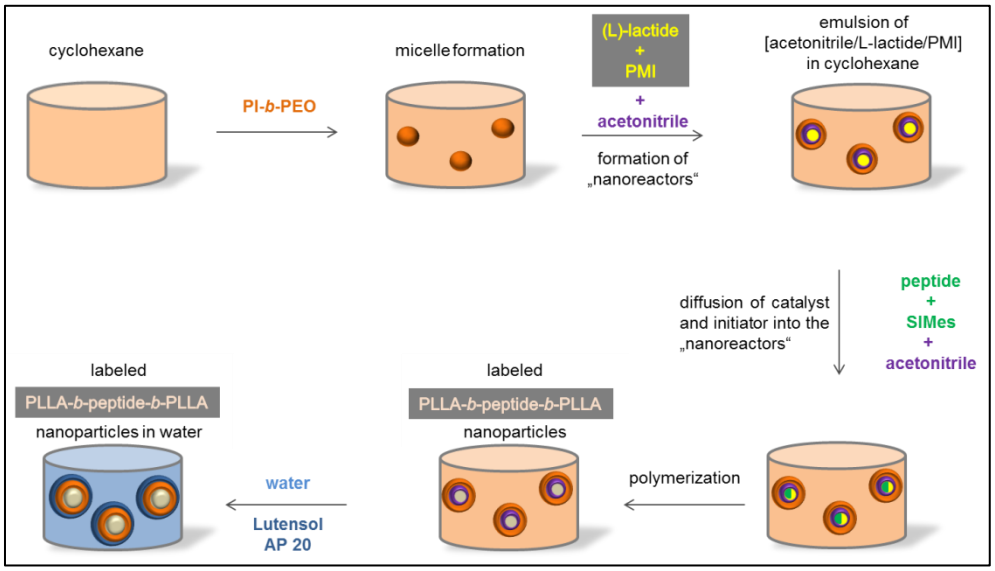

Scheme 4.2.2. Preparation of peptide-initiated, PMI-loaded PLLA-b-Peptide-b-PLLA nanoparticles in non aqueous emulsion and the transfer of these particles into aqueous media.

The monomer conversion in non-aqueous emulsion was 99%, as derived from ^{1}HNMR spectroscopy. The molecular weight correlated with the expected value. Again, a significant downfield shift of the methylene-signals after the polymerization was observed by ^{1}HNMR spectroscopy. The PLLA-*b*-peptide-*b*-PLLA nanoparticles uniformly possessed an approximate diameter of 80 nm, as determined from DLS measurements (Table 4.2.1). To investigate the morphology of the obtained particles, SEM measurements were performed (Figure 4.2.1 a-b).

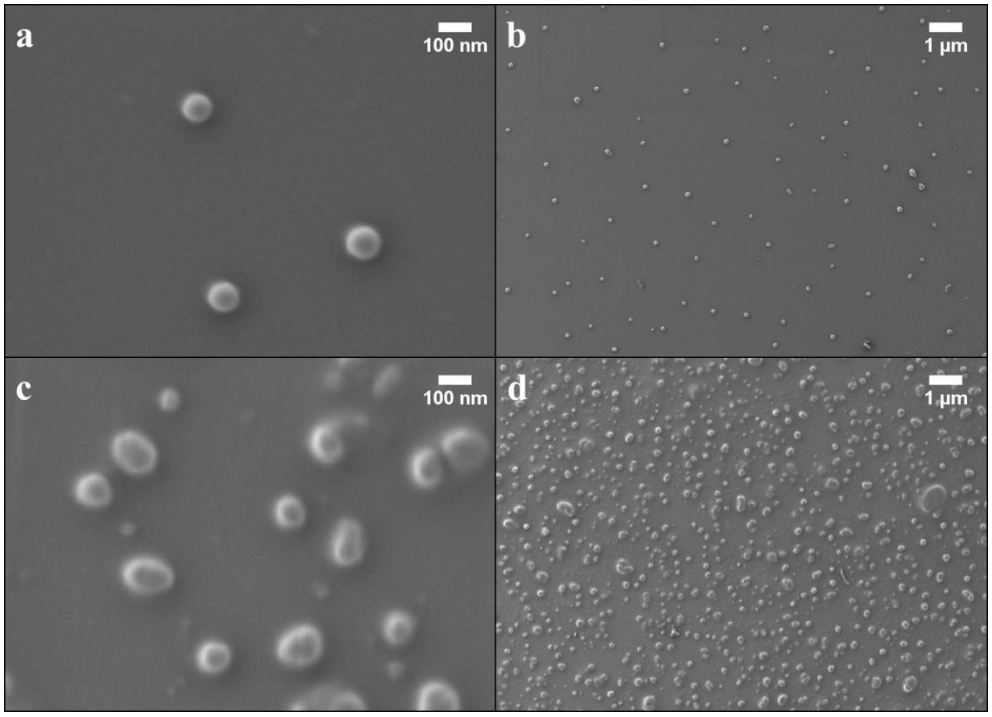

Figure 4.2.1. Typical SEM micrographs of PLLA-b-peptide-b-PLLA nanoparticles prepared in non-aqueous emulsion (a-b) and after transfer into aqueous media (c-d).

Because of the selective solubility of SIMes in the dispersed acetonitrile phase, which partitions into the pre-existing micelles, formation of particles in "nanoreactors" is expected. The largely monodisperse nanoparticles were spherical and possessed a smooth surface, confirming that polymerization must have proceeded exclusively inside the dispersed "nanoreactors". A particle diameter of roughly 80 nm was determined from SEM micrographs (Figure 4.2.1 a-b), which matches the values resulting from DLS measurements. The matching particle sizes indicate that the PI-*b*-PEO copolymer is able to disperse the PLLA-*b*-peptide-*b*-PLLA nanoparticles in cyclohexane very well.

The hydrophobic particles were transferred into aqueous media, namely a 0.05 – 0.2 wt-% Lutensol AP 20 solution, in order to perform cell experiments. Lutensol AP 20 is a PEG-based surfactant. Stabilization of the

nanoparticles in water is achieved through hydrophobic interactions between the surfactant and the polyisoprene block of the emulsifier. The amphiphilic surfactant ensures that the particles remain well-dispersed despite any degradation process within the particle itself.

The determined particle diameters from SEM micrographs were in the range of 100 nm – 120 nm (Figure 4.2.1 c-d, Table 4.2.1: Sample 3a, 4a, 4b). These values are consistent with the results from DLS measurement (particle size 100 nm - 130 nm), since in DLS the hydrodynamic diameter is obtained. Hence, only a slight diameter-increase was observed after transfer of the particles into aqueous media. The increase can be explained by the presence of an additional surfactant shell, compared to the particles in non-aqueous emulsion, as well as possibly the merging processes of the particles. Large aggregates of particles could be excluded, since the DLS results always showed only one monomodal peak. Indeed, SEM micrographs (Figure 4.2.1 c-d) corroborate that the nanoparticles do not substantially aggregate in aqueous media. Aggregations observed in the SEM micrographs may be explained by the drying process during sample preparation. Nevertheless, the perfectly spherical shape of some particles vanished (Figure 4.2.1 c). This was presumably caused by merging of the particles after surfactant-stabilization in water, which led to a slightly broader particle diameter distribution (Table 4.2.1, Sample 3a, 4a, 4b).

As described in the experimental part (Supporting Information) the PLLA-*b*-peptide-*b*-PLLA nanoparticles were labeled by adding a strongly fluorescent PMI dye to the monomer solution before the polymerization (Figure 4.2.2, right). This dye is chemically inert towards the polymerization, possesses outstanding photochemical as well as thermal stability and is selectively soluble in the dispersed phase.[112-113] This should

lead to an encapsulation of the dye after polymerization of L-lactide in non-aqueous emulsion.

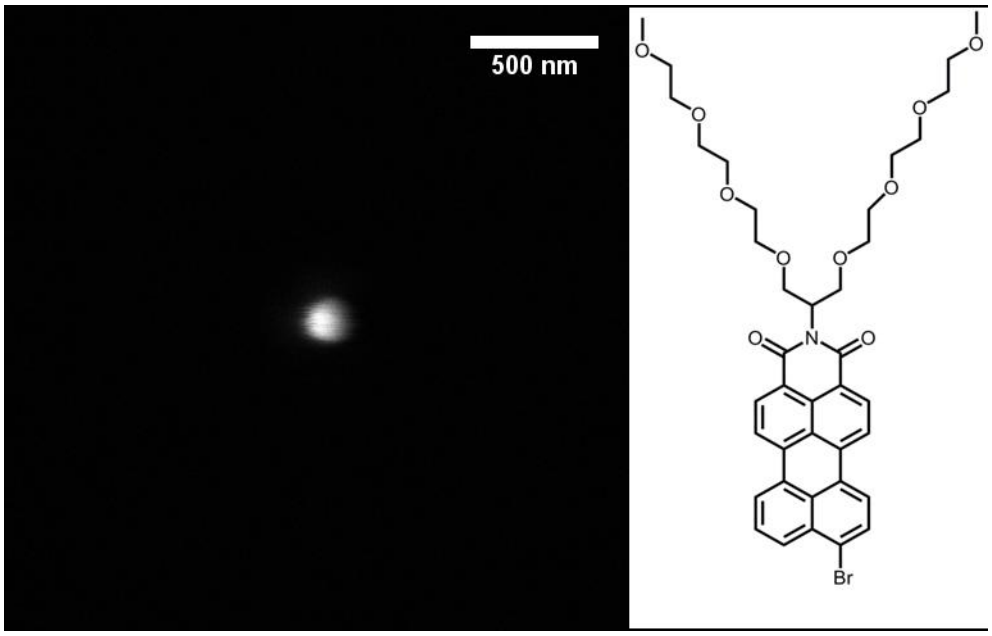

Figure 4.2.2. TPEF image of a single nanoparticle (left); chemical structure of the encapsulated PMI dye (right).

Two-photon fluorescence (TPEF) images of dried nanoparticle samples were recorded at several positions in the sample resulting in an average diameter of 166 nm, which is essentially the diffraction-limited resolution of the imaging system based on the NA of the objective (1.49) and an emission wavelength of 545 nm (Figure 4.2.2, left). The results from DLS showing a narrow monomodal peak between 100 nm and 130 nm combined with the size from TPEF images confirms that particles are well dispersed in solution.

In order to determine the encapsulation efficiency of the particles, the dye concentration was determined through HPLC analysis. Encapsulation efficiencies up to 99% were obtained (Table 4.2.1). This was confirmed by

UV/Vis-spectroscopy measurements of methanol solutions, wherein the precipitation occurred. Such high degrees of loading, taken together with the ideal size of roughly 100 nm, demonstrate the suitability of these PLLA-*b*-peptide-*b*-PLLA nanoparticles as cargo delivery vehicles.

To assess the applicability of these particles as drug delivery vehicles, their uptake in HeLa cells following a 12-hour incubation period was investigated. A combination of TPEF with coherent anti-Stokes Raman scattering (CARS) microscopy was employed.[114] CARS is label-free, multiphoton microscopy technique that derives contrast from the inherent chemistry of the sample. Two photons of different energies, a pump photon (ω_{pump}) and Stokes photon (ω_{Stokes}) excite a vibrationally resonant mode in a sample, and a third (probe) photon (ω_{probe}) is inelastically scattered off this excitation at the CARS wavelength. The CARS wavelength is blue-shifted relative to all lasers ($\omega_{CARS} = \omega_{probe} - \omega_{Stokes} + \omega_{probe}$), which facilitates signal detection. CARS has been used use for three dimensional imaging of polymer blends[115] and cellular imaging in numerous studies.[116-118] Because CARS is a non-linear microscopy technique, it has XY resolution similar to multiphoton fluorescence in lateral plane (~200 nm with appropriately nigh NA objectives) and provides inherent axial sectioning.

CARS was used to provide three-dimensional visualization of the cells based on the local concentration of carbon-hydrogen (CH) vibrations (vibrational energy = 2845 cm^{-1}), which are abundant in lipids and organelle membranes. This corresponds to laser wavelengths of 817 nm for the pump (and probe) and 1064 nm for the Stokes. TPEF, primarily from the 817 nm excitation, was simultaneously used to image the particles, also three dimensionally, within the cells. The combination of CARS with multi-

photon effects has previously been successfully employed for the localization of nanoparticles of different composition in living cells.[119-120]

Controll-experiments showed that HeLa cells solely provided a relatively minimal auto-fluorescence compared to nanoparticles, allowing us to selectively image the particles with TPEF in cells.

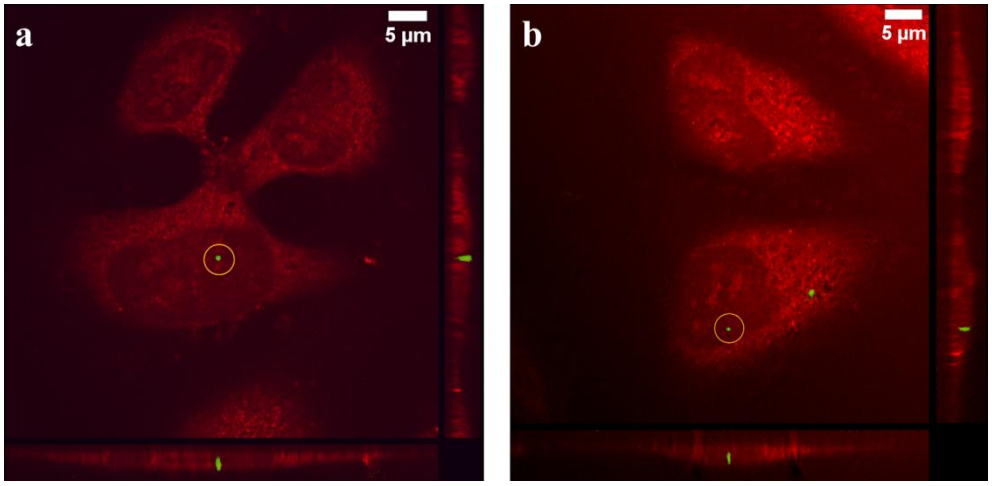

Figure 4.2.3. (a) and (b): Lateral and axial projections of overlayed CARS (red) and TPEF (green) of HeLa cells incubated for 12h with PLLA-*b*-peptide-*b*-PLLA nanoparticle-containing medium. Axial projections (right and below each lateral image) show the YZ and XZ localization of nanoparticle (circled in yellow) within the depth of the cell. In both cases, the fluorescent response of the particles is entirely found within the cell boundaries, demonstrating successful internalization. These projections were reconstructed from a three-dimensional stack with dimensions of 72 x72 μm^2 and slice spacing of 210 nm.

The intensity of the CARS response is presented in red, outlining the cellular components (Figure 4.2.3). The fluorescent response of nanoparticles (green) is visible in the XY projection of panels **a** and **b**, respectively. Axial projections of the particles (circled in yellow) are also presented to the right and below each XY image. Comparison of the three-dimensional localization of the particles relative to the three dimensional cellular outline from CARS allows for direct determination of cellular

uptake versus particle adhesion to the cell surface. As shown in the YZ and XZ projections, the circled particles are entirely contained within the boundaries of the cells. Combined with the XY images, this demonstrates complete internalization of the PLLA-*b*-peptide-*b*-PLLA nanoparticles into HeLa cells within 12 hours.

In the investigated cells ~ 50% of the nanoparticles were completely internalized by the cells. In the remaining cases a determination, whether the internalization was complete or the particles were adsorbed to the cell surface was not possible due to the limited axial resolution of the applied technique. In all uptake experiments performed, the fluorescent features found in cells had lateral dimension between 300 and 500 nm, with an axial dimension of ~ 1 µm, which is larger than the size of a single particle (~ 100 nm). This suggests that either cells could be packaging particles into aggregates during internalization or that particles aggregated in the cell culture medium.

Details of cellular uptake via real-time monitoring will be explored. The challenges like size-preservation after transfer of the particles into aqueous medium, observation of complete cell-internalization and in particular incorporation of peptide into polymer chains of polylactide nanoparticles were solved. The presented method should even be suitable for incorporation of a variety of bioactive peptides. Selectively cleavable peptides, as one example, may act a predetermined breaking point. Its site-selective cleavage should lead to the generation of additional diffusion pathways for the encapsulated species out of the carrier concurrent with an accelerated degradation of the biodegradable polylactide itself. In this way possible obstacles such as poor drug-release, especially for these high encapsulation efficiencies, may be circumvented.

Conclusion

It was demonstrated that bifunctional peptides are able to initiate the ROP of lactide, catalyzed by SIMes, in solution and in non-aqueous emulsion. The polymerization of lactide led to bioinspired PLLA-*b*-peptide-*b*-PLLA triblock structures with number averaged molecular weights up to 11000 $g \cdot mol^{-1}$ and PDIs as low as 1.13. The formation of well-defined spherical PLLA-*b*-peptide-*b*-PLLA nanoparticles was readily achieved in non-aqueous emulsions in one step at ambient temperatures. The generated particles possessed an average diameter of roughly 80 nm and an encapsulation efficiency of up to 99% for a PMI dye. These labeled particles were transferred into aqueous media without aggregation, resulting in particle sizes of approximately 100 nm. In order to assess the efficacy of these hydrophilized nanoparticles as cargo carrier system, their uptake in HeLa cells was investigated. Selective imaging of the PLLA-*b*-peptide-*b*-PLLA particles was possible by a combination of CARS spectroscopy and fluorescence microscopy and proved complete internalization of the loaded nanoparticles. The formation of biodegradable PLLA-*b*-peptide-*b*-PLLA copolymer in a moisture sensitive reaction, the high encapsulation efficiency of the generated particles, their ideal size after transfer into aqueous medium and the successful cell uptake imply these particles are promising drug delivery vehicles.

4.3 Polylactide-*block*-Polypeptide-*block*-Polylactide Copolymer Nanoparticles with Tunable Cleavage and Controlled Drug Release

Authors:

Robert Dorresteijn, Nils Billecke, Mischa Schwendy, Sabine Pütz, Mischa Bonn, Sapun H. Parekh, Markus Klapper, Klaus Müllen

ToC:

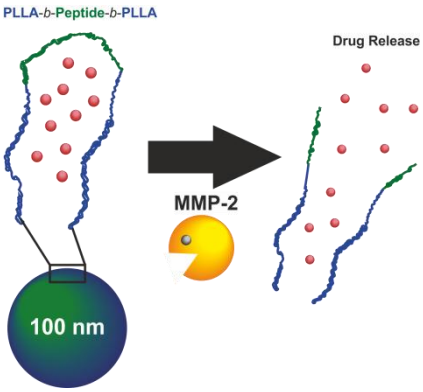

Cover Page:

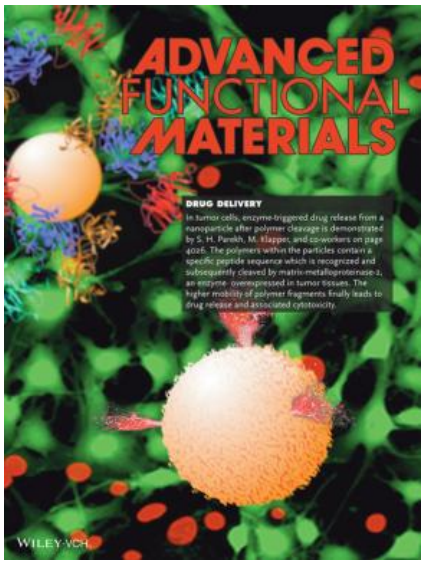

Published in:

Advanced Functional Materials

Abstract

We present a versatile nanoparticle system in which drug release is triggered by enzymatic polymer cleavage, resulting in physicochemical change of the carrier. The polylactide-*block*-peptide-*block*-polylactide triblock copolymer is generated by initiation of the ring-opening polymerization of L-lactide with a complex bifunctional peptide having an enzymatic recognition and cleavage site (Pro-Leu-Gly-Leu-Ala-Gly). This triblock copolymer is specifically bisected by matrix metalloproteinase-2 (MMP-2), an enzyme overexpressed in tumor tissues. Triblock copolymer nanoparticles formed by nonaqueous emulsion polymerization are readily transferred into aqueous medium without aggregation, even in the presence of blood serum. Cleavage of the triblock copolymer leads to a significant decrease of the glass transition temperature (T_g) from 39 °C to 31 °C, likely mediating cargo-release under physiological conditions. Selective drug targeting is demonstrated by hampered mitosis and increased cell-death resulting from drug-release via MMP-2 specific cleavage of triblock copolymer carrier. On the contrary, nanocarriers having a scrambled (non-recognizable) peptide sequence do not cause enhanced cytotoxicity, demonstrating the enzyme-specific cleavage and subsequent drug release. The unique physicochemical properties, cleavage-dependent cargo release, and tunability of carrier bioactivity by simple peptide exchange highlight the potential of this polymer-nanoparticle concept as platform for custom-designed carrier systems.

Introduction

Nanoparticles have proven to be efficient carriers for chemotherapeutics owing to the enhanced permeability of tumor vasculature, resulting in accumulation of nanocarriers in tumor tissues.[59, 121-122] To ensure efficient and selective drug delivery, drug release from the nanocarrier must occur in

response to the dysfunctional environment of the tumor or associated vasculature. Over the past decade, intensive research has focused on polymer-peptide conjugates and tumor-targeted drug delivery using carriers that are recognized and cleaved by proteinases.[2, 69, 99-102, 123-131] Matrix metalloproteinases (MMPs), such as MMP-2, are overexpressed at the invasive front of solid tumors relative to normal tissue and are relatively easy to access by passive accumulation in tissue. By contrast, carriers having reducible or pH-sensitive linkages require transport through cell membranes or diffusion to acidic environments, what might be hard to accomplish.[69, 99-102, 132] In comparison to target molecules such as antigens that are overexpressed only in a subset of tumors, MMPs are overexpressed in a variety of tumors, making them a more attractive target for broad-spectrum diagnostic applications.[69, 132]

MMP-2 overexpression can be exploited for selective targeting by using carrier systems which contain peptide sequences that are recognized and enzymatically cleaved by the enzyme.[101] Specifically, the selective cleavability of the peptide sequence Pro-Leu-Gly-Leu-Ala-Gly (PLGLAG) recognition site by MMP-2 has been extensively investigated.[69, 100, 124] For example, Jiang et al. linked two oppositely charged cell-penetrating peptides by an MMP-2 selectively cleavable peptide, in which a payload was attached to the polycationic peptide.[69] Experiments with scrambled peptides as well as experiments where MMP-2 was knocked out demonstrated the selectivity of the PLGLAG sequence toward MMP-2 recognition and cleavage.[69, 124] Subsequently, Harris et al. used a similar MMP-2 recognizable peptide as a linker between a hydrophilic polymer and a magnetofluorescent nanoparticle.[101] In their system, the cell-internalizing domain of the nanoparticle was veiled by the hydrophilic polymer. MMP-2-induced cleavage of the linker caused detachment of the hydrophilic block resulting in selective accumulation of the hydrophobic vehicle in tumor

tissues.[101] More recently, this concept was used by Matsumura et al. who similarly linked poly(ethylene glycol) (PEG) to a ferritin nanoparticle via a cleavable peptide (PLGLAG), which carried covalently attached doxorubicin.[107]

Despite the advances toward tumor-targeted carrier systems, challenges remain regarding selective and efficient drug release. Besides functionality, carrier size is a key issue in efficient drug delivery: a diameter of 100 nm for delivery systems is ideal, being sufficiently small to prevent both recognition by Kupffer cells and drainage into blood capillaries, which is correlated with potential toxicity.[104-106] For delivery systems, which selectively accumulate in tumor tissue after peptide cleavage, aggregation occurs as a consequence of polarity reversal from hydrophilic to hydrophobic.[107] As a result, the carrier size increases[107], and the carriers can potentially be cleared from the blood stream by Kupffer cells. More importantly, drug release will also be affected by carrier aggregation and resulting local chemical changes, thereby limiting the effectiveness of the strategy. An alternative approach for nanoscale drug delivery is micellar carriers. Micellar carriers are typically less than 40 nm in diameter, which is significantly below the optimal diameter of 100 nm. This small size promotes toxic mechanisms such as redox cycling, and formation of free radicals as well as the aforementioned drainage into blood capillaries.[104-106]

We recently introduced the moisture-sensitive formation of water-stable polylactide-polypeptide triblock copolymers in nonaqueous emulsion (NAE), resulting in poly(L-lactide)-*block*-peptide-*block*-poly(L-lactide) (PLLA-*b*-peptide-*b*-PLLA) triblock copolymer nanoparticles. These particles were readily transferred into an aqueous medium after nonaqueous

formation and showed excellent retention of the original 100 nm particle size.[133]

In the current study, we demonstrate the potential of the NAE technique for the generation of carrier systems having defined bioresponsivity by variation of peptide initiator in the ring-opening polymerization (ROP) of lactide. In this way, a bioactive, cleavable peptide is introduced into this system to act as a pre-determined breaking point for triblock copolymer nanocarriers. As the peptide is centered between two PLLA chains, enzymatic cleavage of the triblock copolymer results in bisection of the molecular weight and coincidental reduction of the glass transition temperature (T_g). This physicochemical change of the polymer promotes increased chain mobility, providing a potential pathway for enzyme cleavage-dependent cargo release, without substantially altering particle morphology. Therefore, obstacles concerning encapsulated drug release and the aforementioned aggregation phenomena are not expected here since these nanocarriers remain hydrophilic even after enzyme-triggered cleavage of peptide.

We show MMP-2 cleavage-dependent cargo release and subsequent cellular toxicity, confirming the specificity and utility of these triblock copolymer NAE nanocarriers as potential drug delivery vehicles. The nonaqueous and mild conditions for their preparation permit the usage of temperature- and moisture-sensitive substances, which may not be used in carrier systems originating from aqueous medium such as micellar systems[58, 95, 97, 134]. This preparation method therefore substantially broadens the portfolio of permissible compounds for polymerization as well as encapsulation into drug carrier systems.

Results and Discussion

PLLA-block-Peptide-block-PLLA Copolymers Synthesis and Enzymatic Cleavage

To benefit from physicochemical change of polylactide regarding enhanced cargo release after polymer cleavage, the peptide must be located near the center of a polylactide chain. Hence, a peptide Ac-Ser-Gly-Phe-Gly-Pro-Leu-Gly-Leu-Ala-Gly-Gly-Phe-Gly-Ser-NH_2 (Ac-SGFG-PLGLAG-GFGS-NH_2) was designed, where the two terminal serine units initiate the lactide polymerization, catalyzed by a well-established *N*-heterocyclic carbene[91, 108], and lead to formation of PLLA-*b*-(Ac)SGFG-PLGLAG-GFGS-NH_2-*b*-PLLA copolymer, carrying a PLGLAG sequence in the center which is cleavable by MMP-2 (Scheme 4.3.1). Gly and Phe units next to serine constitute spacer groups and allow facile determination of the molecular weight by end-group analysis via ^{1}H NMR spectroscopy.

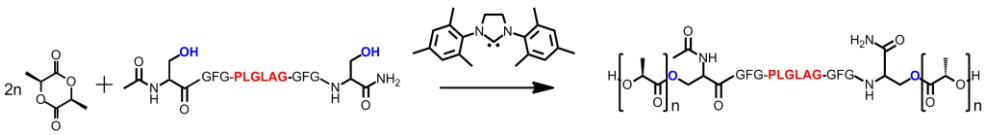

Scheme 4.3.1. Reaction scheme of L-lactide polymerization initiated by bioactive peptide.

In order to distinctively assign cleavage of the triblock copolymer to MMP-2 enzyme activity, a comparison specimen having the exact same amino acids, but with a scrambled sequence (LALGPG instead of PLGLAG), was synthesized (

Table 4.3.1). This peptide was previously shown to not be recognized nor cleaved by MMP-2.[69]

Table 4.3.1. Experimental conditions and results of the preparation of PLLA-b-polypeptide-b-PLLA copolymers in solution and nonaqueous emulsion.

Sample	Sequence	M/Cat/I[a)]	M_n[b] [kDa]	PDI	D_h[c)] (Water) [nm]	D_h[d)] (Serum) [nm]	D_h[e)] (NAE) [nm]	ee[f)] [%]
1[g)]	PLGLAG	17:2:1	2.7	1.17	-	-	-	-
2[h)i)]	PLGLAG	70:2:1	10.0	1.19	98 ± 23	-	92±18	99
3[h)j)]	PLGLAG	70:2:1	8.0	1.07	112±23	176±11	69 ± 3	68
4[g)]	LALGPG	17:2:1	4.7	1.10	-	-	-	-
5[h)i)]	LALGPG	70:2:1	8.0	1.18	107 ± 6	-	106±7	81
6[h)j)]	LALGPG	70:2:1	13.8	1.08	103± 4	-	73 ± 5	66

[a)] monomer/catalyst/initiator ratio (n(L-lactide) / n(SIMes) / n(peptide)); [b)] number-averaged molecular weight determined via GPC vs polystyrene standards; [c)] hydrodynamic diameter of particles in aqueous dispersion determined via DLS; [d)] hydrodynamic diameter of particles in 20 vol-% blood serum determined via DLS; [e)] hydrodynamic diameter of particles in nonaqueous emulsion determined via DLS; [f)] encapsulation efficiency determined via HPLC; [g)] solution polymerization; [h)] nonaqueous emulsion polymerization; [i)] loaded with PMI dye; [j)] loaded with 5-fluorouracil.

PLLA-*b*-(Ac)SGFG-PLGLAG-GFGS(NH_2)-*b*-PLLA copolymers originating from solution polymerization (Sample 1,

Table 4.3.1) were exposed to MMP-2 for certain periods of time (0.5h, 2h, 4h, 4d) and subsequently analyzed by MALDI-ToF MS in order to

determine the cleavability of the polymer-peptide conjugate. The recognition site (PLGLAG) is known to be cleaved between glycine and leucine.[69, 107] Hence, cleavage of peptide should lead to both PLLA-*b*-(Ac)SGFG-PLG-OH and LAG-GFGS(NH_2)-*b*-PLLA copolymers, obviously having different end groups. MALDI-ToF MS measurements of the polymer after exposure to MMP-2 showed cleavage of PLLA-*b*-(Ac)SGFG-PLGLAG-GFGS(NH_2)-*b*-PLLA copolymer. The predicted polymer degradation by MMP-2 was verified by: 1) the decreasing signal-to-noise ratio of the triblock copolymer distribution with MMP-2 incubation time (Figure 4.3.1, top) and 2) detection of both PLLA-*b*-(Ac)SGFG-PLG-OH and LAG-GFGS(NH_2)-*b*-PLLA with various repeating units (Figure 4.3.2, top). To assure the assignment of observed signals to "broken" polymers, we compared the obtained signals after degradation with those of the polymer before enzyme incubation (Figure 4.3.1 and Figure 4.3.2, green).

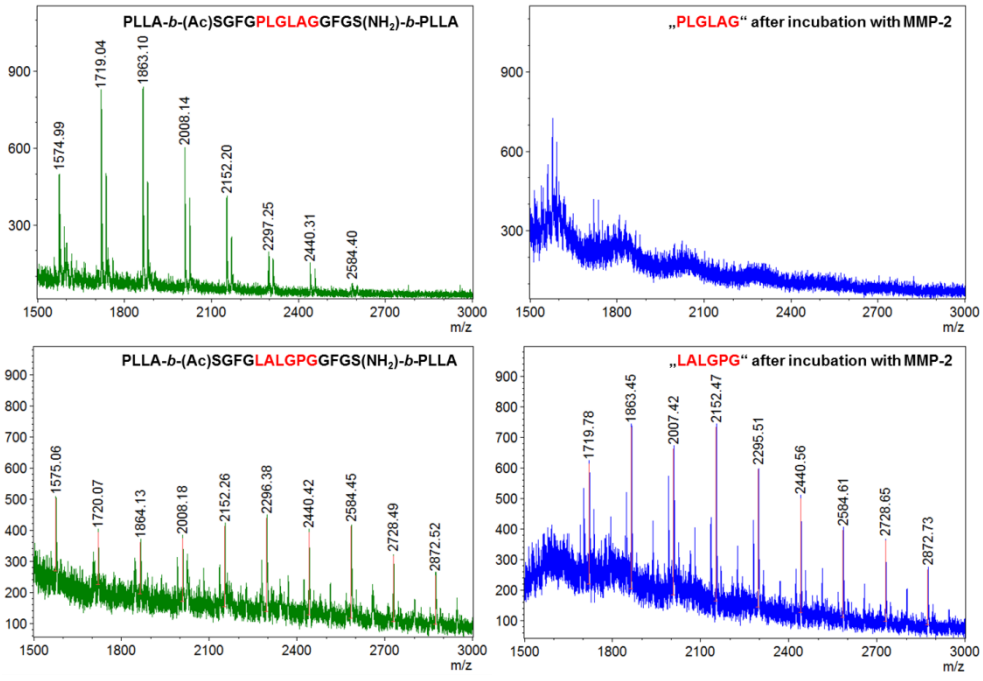

Figure 4.3.1. MALDI ToF MS spectra: PLLA-b-(Ac)SGFG-PLGLAG-GFGS(NH_2)-b-PLLA copolymer sample before (top, green) and after 4 days of incubation with MMP-2 (top, blue); PLLA-b-(Ac)SGFG-LALGPG-GFGS(NH_2)-b-PLLA copolymer sample before (bottom, green) and after 4 days of incubation with MMP-2 (bottom, blue).

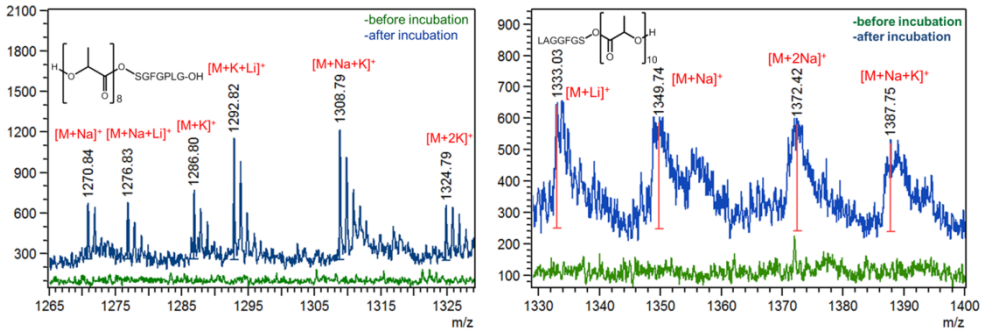

Figure 4.3.2. Exemplary PLLA-b-(Ac)SGFG-PLG-OH (left) and LAG-GGFGS(NH_2)-b-PLLA copolymer fragments (right) before (green) and after 4 days of incubation with MMP-2 (blue).

In contrast to these observations, the matrix-assisted laser desorption/ionization-time-of-flight (MALDI-ToF MS) spectrum of the polymer bearing a scrambled peptide sequence (LALGPG, Sample 4, Table 1) looked identical before and after 4 days of exposure to MMP-2 (Figure 4.3.1, bottom). Furthermore, no cleavage products for this scrambled sequence were detected. This clearly demonstrates the enzymatic cleavability of the polymer with the PLGLAG linker peptide.

The observation of the expected copolymer fragments after degradation in MALDI-ToF MS corroborates the presumed hypothesis of peptide incorporation between two PLLA chains. This result is further supported by diffusion ordered NMR spectroscopy (DOSY) measurements showing covalent attachment of peptide and the narrow polydispersity (PDI), strongly suggesting that initiation occurred by initiating groups having equal nucleophilicity.

Loaded PLLA-block-Peptide-block-PLLA Nanoparticles in Nonaqueous Emulsion

To impart bioactivity of the polymer for selective drug release from a nanocarrier, we created nanoparticles in nonaqueous emulsion (NAE), wherein acetonitrile was dispersed in cyclohexane and stabilized by a poly(isoprene)-*block*-poly(ethylene oxide) (PI-b-PEO) copolymer (DP_{PI} = 441, DP_{PEO} = 357). L-lactide was polymerized in the presence of a cargo molecule (dye or chemotherapeutic agent, Table 1) with either Ac-SGFG-PLGLAG-GFGS-NH_2 or Ac-SGFG-LALGPG-GFGS-NH_2 as initiator resulting in nanoparticles bearing triblock copolymers (Figure 4.3.2).

The particles were transferred from the nonaqueous into an aqueous phase and were stabilized with a PEG based surfactant (Lutensol AP20) in order to investigate bioactivity of these nanocarriers. According to dynamic light scattering (DLS) measurements, the particles had an approximate diameter of 100 nm (Table 1), which was similar to that inferred from scanning electron microscopy (SEM) micrographs (Figure 4.3.3). A monomodal distribution in the DLS measurements provided evidence of well-dispersed, non-aggregated nanocarriers in the aqueous solution. Even in 20-vol% blood serum only a single monomodal peak was observed demonstrating that, on average, no aggregation occurs under physiological conditions. The cargo encapsulation efficiencies (Table 1) exhibited values as high as 99%, as determined by high-performance liquid chromatography (HPLC), demonstrating the high loading capacity of this carrier system.

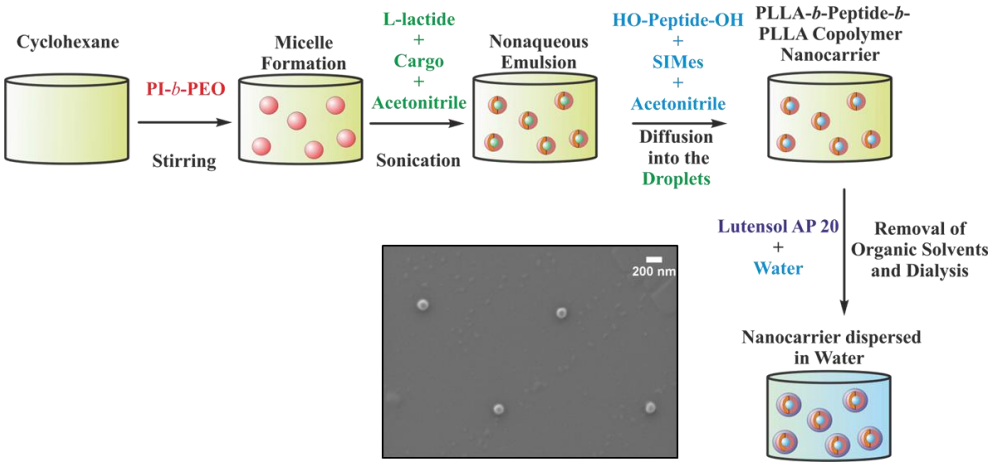

Figure 4.3.3. Scheme for preparation of nanoparticles bearing the triblock structure and a typical SEM image of the nanoparticles.

Cleavage and Release Studies of Loaded Nanoparticles

Dye-Loaded Nanoparticles

To test for enzymatic specific cleavage of the nanocarrier system and subsequent cargo release, dye-loaded nanoparticles were incubated with MMP-2 for 4 days. After incubation, particle suspensions were centrifuged to pellet the nanocarriers and isolate the released dye from that still contained in the particles. The dye concentration in the supernatant was determined via fluorometry and compared to control samples not incubated with MMP-2. Significantly higher dye release was observed for nanocarriers having an MMP-2 recognition site in the polymer chain (Figure 4.3.4).

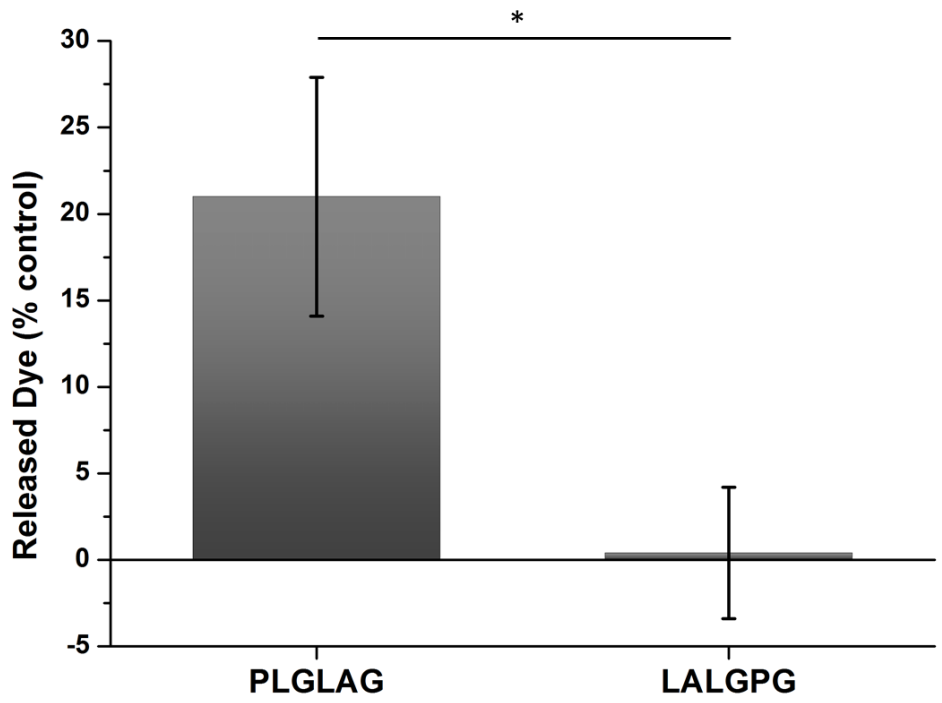

Figure 4.3.4. Dye release from nanocarriers bearing either the cleavable sequence (PLGLAG) or the scrambled sequence (LALGPG) in the polymer chain after 4 day incubation time. Each measurement is presented as % released relative to control specimens not incubated with MMP-2. Error bars are standard deviation from three experiments and * marks statistically significant differences between samples with $P < 0.05$.

This experiment demonstrates that nanocarriers having the MMP-2 recognition sequence (PLGLAG) in the polymer chain undergo selective cargo release owing to the bioactive polymer constitution of the nanoparticle.

In addition to the fluorometry dye release study, the MMP-2 degraded polymer nanoparticles (containing PLGLAG, sample 3) were further analyzed using gel permeation chromatography (GPC), differential scanning calorimetry (DSC) and DLS. GPC results confirmed that bisection of the original triblock copolymer was accomplished with polymer nanoparticles (Figure 7.2.1). DSC measurements of triblock copolymers showed a clear decrease in the glass transition temperature (T_g) from 39 °C before degradation to 31 °C after degradation (Figure 4.3.5 a). This decrease is

expected based on the severing of longer triblock chains into shorter fragments. DLS measurements revealed a slight increase in particle size (~ 10%) before and after enzymatic cleavage (Figure 4.3.5 b).

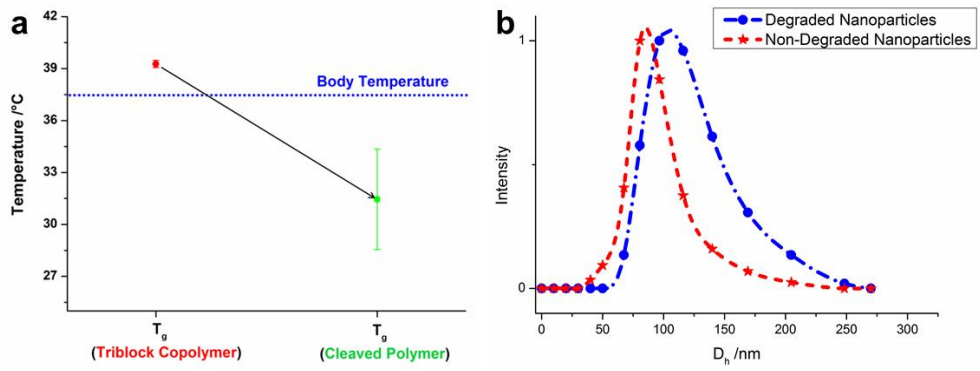

Figure 4.3.5. a) Glass transition temperatures of PLGLAG triblock copolymers before (red) and after peptide cleavage (blue) by MMP-2; b) DLS graph of PLGLAG nanoparticles before (non-degraded) and after (degraded) MMP-2 incubation (sample 3).

The change in T_g is well-suited for promoting enhanced mobility of cleaved chains within a physiological context to enable diffusion of water molecules into the particles and subsequent cargo release by concentration gradient. Taken together with the dye release results, these data demonstrate enzymatic cleavage is robust in our NAE particles and suggest a potential cargo-release mechanism based on enhanced polymer chain mobility due to reduced molecular weight after cleavage.

Drug-Loaded Nanoparticles

Based on selective cargo release, we incubated fluorescent PLGLAG-particles with C2C12 cells expressing MMP-2[135] and noted strong interaction between the cells and particles (**Figure 7.2.2**). To determine the applicability of the triblock nanoparticles for specific drug delivery, we synthesized nanocarriers with 5-fluoruracil (5-FU) as the cargo molecule. 5-

FU is an extensively investigated chemotherapeutic agent that disrupts RNA transcription and is known to prohibit cell proliferation and cause cell death.[136-138] Both PLGLAG and LALGPG nanocarriers containing 5-FU were synthesized and incubated with C2C12 cells in order to examine cytotoxicity (and specificity) as a response to the bioactive domain (**Figure** 4.3.6).

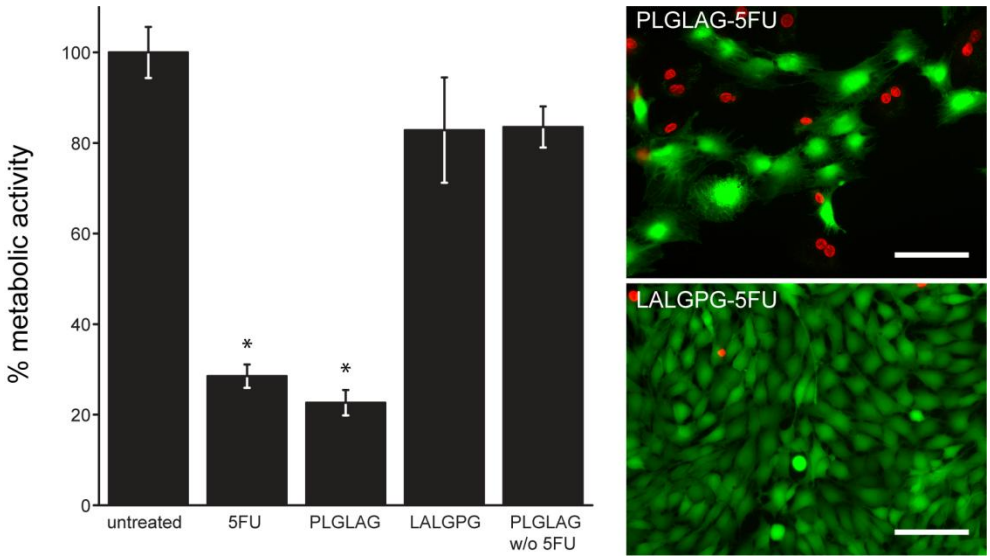

Figure 4.3.6. Cytotoxicity by 5-FU-encaspulated nanocarriers bearing the PLGLAG sequence or the LALGPG sequence. Quantitative analysis reveals cytotoxicity for cleavable particles is comparable to soluble 5-FU (10 μg/mL) whereas LALGPG-5-FU and PLGLAG without 5-FU particles show similarly limited toxicity as untreated cells. Images show more living cells retaining calcein-AM (green) and fewer dead cells containing ethidium homodimer (red) in the LALGPG-5FU particles. Error bars are standard deviation from three experiments, * marks statistically significant differences between samples and untreated with $P < 0.05$.

Figure 4.3.6 shows increased metabolic senescence, decreased cell density, and more pronounced cell death after C2C12 incubation with MMP-2 degradable nanocarriers loaded with 5-FU. The cytotoxic effect of PLGLAG particles was slightly higher than that of free 5-FU (~17%). By comparing this value with the maximum drug content in the particles, calculated from the original sample weight, a high drug release efficiency of greater than 35% within 3 days of incubation was determined. To further

verify where the drug molecules are exactly located within the cell after incubation and degradation, it is conceivable to encapsulate molecules which become fluorescent upon activation by specific cell-associated enzymes, as described in previous works.[129]

Incubation of non-degradable nanocarriers with C2C12 cells showed no enhanced cytotoxicity, even at extended times (**Figure 7.2.3**). This experiment demonstrates selective drug release and associated cytotoxicity owing to MMP-2 cleavage of non-leaching defined bioactive polymer-peptide conjugates within the PLGLAG nanocarrier.

Conclusion

We have introduced biocompatible, triblock copolymer nanoparticles with enzyme-specific cleavage and tunable functionality. These particles have excellent loading capability that shows targeted drug release in response to MMP-2 enzymatic cleavage. The carrier was generated by ROP of L-lactide with a bioactive, bifunctional peptide initiator in nonaqueous emulsion. The nanoparticles were readily transferred into aqueous medium with 100 nm size retention. The peptide between two PLLA chains acted a predetermined breaking point for the triblock copolymer nanocarriers, which after cleavage by MMP-2 created hydrophilic end groups on each PLLA fragment. The reduced molecular weight of the polymer as well as the end group addition cooperate to reduce the T_g compared to the non-degraded polymer. Under physiological conditions (37 °C), decrease of T_g (to 31 °C) results in higher mobility of the constituent polymers in the particle, which is likely responsible for triggered diffusion of the cargo out of the carrier. This triggered physicochemical change of polymer is most likely imparted to other polyester or even polyurethane systems by using the bifunctional peptide as initiator or comonomer within this facile method.

Selective cleavage and drug release resulting in cell-death and hampered mitosis was demonstrated by comparing cellular effects using nanocarriers having a scrambled peptide sequence as a linker. Hence, drug release is selectively imparted by polymer cleavage of the carrier with an enzyme overexpressed in tumor tissues, showing that drug release can be tuned with polymer constitution alone. Changing the linking peptide permits custom-designed bioresponsivity, making this a highly promising platform for targeted drug delivery. The current study demonstrates the versatility of our NAE/peptide-initiated polymerization method to construct stable, well-loaded, and selectively-cleavable nanoparticles.

Experimental Section

General Remarks

All solvents and reagents were purchased from Sigma Aldrich if not stated otherwise. The poly(isoprene)-*block*-poly(ethylene oxide) (PI-*b*-PEO) copolymer was prepared using a sequential anionic polymerization technique.[82] L-lactide and 1,3-bis(2,4,6-trimethylphenyl)-2-ididazolidinylidene (SIMes) were used as received. SIMes was stored under inert atmosphere at -20 °C. Lutensol AP 20 was obtained from BASF SE in Ludwigshafen. Peptides (Ac-SGFG-PLGLAG-GFGS-NH_2 and Ac-SGFG-LALGPG-GFGS-NH_2) were obtained from Genosphere Biotechnologies in Paris. 9-bromo-*N*-(2,5,8,11,15,18,21,24-octaoxapentacosan-13-yl)perylene-3,4-dicarboxy monoimide (PMI) was prepared according to the literature.[133] To determine the molecular weight and the molecular weight distribution (MWD) of the polylactide-peptide conjugate a gel permeation chromatography (GPC) was carried out at 30 °C using MZ-Gel SDplus 10E6, 10E4 and 500 columns in tetrahydrofuran (THF) as eluent vs.

polystyrene standards. The detector was an ERC RI-101 differential refractometer. The composition of the block copolymers was determined by ^{1}HNMR spectroscopy in deuterated dichloromethane (DCM-d2) via peak analysis, using a Bruker Avance III spectrometer operating at 700 MHz. The structure of the polylactide-peptide conjugate was investigated via ^{1}HNMR spectroscopy, diffusion ordered spectroscopy (DOSY) in deuterated dimethylsulfoxide (DMSO-d6) and MALDI-ToF MS. For a ^{1}HNMR spectrum 128 transients were used with an 13.8 µs long 90° pulse and a 12600 Hz spectral width together with a recycling delay of 5 s. The temperature was kept at 298.3 K and regulated by a standard ^{1}H methanol NMR sample using the Topspin 3.1 software (Bruker). The DOSY experiments were done with a 5 mm BBI ^{1}H/X z-gradient probe and a gradient strength of 5.516 [G/mm] on the 700 MHz spectrometer. In this work, the gradient strength was 32 steps from 2 % to 100 %. The diffusion time d20 was optimized to 80 ms and the gradient length p30 was kept at 1.4 ms. For MALDI-ToF MS measurements the polymer was dissolved in THF and analyzed with alpha-cyano-4-hydroxycinnamic acid as matrix. Scanning electron microscopy (SEM) images were taken using a Zeiss Gemini 912 microscope. The SEM sample preparation proceeded the following way: the nanoparticles were dispersed in cyclohexane and drop casted on a silica wafer. The average diameters of the particles visualized in SEM images were determined by diameter measurements of 100 randomly chosen particles. Dynamic light scattering (DLS) was used to determine the mean size of generated polylactide-peptide nanoparticles (number distribution). The DLS measurements were performed on a Malvern Zetasizer 3000 with a fixed scattering angle of 90° and on an ALV/LSE-5004-correlator using a He/Ne-laser operating at 632.8 nm. The glass transition temperature (T_g) of polymers was determined by peak analysis of differential scanning calorimetry (DSC) graphs using a DSC822e differential scanning calorimeter. The initial temperature of -100°C was raised to +180°C with a heating rate of 10 K/min.

Typical preparation of poly(L-lactide)-b-polypeptide-b-poly(L-lactide) copolymer

L-lactide (37.5 mg, 0.26 mmol), SIMes (9.36 mg, 30.6 µmol) and the peptide (9.30 mg, 7.36 µmol) were dissolved in acetonitrile (0.203 g, 4.94 mmol) and stirred for 15 min at room temperature. After removal of the solvent *in vacuo*, the triblock copolymer was analyzed with ^{1}H NMR spectroscopy, DOSY, GPC and MALDI-ToF MS.

Typical preparation of poly(L-lactide)-b-polypeptide-b-poly(L-lactide) nanoparticles loaded with either dye or chemotherapeutic agent

PI-*b*-PEO copolymer (0.050 g) was magnetically stirred in cyclohexane (14.4 g, 171 mmol) at room temperature. L-lactide (76.0 mg, 0.53 mmol) and PMI (0.30 mg, 0.39 µmol) or 5-fluorouracil (5-FU) (2.6 mg, 0.02 mmol), respectively, were dissolved in acetonitrile (0.230 g, 5.59 mmol). The emulsion was formed by dropwise addition of the monomer/cargo solution to the cyclohexane/PI-*b*-PEO dispersion and subsequent treatment with sonication for 15 min using a Bandelin Sonorex RK255H ultrasonic bath operating at 640 W. SIMes (9.36 mg, 30.6 µmol) and the peptide (9.30 mg, 7.36 µmol) were dissolved in acetonitrile (0.176 g, 4.29 mmol) and added dropwise to the emulsion under inert atmosphere. The emulsion was stirred for 15 min at room temperature to produce poly(L-lactide)-*block*-peptide-*block*-poly(L-lactide) (PLLA-*b*-peptide-*b*-PLLA) nanoparticles. A sample was taken out of the emulsion in order to analyze the particle size and morphology via DLS and SEM. 5 ml of the emulsion were precipitated in methanol, separated by centrifugation and dried *in vacuo.* The polymer was investigated via NMR spectroscopy and via GPC. Furthermore, this solid was dissolved in dioxane

and investigated by HPLC analysis in order to determine the encapsulation efficiency.

The remaining emulsion was mixed with a 20 mL of a 0.05 wt-% Lutensol AP 20 solution in order to disperse the obtained particles in aqueous medium. The organic solvents were evaporated and the aqueous dispersion was dialyzed against deionized water for 5 days in order to remove unreacted components and organic solvents. Two samples were taken out of the dispersion: one sample was diluted with water and investigated via DLS and SEM to study the morphology. The other sample was dried *in vacuo* and the resulting solid was analyzed via GPC and NMR spectroscopy. The remaining aqueous dispersion was used for cargo release and cell toxicity studies.

Cleavage Study of the Polymer

PLLA-*b*-peptide-*b*-PLLA copolymer (0.5 mg) was dissolved in 1 mL buffer (100 mM Tris, 10 mM calcium chloride, and 150 mM sodium chloride, pH 8.0). The buffer solution was agitated at 37 °C under 300 revolutions per minute. From a stock solution of MMP-2 (100 µg/mL), 25 µL were incubated with DMSO-solution of APMA (*p*-aminophenylmercuric acetate, 1 mM of APMA) over 2 h at 37 °C under 300 revolutions per minute agitation. After activation, MMP-2 was added to the buffer solution. After certain periods of time (0.5 h, 2 h, 4 h, 4 d) 5 µL of the buffer solution was collected and mixed with 15 µL of CHCA solution (THF) for analysis via MALDI-ToF MS.

Cleavage Study of Particle Dispersions

250 µL of PMI-loaded particle dispersion was mixed with 250 µL of buffer solution (100 mM Tris, 10 mM calcium chloride, and 150 mM sodium chloride, pH 8.0). From a stock solution of MMP-2 (100 µg/mL in 100 mM Tris, 10 mM calcium chloride, 150 mM sodium chloride, pH 8.0), 15.6 µL was activated with 1mM APMA for 2 h at 37 °C under 300 revolutions per minute agitation. After activation, MMP-2 was added to the particle dispersions in a ratio of 150 µL particles: 250 ng of activated MMP-2. This reaction was incubated in a 300 µL total volume of TCNB buffer (50 mM Tris, 10 mM calcium chloride, 150 mM sodium chloride, pH 7.5) for 4 days at 37 °C under 300 revolutions per minute agitation. Following this incubation, the reaction was centrifuged at 13.4 rpm for 20 min. 200 µL of the supernatant was analyzed via fluorescence spectroscopy in order to determine the concentration of released dye during incubation. Control reactions in which no MMP-2 was used were run in parallel and analyzed in the same way.

Encapsulation Efficiency through High-Pressure-Liquid-Chromatography (HPLC)

The HPLC analysis was carried out with a reversed phase HD C8 column (Macherey-Nagel) using a series 1100 pump (Hewlett Packard). The components, containing in the particles, were detected by a UV-Vis detector S-3702 (Soma). The encapsulation efficiency was calculated by determination of the concentration of either PMI or 5-FU in the solid and its comparison to the applied amount of encapsulated species before the polymerization.

Cellular Interaction Imaging

The interaction of nanoparticles with living cells was done with immortalized C2C12 myogenic cells cultured in chamber slides having coverglass (Thermo Scientific™ Nunc Lab-Tek) bottoms. Cells were allowed to attach to the glass surface and grown to near confluence in growth medium (DMEM low glucose, Gibco) supplemented with 10% fetal bovine serum (Gibco). Directly before imaging, cells were washed 3 times with PBS and PLGLAG particles loaded with the fluorescent dye (9-bromo-N-(2,5,8,11,15,18,21,24-octaoxapentacosan-13-yl)perylene-3,4-dicarboxy monoimide, PMI) suspended in growth medium were added. The chambered coverglass was then transferred to a stage-top incubation chamber (Ibidi) mounted on a Leica SP 5 II TCS CARS (Leica Microsystems GmbH) microscope equipped with transmitted and reflected light photomultiplier tubes (PMT). The interior of the incubation chamber was maintained at 37°C and gassed with ambient air with 5% CO_2. Nanoparticles were detected using laser-based, multiphoton fluorescence in the reflected (epi) PMT while the transmitted PMT was used for forward, label-free coherent anti-Stokes Raman scattering (CARS) microscopy. Briefly, CARS is a multi-photon coherent Raman microscopy that derives contrast from the chemistry of the sample itself without any labels. Using this imaging system, we targeted the CH_2 symmetric vibration in CARS (2845 cm^{-1}) to image the cell borders, intracellular membranes, lipid deposits while imaging the multiphoton fluorescence of PMI in the epi PMT. The excitation source for CARS was two picosecond lasers at 1064 nm and 817 nm (energy difference equal to 2845 cm^{-1}) while multiphoton fluorescence excitation was the 817 nm laser alone (picoEmerald, Angewandte Physik & Eletronik GmbH).

The epi-detection path contained a shortpass filter (750 nm, Chroma Technology) to exclude excitation laser light (and pass PMI two-photon fluorescence) while the forward detection path was equipped with a 750 nm shortpass and additional narrow bandpass filter (660 nm / 8 nm bandwidth, Omega Optical) to exclude any two photon fluorescence signal and pass only the CH_2 symmetric CARS signal. Images were acquired every 5 min for 24 h. All images were acquired with a 60X 1.49 NA TIRF objective(Nikon) and subsequently analyzed with ImageJ. Individual time points are shown below (Fig. S2).

Cytotoxicity with 5-FU

Cytotoxicity analysis of nanoparticles was done using the immortalized myogenic cell line C2C12. This line has been previously shown to express MMP-2 but not the similar MMP-9.[135] Cells were cultured in growth medium supplemented with 10% fetal bovine serum and grown to ~70% confluence in 96-well plates. To determine particle toxicity, cells were incubated with nanoparticle dispersions bearing either PLGLAG or LALGPG sequence with 5-FU loading (final concentrations of ~8 – 35 µg/mL) prepared in fresh growth medium. Negative control experiments were done using standard growth medium, and positive control experiments were done using growth medium supplemented with soluble 5-FU at 10 µg/mL. At indicated times, metabolic activity was quantified with standard 3-[4,5-dimethylthiazol-2-yl]-2,5- diphenyltetrazolium bromide (MTT) assays. Briefly, MTT was added directly to each well to a final concentration of 0.7 mg/mL. Cells were then incubated for 3 h at 37°C. After centrifugation, the supernatant was removed, and the cells were allowed to dry for at least 1h before lysing with 200 µL isopropanol. Formation of formazan crystals was analyzed via the optical density at 560 nm using 670 nm as reference in a spectrophotometer (Tecan). Each

experiment was taken out as quintet of wells and repeated three times. Statistical analysis (one-way ANOVA) was performed with Origin 8.5 for Windows, p-Values ≤ 0.05 were considered statistically significant.

Live/Dead Staining

Cells were grown in growth medium in Lab-Tek® Chamber Slides (Thermo Scientific™ Nunc Lab-Tek) to near-confluence similar to cytotoxicity assays. Cells were then incubated for 3 days with PLGLAG or LALGPG nanoparticles with 5-FU loading at a final concentration between 8- 35 µg/mL in fresh growth medium. Plain growth medium and medium supplemented with 5 FU (10 mg/mL) served as negative and positive controls, respectively. Following incubation, the medium was exchanged with 2 µM calcein-AM and 4 µM ethidium homodimer (Invitrogen) dissolved in PBS at room temperature. After 30 min of incubation, cells were directly imaged in the chamber slides on an IX81 inverted microscope (Olympus). Images were collected using the green (excitation BP472/30, emission BP520/35) and red (excitation BP540/20, emission LP590) channels with a 20X, 0.4 NA objective (Olympus). Images were processed with ImageJ.

4.4 Polarity Reversal of Nanoparticle Surfaces by the Use of UV-Sensitive Polymeric Emulsifiers

Authors:

Robert Dorresteijn, Nils Billecke, Sapun H. Parekh, Markus Klapper, Klaus Müllen

ToC:

Published in:

Journal of Polymer Science Part A: Polymer Chemistry

(Reprinted with permission from (*J. Polym. Sci. A Polym. Chem.*, **2014**, *53*, 200-205.)

Abstract

A polarity reversal of a nanoparticle surface with a light-sensitive PEG-*block*-poly((1-pyrenyl methyl) glutamate) (PEG-*b*-PGlu(Pyr)) copolymer is presented. The copolymer is successfully applied as emulsifier in a nonaqueous emulsion polymerization of lactide. The hydrophobic pyrenyl methylene-units are readily cleaved from the outer hydrophilic PGlu-block by UV irradiation. The initially hydrophobic particles can now be dispersed in aqueous medium without the need of additional surfactants.

Introduction

Organic nanoparticles find use in colorants, as adhesives and as pharmaceuticals.[2, 100, 130, 139-146] Their synthesis is usually conducted in shape giving processes such as the common aqueous emulsion polymerization. However, the applied aqueous conditions limit both the applicable polymerization technique and the permissible compounds (monomer, initiator, catalyst, etc.). Typically, water-stable components are polymerized radically giving polymer nanoparticles with carbon-carbon bonds in the polymer main chain. The recently introduced nonaqueous emulsion polymerization overcame this limitation and substantially broadened the portfolio of applicable compounds and polymerization techniques.[3, 30, 35, 108, 133, 147] For instance, this method was used for the single step synthesis of poly(ester) nanoparticles at room temperature[30, 108], which are of particular interest in biomedical fields owing to their biocompatibility and biodegradability.[64-65]

Despite the versatility of nonaqueous techniques, the resulting particles are dispersed in a nonpolar organic solvent and often must be transferred into aqueous medium for their final utilization.[1-2] This transfer has remained a huge challenge: complex purification and the addition of a second surfactant

layer allow particle transfer, yet causing aggregation which potentially has a negative impact on particle functionality and therefore its usability.[2, 131, 133, 140, 148-149] In particular for nanoparticles that are used as intravascular drug delivery systems, aggregation resulting in carrier sizes >250 nm is a serious issue as those systems are removed from the blood stream by Kupffer cells.[104-106] Therefore, an emulsifier is needed that is capable of stabilizing particles in both nonpolar solvents and aqueous medium without the necessity of additional surfactant layers.

Recently, an amphiphilic PEG-*block*-poly((1-pyrenyl methyl) methacrylate) copolymer was synthesized by atomic-transfer radical-polymerization (ATRP). This polymer contains 1-pyrenyl methylene-units in the side chains that are readily cleaved from a poly(methacrylate) backbone via radical transition state.[150-152] In water, the micelles were proven to be broken upon UV irradiation owing to the removal of the hydrophobic side groups and the resulting hydrophilic nature of the entire polymer.[150] Different from the concept of generating potential light-sensitive "drug containers", we designed an amphiphilic PEG-*block*-poly((1-pyrenyl methyl) glutamate) (PEG-*b*-PGlu(Pyr)) copolymer that can stabilize particles in hydrophobic solvents and in water upon photolysis. Specifically, the hydrophobic pyrenyl methylene-units in the side chains of PGlu are photolytically cleaved, resulting in particles having a fully hydrophilic and biocompatible PEG-*b*-PGlu shell. Hence, this copolymer allows transfer of hydrophobic particles into water without the necessity of adding further surfactant layers.

Results and Discussion

The PEG-*b*-PGlu(Pyr) copolymer was intended to effectively disperse a polar organic solvent in a nonpolar organic solvent. PEG stabilizes the polar dispersed phase (acetonitrile), whereas stabilization of the nonpolar continuous phase (cyclohexane) is attained by the PGlu(Pyr)-block. In order

to achieve maximum emulsifying efficiency, the block copolymer must possess a molecular weight ≥ 30 kg·mol^{-1} and a molar block composition of 2:1 in favor of the block facing the continuous phase.[20-21, 28] Therefore, we synthesized a PEG-*b*-PGlu(Pyr) copolymer having 45 repeating units of ethylene glycol (EG) and 90 repeating units of 1-pyrenyl methyl glutamic acid (Glu(Pyr)), resulting in a total molecular weight of approximately 33 kg·mol^{-1}.

Synthesis

The reaction of γ-benzyl glutamic acid (**1**) and triphosgene under release of hydrogen chloride gave the monomer γ-benzyl glutamic acid *N*-carboxy anhydride (Glu(Bz)-NCA) (**2**) in a 75% yield, which is in accordance with the literature.[153] The backbone of the photosensitive block copolymer was synthesized by a literature-known ring-opening polymerization of **2** with α-methoxy-ω-amino-PEG (PEG-NH_2) as macroinitiator having a degree of polymerization (DP) of ~45 (Scheme 4.4.1).[154-155]

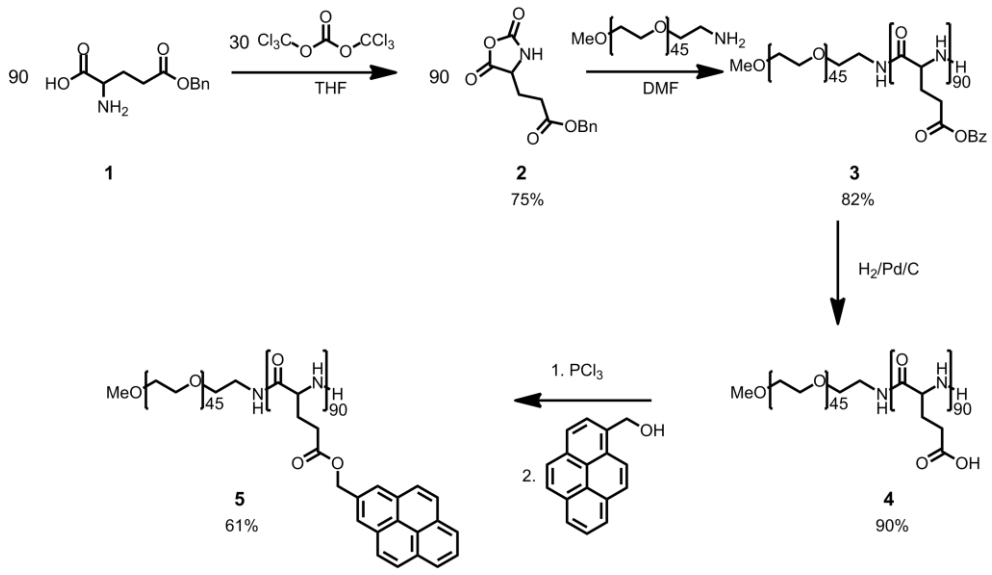

Scheme 4.4.1. Synthetic route toward the PEG-b PGlu(Pyr) copolymer.

The PEG-*b*-PGlu(Bz) copolymer (**3**) was subsequently analyzed via ^{1}H NMR spectroscopy and diffusion ordered spectroscopy (DOSY). The ^{1}H NMR measurement of **3** revealed a molar block composition of 2:1 in favor of the PGlu(Bz)-block (DP_{PEG}=45; $DP_{PGlu(Bz)}$=90). DOSY measurements depicted equal diffusion of both blocks demonstrating covalent attachment of the PEG-block to the PGlu(Bz)-block and the formation of **3**. The copolymer was subsequently reduced with hydrogen on Pd/C in order to cleave the benzyl protecting group. ^{1}H NMR measurement of PEG-*b*-PGlu copolymer (**4**) demonstrated complete reduction (Figure 7.3.1). To esterify **4** with 1-pyrenyl methanol, the PEG-*b*-PGlu copolymer was first converted into the corresponding acid chloride with phosphorous trichloride and then esterified giving the PEG-*b*-PGlu(Pyr) copolymer (**5**). The degree of esterification was 86%, as determined by relative signal intensities of the aromatic pyrenyl protons (δ = 8.6 - 7.6 ppm) and the aliphatic protons of PEG (δ = 3.6 ppm) in the ^{1}H NMR spectrum (Figure 7.3.3). Higher degrees of esterification could not be achieved, even at extended reaction times. As pyrene tends to aggregate in solution, aggregation of the esterified polymer most likely caused an inaccessibility of remaining reaction centers.

Self-assembly in a nonpolar organic solvent

After synthesis of the block copolymer, its self-assembly in a nonpolar organic solvent before and after UV irradiation was investigated to study whether a pyrenyl substituent in the polymer side chain suffices to stabilize a nonpolar solvent and to elucidate the effect of photolysis on the polymer's assembly. The aggregates of PEG-*b*-PGlu(Pyr) copolymers in cyclohexane (c = 2.4 mg·mL^{-1}) were spherical and possessed a smooth surface (Figure 4.4.1 a, b). They were monomodal and had hydrodynamic diameters (D_h) of 99 ± 38 nm, as determined via DLS.

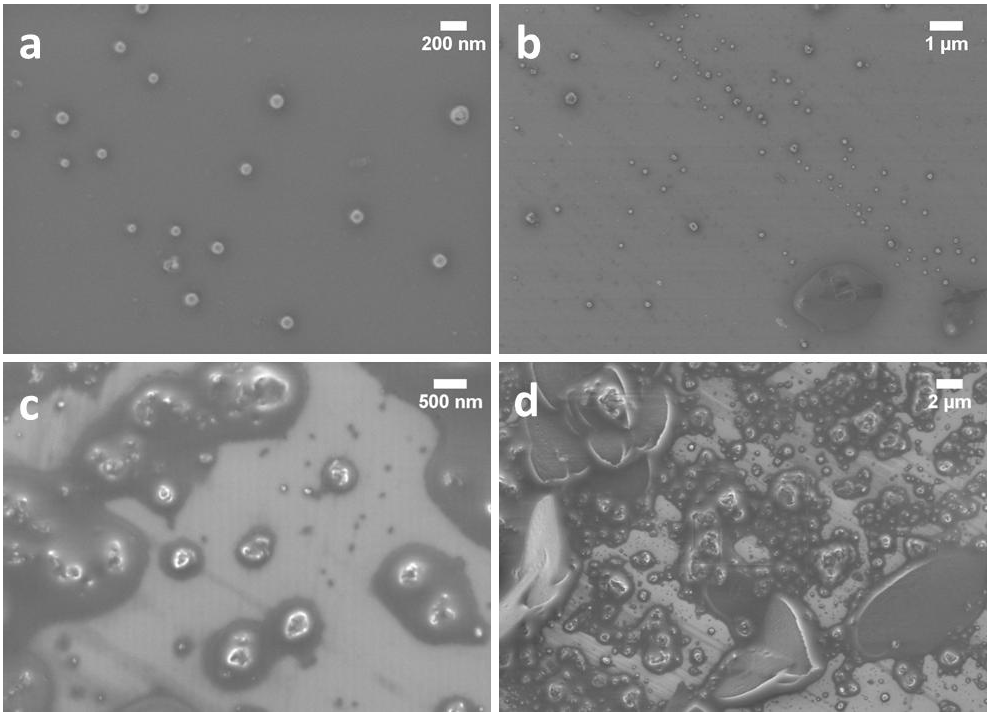

Figure 4.4.1. SEM micrographs of a PEG b PGlu(Pyr) copolymer/cyclohexane dispersion before (a,b) and after UV irradiation (λ = 366 nm, P = 4 W, t = 3h).

Particle analysis via SEM micrographs corroborated the D_h obtained from DLS (D = 86 ± 23 nm) (Figure 4.4.1 a, b), implying that the chosen block length (DP = 90) and the degree of esterification (86%) sufficed to stabilize the nonpolar organic phase.

After addition of small amounts of water and UV irradiation, D_h of the aggregates in cyclohexane significantly increased to D_h = 675 ± 523 nm, indicating strong aggregation of photolytically cleaved polymers (Figure 4.4.1 c, d). To verify this assumption, both the cyclohexane and the water phase were investigated by ^{1}H NMR and DOSY. Verification of 1-pyrenyl methanol in the cyclohexane phase and of water-soluble PEG-*b*-PGlu copolymer in the aqueous phase demonstrated photo-induced cleavage of the hydrophobic group from the hydrophilic PGlu-backbone.

These results strongly suggest efficient stabilization of the nonpolar solvent by the PGlu(Pyr) block before UV irradiation. Upon UV irradiation and

subsequent removal of hydrophobic pyrenyl derivative, the former hydrophobic block PGlu(Pyr) becomes more hydrophilic (PGlu), resulting in increased aggregate size of copolymers that remained in cyclohexane.

Nonaqueous emulsion polymerization and photo-induced particle transfer

Based on photo-induced polarity change of the initially amphiphilic PEG-*b*-PGlu(Pyr) copolymer, a nonaqueous emulsion polymerization with PEG-*b*-PGlu(Pyr) as emulsifier was conducted to investigate potential nanoparticle transfer from a nonpolar organic solvent into an aqueous medium. Poly(L-lactide) (PLLA) nanoparticles were synthesized via ring-opening polymerization of L-lactide with a moisture-sensitive catalyst in a nonaqueous emulsion consisting of acetonitrile, cyclohexane and the PEG-*b*-PGlu(Pyr) copolymer as emulsifier.

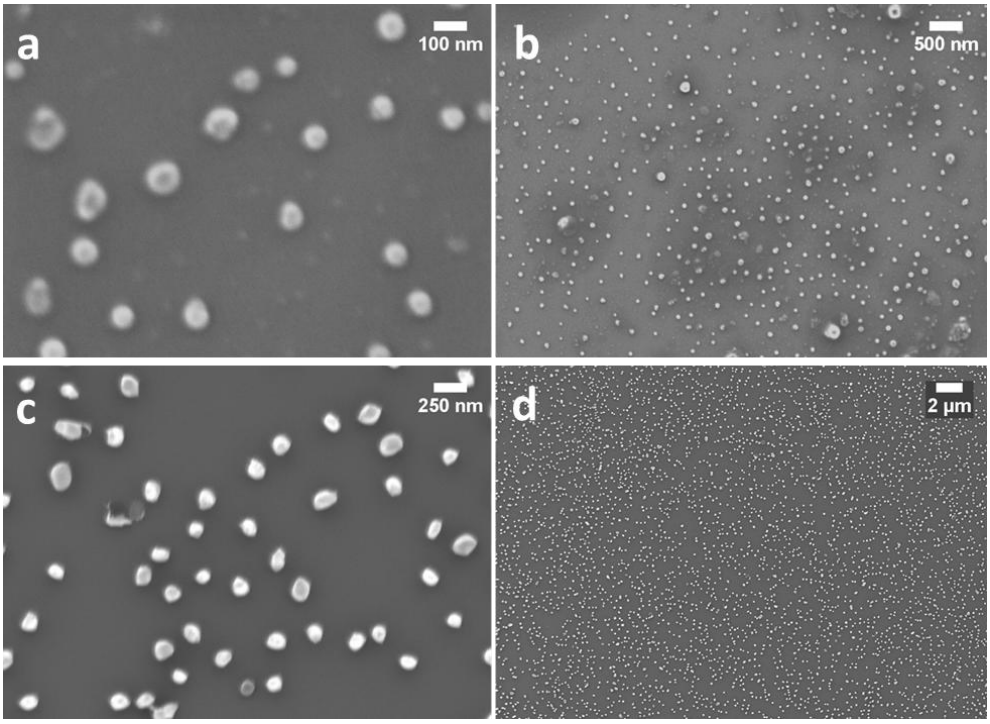

Figure 4.4.2. SEM micrographs of PLLA nanoparticles before (a, b) and after photo induced cleavage of pyrenyl methylene units from the PEG b PGlu(Pyr) copolymer (c, d) (λ = 366 nm, P = 4 W, t = 3h).

The PLLA nanoparticles had diameters of $D_h = 130 \pm 19$ nm, which was corroborated by particle analysis of SEM micrographs ($D = 93 \pm 17$ nm, Figure 4.4.2 a, b). Compared to the block copolymer aggregate sizes in cyclohexane, the PLLA particle diameters were significantly higher implying sufficient stabilization of the polymer components in the acetonitrile droplets. Subsequently, the emulsion was mixed with water and irradiated with UV light ($\lambda = 366$ nm) to cleave the hydrophobic 1-pyrenyl methylene-units from the PGlu-block. After photolysis, the cyclohexane phase was removed *in vacuo* and the resulting aqueous dispersion was purified by dialysis. UV-vis spectroscopy measurement proved complete removal of pyrenyl residues. The PLLA nanoparticles had a D_h of 199 ± 6 nm, indicating a larger hydrophilic shell around the particles in aqueous medium as compared to organic emulsions. Analysis of the aqueous nanoparticle dispersion via SEM gave a mean particle diameter of

D = 105 ± 18 nm, proving size retention without occurrence of aggregation. Size retention was expected as the addition of a second surfactant was not necessary for the transfer.

The resulting particle dispersions were dried, washed several times with water and subsequently dialyzed for 7 days against water to investigate potential removal of entirely hydrophilic PEG-*b*-PGlu copolymer from the hydrophobic PLLA particles. After dialysis, the particle dispersions were dried and a THF/water mixture was added to the resulting solid to dissolve both PLLA and the block copolymer. Subsequently, the solution was poured into an excess of water to precipitate PLLA. Precipitated PLLA had a molecular weight of M_n = 5800 g·mol^{-1} and a PDI of 1.34, as determined via ^{1}H NMR end-group analysis and GPC. The molecular weight is close to the theoretical one (M_{theo} = 5000 g·mol^{-1}) proving successful polymerization and inertness of the emulsifier (PEG-*b*-PGlu(Pyr)) toward the polymerization. After centrifugation and removal of PLLA, the aqueous solution was dried and the remaining solid was investigated via ^{1}H NMR spectroscopy and DOSY. The measurements verified the solid to be the cleaved PEG-*b*-PGlu copolymer (Figure 7.3.4).

This strongly suggests that PLLA chains are entangling predominantly with the PEG chains of the PEG-*b*-PGlu(Pyr) copolymer since they face the dispersed phase during particle formation (in the nonaqueous emulsion polymerization). The entanglement is most likely responsible for the fact that PEG-*b*-PGlu copolymer could not be removed from the PLLA particle surface and that PLLA particles are efficiently stabilized in water by the entirely hydrophilic PEG-*b*-PGlu copolymer.

Finally, the biocompatibility of the PEG-*b*-PGlu emulsified PLLA nanoparticles was assessed by 24-hour incubation with human mesenchymal stem cells. Particles incubated with significantly higher concentration (10-fold dilution) than in our previous PEG-*b*-PI copolymer emulsions[133,

[148] (30-fold dilution) showed identical cell viability with non-particle-incubated controls. In all cases the viability was nearly 100% (Figure 4.4.3).

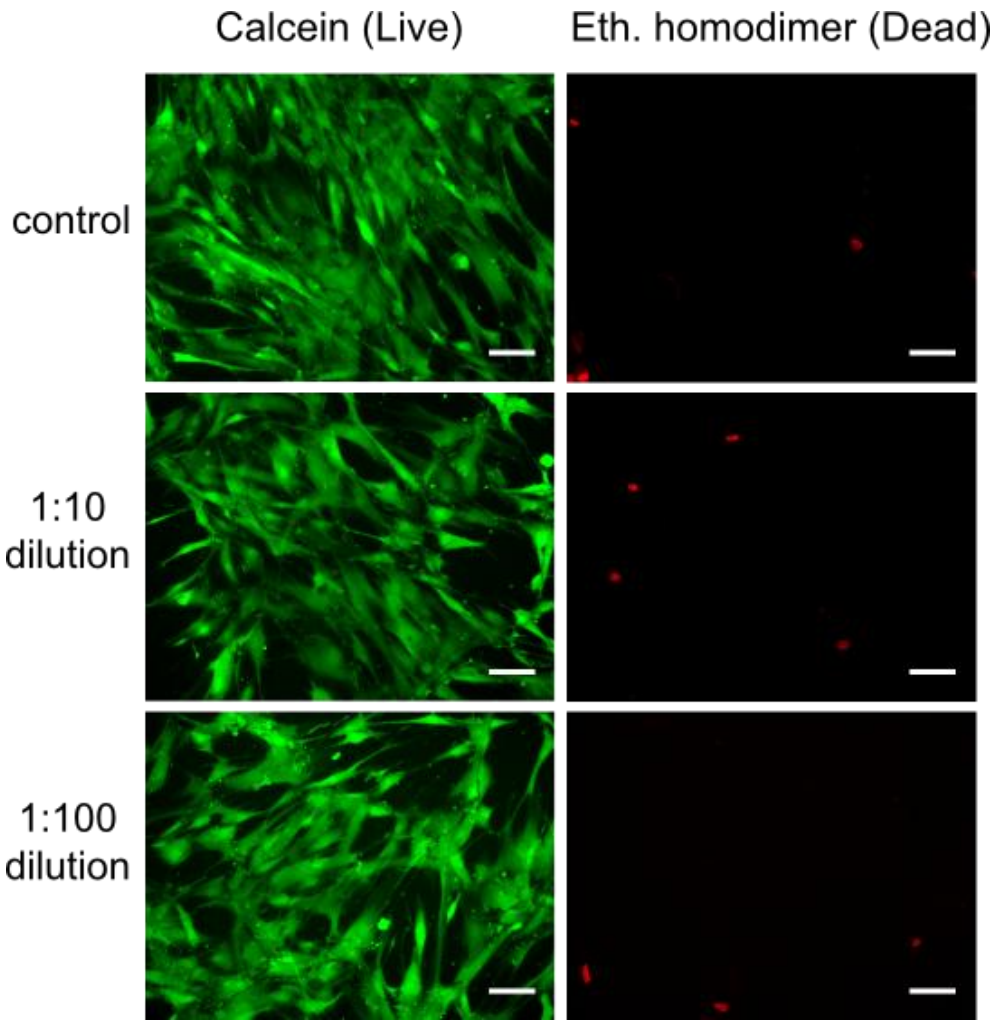

Figure 4.4.3. Live/dead staining of hMSC cells after 24-hour incubation of PEG-b-PGlu(Pyr) emulsified PLLA nanoparticles at various dilutions. Live cells stained positive for calcein (green) whereas dead cells stained positive for ethidium homodimer (red). Scale bar = 100 μm.

Conclusion

It was demonstrated that an amphiphilic PEG-*b*-PGlu(Pyr) copolymer stabilized a nonaqueous emulsion polymerization of lactide giving hydrophobic PLLA nanoparticles. The addition of water and subsequent UV

irradiation of the particle dispersion caused cleavage of hydrophobic 1-pyrenyl methylene-units from the hydrophilic PGlu-side chains. The resulting polarity change of the particle surface from hydrophobic to hydrophilic enabled its final transfer into water. Since additional surfactants were not necessary for solvent exchange, the particles did not aggregate and their size was retained. Therefore, potential functions, for example targeting or responsiveness in drug delivery systems, are not expected to be negatively affected by this transfer reaction.

Since the emulsifier had no negative impact on the sensitive catalytic polymerization of lactide, this change of surface polarity is most likely imparted to other systems necessitating solvent transfer reaction with retention of particle morphology and functionality. More importantly, this emulsifier design addresses two major challenges that previous approaches have been struggling with[2, 156-161]: 1) dispersing hydrophobic latex particles in water without aggregation; 2) synthesizing fully biocompatible latex particle, avoiding the use of non-biocompatible block copolymers or toxic ionic tensides[162] as stabilizing agents. Taken together with potential functionalization of the emulsifier's terminal amine group with targeting molecules, this emulsifier offers a pathway to new drug delivery systems consisting solely of FDA-approved PLLA, PEG and PGlu.

Experimental Section

Photosensitive Emulsifier Synthesis

Glu(Bz)-NCA

In a dry Schlenk flask γ benzyl α glutamic acid (10.0 g, 42.2 mmol) was dissolved in dry THF (100 mL) under inert atmosphere. The suspension was heated to 50°C under reflux and subsequently treated with triphosgene (4.17 g, 14.1 mmol). After 1h of stirring, additional triphosgene (1.26 g, 4.24

mmol) was added. The suspension became a solution after a total reaction time of 3 h. The solution was poured into 300 mL dry *n*-hexane and heated to recrystallize. The *N*-carboxy anhydride was recrystallized twice and subsequently stored in a freezer overnight. The flask was transferred into a glove box. The solid was isolated by filtration and stored in the glove box after drying *in vacuo*.

Yield: 75%; 1H NMR (500 MHz, CD_2Cl_2, δ): 7.37 (m, 5H, Ar H), 6.51 (s, 1H, NH), 5.13 (s, 2H, OCH_2Ph), 4.40 (t, J = 6.2 Hz, 1H, CHC(O)), 2.59 (m, 2H, γ-CH_2), 2.25 (m, 1H, β-CH_2), 2.13 (m, 1H, β-CH_2); 13C NMR (500 MHz, CD_2Cl_2, δ): 172.9 (OC=O), 170.2 (OC=O), 152.2 (HNC=O), 136.2 (Ar), 129.2 (Ar), 129.0 (Ar), 128.8 (Ar), 67.5 (CH_2Ar), 57.5 (CH), 30.3 (CH_2), 27.4 (CH_2).

PEG-*block*-PGlu(Bz) Copolymer

In a glove box Glu(Bz)-NCA (9.00 g, 34.2 mmol) and urea (4.00 g, 66.6 mmol) were placed in a dry Schlenk flask and dissolved in dry DMF (240 mL). A solution of PEG-NH2 (Mn ~ 2000 $g \cdot mol^{-1}$, 0.76 g) in dry DMF (90 mL) was added. The polymerization was conducted under stirring at room temperature for 4 d. The PEG-*b*-PGlu(Bz) copolymers were precipitated into diethyl ether and subsequently freeze dried.

Yield: 82%; ^{1}H NMR (500 MHz, DMF, δ): 8.53 (br, 1H, NH), 7.36 (m, 5H, Ar), 5.10 (m, 2H, Ar-CH_2), 4.13 (br, 1H, CH), 3.59 (s, 4H, OCH_2CH_2), 3.30 (s, 3H, OCH_3), 2.30 (m, 4H, CH_2CH_2). M_n (1H NMR) = 21,900 $g \cdot mol^{-1}$; M_w/M_n (GPC) = 1.24.

PEG-*block*-PGlu Copolymer

PEG-*b*-PGlu(Bz) copolymer (4.00 g) was dissolved in dry DMF (140 mL). Small amounts of Pd/C (10%) were added and the reaction chamber was filled with hydrogen and stirred vigorously. After removal of Pd/C powder,

the polymer was dropped into an excess of n hexane. For purification, the product was dialyzed against water for 4 d (MWCO = 1000 g·mol^{-1}).

Yield: 90%; ^{1}H NMR (500 MHz, D_2O, δ): 8.45 (s, 2H, 2xNH), 4.31 (m, 2H, 2xCH), 3.70 (s, 4H, OCH_2CH_2), 3.38 (s, 3H, OCH_3), 2.20 (m, 8H, $2xCH_2CH_2$).

PEG-*block*-PGlu(Pyr) Copolymer

PEG-*b*-PGlu copolymer (80.0 mg) was mixed with phosphorus trichloride (PCl_3) (5.25 mL) and stirred under reflux and inert atmosphere at 60°C for 3 d. Excess of PCl_3 was removed in vacuo. 1-pyrenyl methanol (120 mg, 0.52 mmol) was dissolved in dry methylene dichloride (4 mL) and added to the solid under inert atmosphere and light exclusion. The mixture was vigorously stirred at room temperature for 3 d. The polymer was precipitated in diethyl ether, washed with n hexane and subsequently dried *in vacuo*.

Yield: 61%; ^{1}H NMR (500 MHz, CD_2Cl_2, δ): 8.20 (m, 16H, 0.86x2xpyrene(9H)), 5.53 (b, 3H, 0.86x2xCH_2), 4.01 (br, 2H, 2xCH), 3.57 (s, 4H, OCH_2CH_2), 3.31 (s, 3H, OCH_3), 2.30 (m, 8H, $2xCH_2CH_2$).

Self-Assembly Study of PEG-b-PGlu(Pyr) copolymers in Cyclohexane

PEG-*b*-PGlu(Pyr) copolymer (12.0 mg) was dispersed in cyclohexane (5.00 mL; c = 2.4 mg·mL-1). The dispersion was mixed with water (0.50 mL) and subsequently irradiated with UV light (λ = 366 nm; P = 4W), followed by vigorous stirring at room temperature for 3 h. A sample was taken out to analyze the aggregates via DLS and SEM. Cyclohexane of the remaining sample was removed under reduced pressure and an additional amount of water (1.50 mL) was added. After filtration, the aqueous dispersion was analyzed via ^{1}H NMR spectroscopy and DOSY.

Preparation of Aqueous Poly(L-lactide) Nanoparticle Dispersions

PEG-*b*-PGlu(Pyr) copolymer (45.0 mg) was magnetically stirred in cyclohexane (14.4 g, 171 mmol) at room temperature. L-lactide (76.0 mg, 0.53 mmol) was dissolved in acetonitrile (0.203 g, 0.26 mL, 4.94 mmol). The emulsion was formed by dropwise addition of the monomer solution to the cyclohexane/PI-*b*-PGlu(Pyr) dispersion and subsequent treatment with sonication for 5 min using a Bandelin Sonorex RK255H ultrasonic bath operating at 640 W. SIMes (4.68 mg, 15.3 µmol) and the 1-pyrenyl butanol (4.20 mg, 15.3 µmol) were dissolved in acetonitrile (0.203 g, 4.94 mmol) and added dropwise to the emulsion under inert atmosphere. The emulsion was stirred for 15 min at room temperature to produce poly(L-lactide) (PLLA) nanoparticles. A sample was taken out of the emulsion in order to analyze the particle size and morphology via DLS and SEM. To the remaining emulsion water (18.5 mL) was added. After UV irradiation (λ = 366 nm) and vigorous stirring for 3 h at room temperature, the organic solvent was removed *in vacuo* and the dispersion was isolated from the precipitated 1-pyrenyl methanol. The remaining aqueous dispersion was dialyzed against water for 3 days (MWCO = 1000 $g \cdot mol^{-1}$). The resulting particles were analyzed via DLS and SEM. To evaluate the polymerization of LLA and quality of photo induced particle transfer, a sample of the aqueous dispersion was dried and dissolved in a THF/water mixture. The solution was poured into an excess of water and THF was removed *in vacuo* to precipitate PLLA. After centrifugation, the dried solid was analyzed via GPC, ^{1}H NMR spectroscopy and DOSY. The supernatant of the centrifuged sample was collected and analyzed for cleaved PEG-*b*-PGlu copolymer.

Biocompatilibty of PEG-b-PGlu(Pyr) emulsified Poly(L-lactide) Nanoparticles

hMSCs below passage 5 (Lonza, Cologne, Germany) were cultured in 12-well polystyrene plates in growth medium (α-MEM, Lonza, Cologne, Germany) supplemented with 15% FCS (Life, Frankfurt, Germany) at 37°C and 5% CO_2 under humidified atmosphere. When reaching ~80%

confluence, medium was exchanged with 1:10 and 1:100 dilutions of PLLA particle dispersion (stock in milliQ water) in pre-warmed growth medium; media with 10% sterile milliQ water was as the control. After 24h, medium was aspirated and cell were washed 3x in pre-warmed PBS. Cell viability was assessed using a live-dead staining kit according to the manufacturers instructions (LIFE/DEAD®, Life, Frankfurt, Germany). Images of cells were acquired using an IX81 inverted microscope (Olympus, Hamburg, Germany) and processed with ImageJ Software. The experiment was performed in triplicates and representative pictures are shown in Figure 4.4.3.

4.5 Metallocene Supported on Porous and Nonporous Polyurethane Particles for Ethylene Polymerization

Authors:

Robert Dorresteijn, Sven Nietzel, Daejune Joe, Yi Gerkmann, Gerhard Fink, Markus Klapper, Klaus Müllen

ToC:

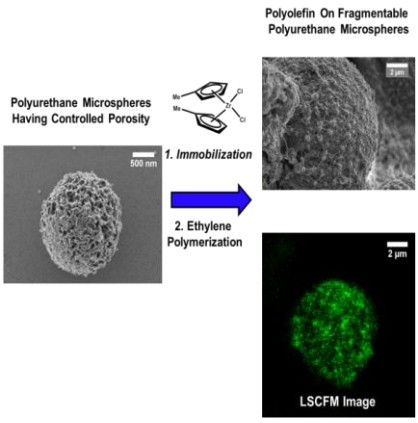

Cover Page:

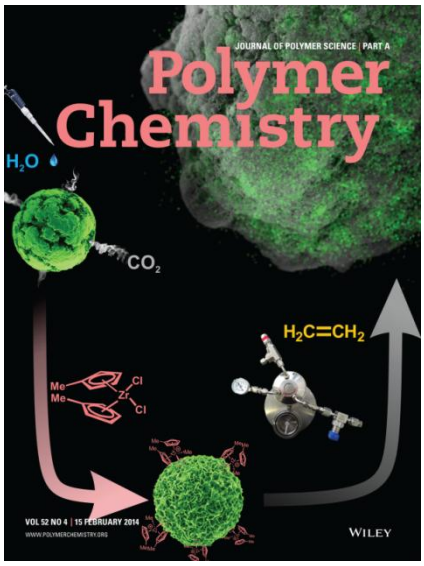

Published in:

Journal of Polymer Science Part A: Polymer Chemistry

Abstract

Porous polyurethane particles are presented as uniform fragmentable supports for metallocene catalysts in polyolefin synthesis. The micrometer-sized particles which have a narrow size distribution and a controlled porosity are prepared by a nonaqueous emulsion polymerization in a single step. The porosity of the PU particles is controlled by introducing a defined amount of water into the emulsion polymerization. A complex of metallocene/methylaluminoxane is immobilized on the PU supports and used for the ethylene polymerization in a gas phase reactor. The surface and morphology of the polyethylene/polyurethane particles are characterized by using scanning electron microscopy. Homogeneous fragmentation of the support material is observed during the polymerization and affords product particles with a spherical shape and narrow size distribution. The fragmentation behaviors of the polyurethane microspheres throughout the ethylene polymerization are monitored by laser scanning confocal fluorescence microscopy (LSCFM) which is a non-destructive method in contrast to other techniques. A homogeneous distribution of PU in the polyethylene particles is proven by the optical sectioning of LSCFM.

Introduction

The combination of metallocenes with trialkylaluminoxane has opened a new era of producing polyolefins with tailor-made properties.[163-164] The novelty of metallocene catalysis, in contrast to Ziegler-Natta systems, is the single-site character of the active species which generates polymers with narrow, monomodal Flory-size distributions. By tailoring the ligands of the metallocenes, polyolefins with specific properties can be produced through the control of tacticity and the incorporation of discrete ratios of comonomers.[165-166] Despite these outstanding properties, however, their use in industrial applications under homogeneous conditions at

polymerization temperature below the melt point encounters some problems such as low bulk density of the product, a very large amount of methylaluminoxane (MAO) as co-catalyst, lack of morphology control and reactor-fouling. The polymers produced from homogeneous olefin polymerization via metallocenes are obtained only in dust or lump form which is not suitable for industrial applications. For better processability, a flowable powder is required which can only be produced by supporting metallocenes on solid carriers.[167] Such a heterogeneous approach provides better morphology control and higher bulk densities of the obtained particles, prevents reactor-fouling. Additionally, the use of a supporting material is the only way to run metallocene polymerizations without a solvent in a gas phase reactor.

The proper choice of supporting materials is an important factor:[168-173] i) The supporting material should consist of micrometer-sized spherical particles to avoid dust formation and possess a high surface area, well-defined pore diameters and uniform size distributions; ii) the supporting material should be fragmentable into nanometer-sized particles throughout the polymerization process to achieve a high density product and to avoid light scattering in the final product; and iii) the active sites of the supports should be homogeneously distributed on the surface and in the pores to achieve uniform product particles, although there is emulsion-based supports such as Sirius technology that dispersed active sited in a fragmentable support without porosity.

Immobilization of metallocenes onto supporting materials such as silica,[174-176] magnesium chloride,[177] alumina,[178] and organic materials[179-181] has been intensively investigated. Among the supporting materials, highly porous silica particles have become the most widely used supports and have been extensively applied in industrial polyolefin production. Commercially applied porous silica particles are agglomerates (*secondary particles*) composed of nanometer-sized non-porous granulates (*primary*

particles).[182] These primary particles are commonly prepared by neutralization of aqueous alkali metal silicates with an acid.[183] The average sizes of these secondary particles, which should be in micrometer-range, are mainly altered by the nozzle pressure of a spray drying process with the primary particles. This process is suitable for large-scale production. Despite many efforts, these secondary particles still have limitations including irregular shape, broad size distributions, and broad ranges of surface area.[183] These drawbacks might also affect the properties of the final polyolefin products having heterogeneous morphology, irregular shape by the "replica" effect, and broader product particle distribution. For better results, secondary particles should be micrometer-sized and have pore structures in which metallocenes can be immobilized. Secondary particles tend to fragment into nanometer-sized primary particles beginning with the onset of metallocene-catalyzed polymerization after which, the primary particles remain homogeneously dispersed in the polymer particle over the whole process.[184] Although silica supports are generally applied for metallocene-catalyzed polyolefin synthesis, once could consider there is a room to be improved.

Organic supports which allow for relatively easy modification of the surfaces have been investigated for olefin polymerizations,[181, 185-186] since modification of the chemical and structural properties of the supporting materials is still desired to improve the immobilization process. Additionally, organic supports hold promise for better incorporation into the final polyolefin products owing to their hydrocarbon-rich matrix.[182, 185] Due to their well-defined structure and the possibility of direct surface modification via functionalized styrene derivatives, micrometer-sized polystyrene (PS) particles, crosslinked with 1-2 mol% divinylbenzene (merryfield resins), have been introduced.[187] However, the fragmentation of PS particles is hindered due to irreversible cross-linking. As a result, in contrast to that of the porous silica supports, a lower effective surface area is

achieved which lowers the activity, and the unfragmented large PS particles induce light scattering in the obtained product. To overcome these problems, we have introduced PS particles with sizes ranging from 50 to 200 nm produced by miniemulsion polymerization.[188-190] The PS nanoparticles (*primary particles*) agglomerate reversibly to micrometer-sized secondary particles through nucelophilic interaction with the methylaluminoxane (MAO) during the immobilization process of metallocenes.[186] Similar to the inorganic supports during olefin polymerization these secondary particles (*agglomerates*) break down to their primary particles, and the nanometer-sized primary particles are distributed homogeneously over the obtained polyolefin products. Even though better fragmentation is observed, it should be noted that the problem of obtaining uniform shape and size of the secondary particles still has remained, along with the need to increase surface area by introducing porosity.

In both cases using silica and crosslinked PS particles, the agglomeration of their corresponding primary particles to the secondary particles does not lead to the desired uniform spherical systems required for modified supports. As such, alternative methods for obtaining uniform, spherical, porous, and fragmentable supports, these particles are needed and would be an important progress in the gas phase (or slurry) polymerization processes. Herein, we address micrometer-sized porous polyurethane (PU) particles, prepared via a one-pot synthesis, as new supports for metallocene-catalyzed olefin polymerization. The preferred method of choice for the synthesis of suitable PU microspheres is via nonaqueous emulsion polymerization. The porosity and surface area of the PU microspheres are tailored by adding small amounts of water which controls the formation of pores, since its reaction with the isocyanate generates CO_2. Their applicability as porous organic supporting materials is demonstrated in a heterogeneous catalytic system with immobilized metallocenes.

Results and Discussion

Porous Polyurethane Particles

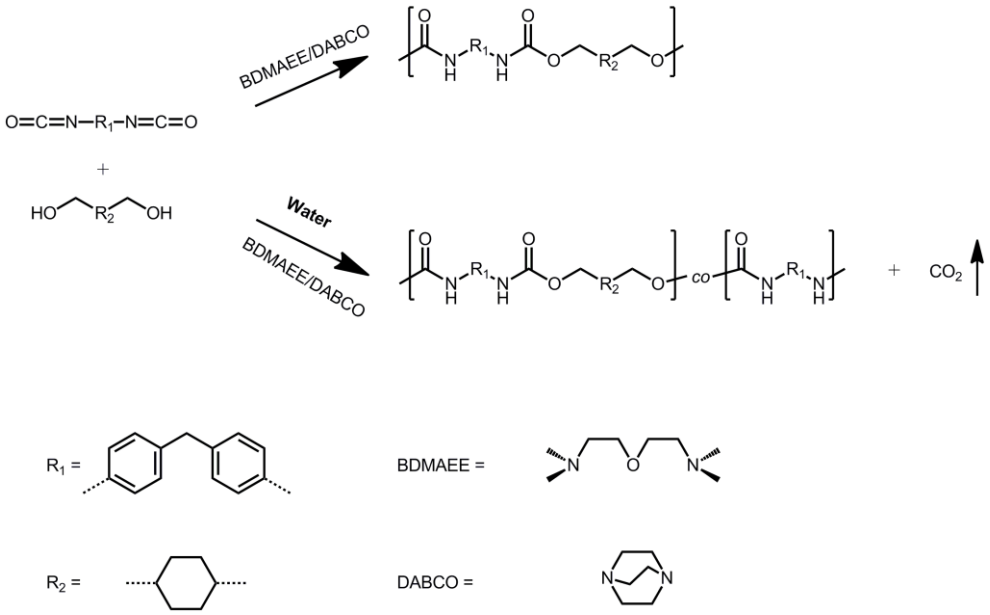

Figure 4.5.1. Reaction scheme for the formation of polyurethane and polyurea.

In order to form porous polyurethane (PU) microspheres, the polymerization of a diol with a diisocyanate with concurrent CO_2 release in a shaping procedure, like an emulsion, is performed.[191] The presence of water in a diisocyanate-containing emulsion leads to both a release of CO_2 and the generation of polyurea (Figure 4.5.1).[192] The amount of water controls the quantity of released CO_2 which is responsible for the resulting porosity and pore size.[193-194] In an aqueous emulsion, this process is rather uncontrolled due to the continuous phase. We introduce a nonaqueous system, which is predestinated to generate PU particles with a defined porosity due to the exact amount of water employed. This system has previously proven its applicability towards the formation of PU nanoparticles.[195] A typical nonaqueous emulsion system consists of two immiscible organic solvents that are stabilized by an amphiphilic block copolymer.[195-196] In particular, a

mixture of DMF and cyclohexane is well-stabilized by a polyisoprene-*block*-polymethyl methacrylate (PI-*b*-PMMA) copolymer and leads to the generation of "microreactors", wherein the polymerization can occur. The PI-*b*-PMMA copolymer has a number average molecular weight of 60 $kg \cdot mol^{-1}$ with a polydispersity (PDI) of 1.03. Due to the low interfacial tension between the two organic solvents, high molecular weight is necessary. The molar block composition of this copolymer is 69 % PI and 31 % PMMA (DP_{PI} = 677; DP_{PMMA} = 142). This composition leads to both a good steric repulsion between the dispersed droplets and to an anchoring effect inside the droplets.[147, 197]

The polymerization of PU microspheres was performed using two different catalysts: bis(2-dimethylaminoethyl) ether (BDMAEE) and 1,4-diazobicyclo[2.2.2]octane (DABCO). In general, higher intermolecular forces between water and catalyst result in a greater ability to decompose the isocyanate to CO_2 and amine.[191] Whereas BDMAEE effectively promotes the reaction of water and isocyanate leading to urea formation, DABCO coordinates larger isocyanates and alcohol and favors the urethane formation.[191] Due to this selectivity of the catalysts, a polymerization of only one catalyst does not lead to porous PU particles, since either no particles at all (catalyst: BDMAEE) or non-porous PU particles (catalyst: DABCO) are obtained. Hence, a combination of the both catalysts is necessary for the formation of both PU and polyurea and to produce porous particles, depending on the amount of water in the emulsion (Table 4.5.1).

Table 4.5.1. Experimental conditions and results of the preparation of PU microspheres in nonaqueous emulsion polymerization.

Sample	Amount of Water (mmol)	Surface Area [a] ($m^2 \cdot g^{-1}$)	D_h [b] (DLS) (µm)	D [c] (SEM) (µm)	M_n [d] ($kg \cdot mol^{-1}$)	PDI [e]	Molar ratio urethane /urea [f] (%)
1	0	2.8	2.03 ± 0.39	2.07 ± 0.34	5.3	1.65	79
2	0.78	3.7	2.02 ± 0.23	1.74 ± 0.41	8.7[g]	1.52[g]	24
3	1.67	15.1	2.36 ± 0.30	1.93 ± 0.24	6.6[g]	1.37[g]	18
4	3.27	6.8	2.27 ± 0.19	1.86 ± 0.46	6.5[g]	1.36[g]	14

Emulsion: DMF (26.0 mmol) dispersed in cyclohexane (185 mmol) stabilized by PI-*b*-PMMA (0.21 g); Polymerization: BHC (1.5 mmol) + MDI (1.6 mmol) + DABCO (0.10 mmol) + BDMAEE (0.31 mmol) + water (0 – 3.27 mmol) at ambient temperature for 15 min. The errors are standard deviation from 10 DLS measurements.
[a] Surface area determined via nitrogen adsorption and desorption isotherms. [b] hydrodynamic diameter determined via DLS. [c] average diameter of 200 randomly chosen particles from various SEM micrographs. [d] degree of polymerization determined via GPC vs. PMMA standards. [e] polydispersity index determined via GPC vs. PMMA standards. [f] derived from FTIR-spectroscopy measurements. [g] *N*-methylated polyurea and polyurethane.

In an emulsion polymerization in the absence of water (sample 1, Table 4.5.1), the polymer displays the molecular weight of 5.3 $kg \cdot mol^{-1}$ and the PDI of 1.65 measured by gel permeation chromatography (GPC). According to the Carothers equation, this implies a conversion of 0.99 for this step-growth reaction against the used PMMA standard.[198] The molecular weights of the polymers (samples 2-4, Table 4.5.1), obtained from the polymerizations in the presence of water, could not be measured at first. This is due to the insolubility of these polymers originating from the "hard" urea-segments in the polymer chain, which form hydrogen bonds.[199-200] By *N*-methylation,[201] the hydrogen bonds of the urea-segments can be broken, and thus, the *N*-methylated polymers were well-soluble in DMF for GPC measurements. These polymers are observed with molecular weights up to 8.7 $kg \cdot mol^{-1}$ and a PDI as low as 1.36.

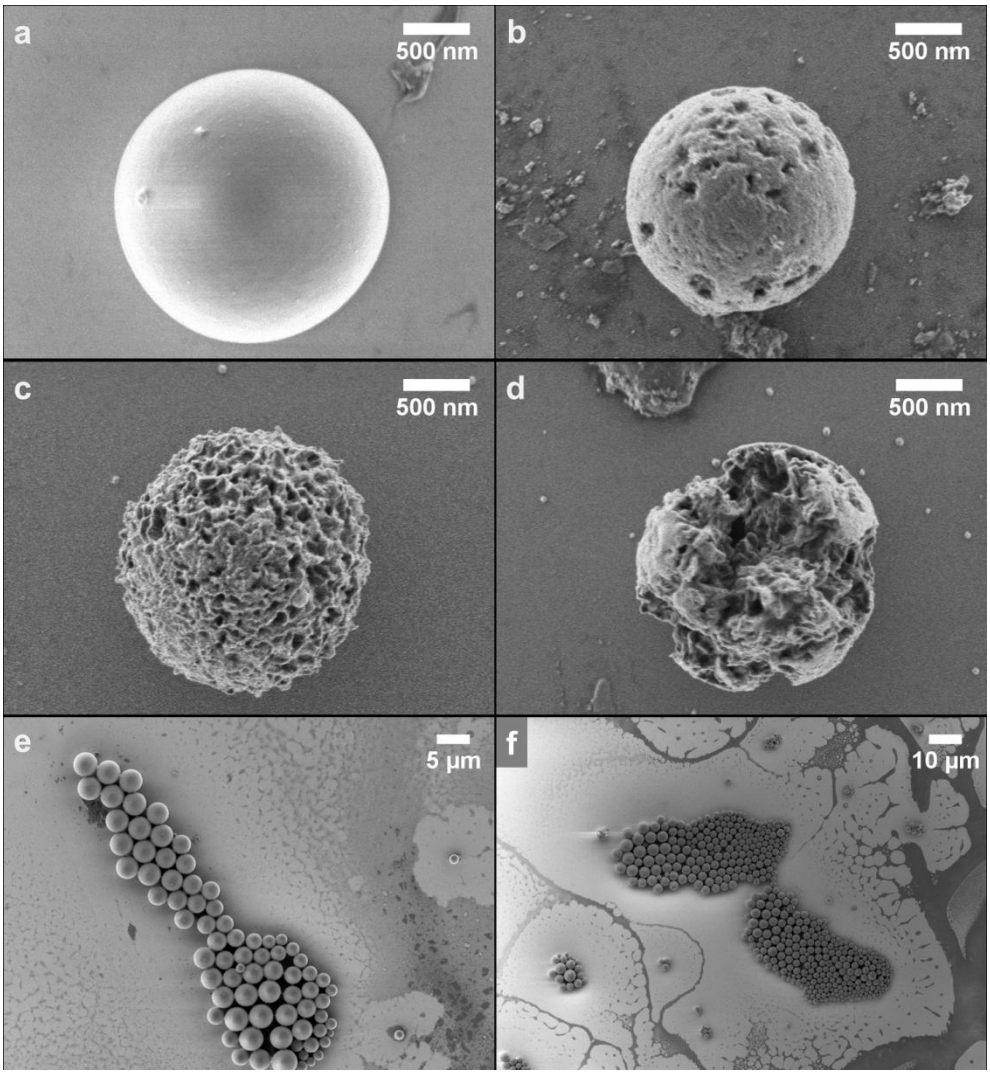

Figure 4.5.2. SEM micrographs of (a, e) non-porous and (b-d, f) porous PU particles. The amount of water during the polymerization was varied (a-d: 0, 0.78, 1.67, and 3.27 mmol of water).

In order to determine the size of the polymers, the PU particles were studied by dynamic light scattering (DLS) and scanning electron microscopy (SEM). As derived from SEM micrographs (Figure 4.5.2), they exhibit approximate diameters of 2 µm with a narrow distribution, which are similar to the data from the DLS measurements (Table 4.5.1). The isotropic shape of the particles originates from the exclusive solubility of all reaction components in the dispersed phase. By increasing the amount of added

water from 0 to 1.67 mmol (Figure 4.5.2 a-c), the surface morphology of the particles is drastically changed from smooth to porous particles. It can be attributed to the added water, which controls the amount of released CO_2. This results in the porous structure of the spherical particles. In the case of sample 4 (Figure 4.5.2 d, Table 4.5.1), the amount of released CO_2 appears to be sufficient for rupturing the resulting particles. The mean pore diameters of the spherical porous particles ranged from 58 ± 27 nm (sample 2; Figure 4.5.2 b) to 89 ± 27 nm (sample 3; Figure 4.5.2 c), that indicates a growth in pore diameter due to the blowing effect caused by the higher amount of released CO_2.

The surface areas of these particles increase for samples 1-3 from 3 $m^2 \cdot g^{-1}$ to 15 $m^2 \cdot g^{-1}$, depending on the employed amount of water (Table 4.5.1). From the low surface areas of these particles, it is assumed very small nanopores are not formed. This is desirable since MAO activated complexes can only be adsorbed into larger pores.[172] Sample 4 shows even lower surface area, and we assume that in this case too much CO_2 was formed causing the rupture of the particles. These results show that porosity can be well adjusted by the addition of water without losing shape control. Comparing these results with silica, which delivers broad particle size distribution and irregular shape of secondary particles[170], the porous PU particles are advantageous: they possess uniform shape, a controlled size with a narrow size distribution and a well-defined morphology.

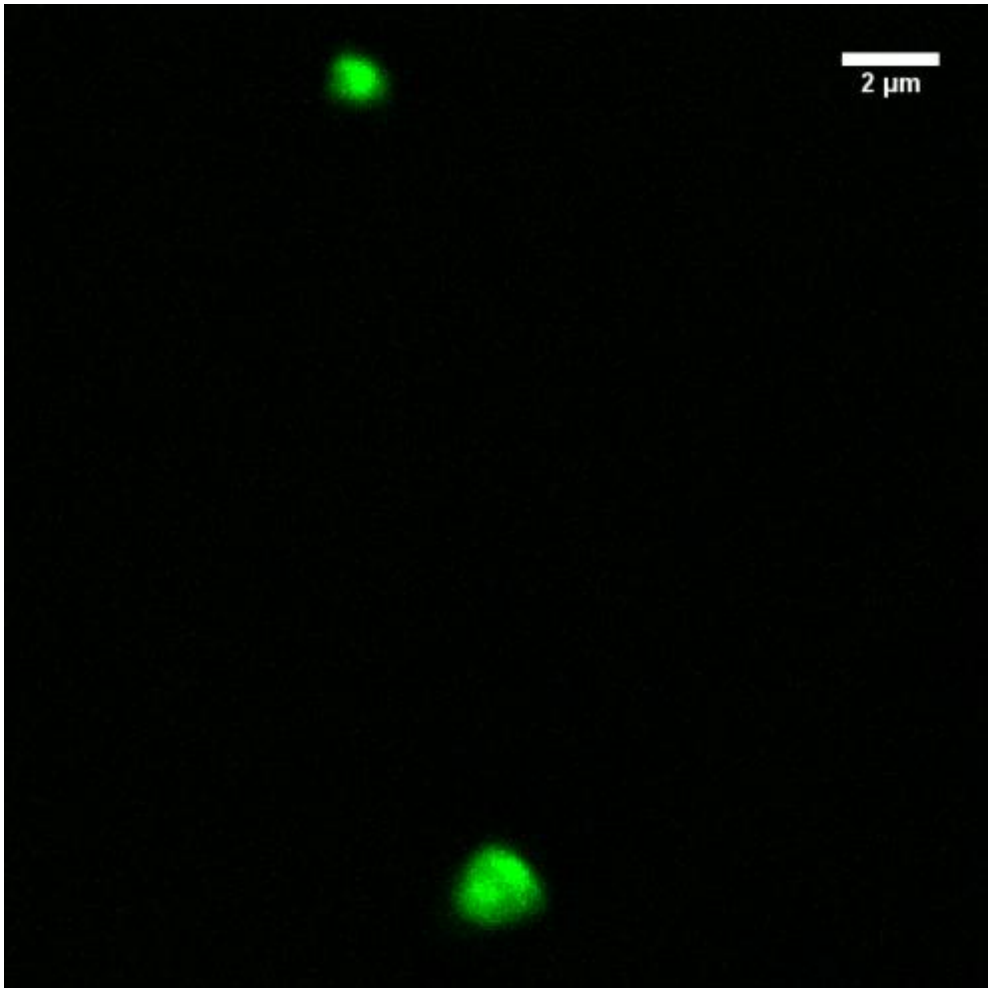

Figure 4.5.3. LSCFM image of the porous particles stained with Rhodamine B.

To homogeneously immobilize metallocene catalyst/MAO complexes onto supporting materials, the pores in the supports should be interconnected with one another. In order to demonstrate the presence of an open pore architecture, the porous particles (sample 3; Figure 4.5.2 c) were stained with a fluorescence dye and visualized via laser-scanning confocal fluorescence microscope (LSCFM). Rhodamine B (RhoB) was chosen as the staining dye due to its high solubility in methanol and the suitable emission wavelength for LSCFM studies.[202] In Figure 4.5.3, RhoB-stained porous PU particles show the accessibility of the inner particle-pores, since the dye is well distributed over the whole PU microspheres and not only on the surface. The fluorescence image of the RhoB-stained porous PU

particles indicates that they have “interconneted-pores”. In case the pores are not connected, a fluoresence dye can be detected exclusively at the surface of the particles. This demonstrates that two main requirements for a good support, a very homogeneous particle size and an open porous structure, for metallocene-catalyzed polymerizations have already been fulfilled.

Ethylene polymerization on polyurethane particles

To investigate the feasibility of polyurethane (PU) microspheres for heterogeneous polyolefin (PO) synthesis, bis(methylcylcopentadienly)zirconium(IV) dichloride (MCP) was chosen as a model catalyst. For the immobilization on the organic supports, the catalyst was dissolved in toluene and pre-activated with methylaluminoxane (MAO) which is the most common co-catalyst for metallocenes. The PU microspheres obtained via nonaqueous emulsion polymerization were dried under vacuum at elevated temperature and the MAO/MCP mixtures were added. These MAO/MCP complex-containing PU particles were obtained after filtration through a glass frit and were used after drying under vacuum. The correlation between catalytic activity towards ethylene polymerization and surface areas of PU microparticles was studied. The polymerizations were performed in a gas phase reactor at 3 bar and 40 °C. To facilitate a comparison, all samples were prepared under the same conditions with respect to the amount of PU particles, concentration of metallocene catalyst, ratio of MAO/MCP, temperature and drying time under vacuum. The results of the ethylene polymerization in the gas phase reactor are summarized in Table 4.5.2.

Table 4.5.2. Ethylene polymerization results of the PU particles in a gas phase reactor.

Sample [a]	Loading of catalyst system (µmol Zr ·(g Cat.)$^{-1}$)	Amount of catalyst (µmol)	MAO (µmol)	[Al]/[Zr]	Activity (kgPE·(mol Zr·h·bar)$^{-1}$)	T_m [b] (°C)	M_w [c] (kg·mol^{-1})	PDI [c]
1	25	3.1	310	100	6	n/d	n/d	n/d
2	25	3.1	310	100	39	137.5	1077	5.8
3	25	3.1	310	100	202	139.0	657	15.8
4	25	3.1	310	100	177	139.6	627	17.1

Polymerization conditions: 3 bar of ethylene at 40 °C for 30 min.
[a] Corresponding sample number in Table 1. [b] Determined by DSC. [c] Analyzed by GPC (PS-standard).

The final polyethylene products were obtained as well-defined beads. Neither dust-like products nor reactor fouling was observed due to the gas phase reactor setup, preventing catalyst leaching and aggregation of particles. Activities of MAO/MCP-supported PU particles toward ethylene polymerization were in the range of 6 to 202 kg of polymer (mol of Zr·h·bar)$^{-1}$. Sample 3 displayed the highest catalytic activity, since the applied PU microspheres possess the highest surface area (sample 3, Table 4.5.1). Sample 1 having the lowest surface area showed the lowest activity among the samples under the same polymerization conditions (Table 4.5.2). Although the value of activity is quite low as compared to conventional silica support system, these results demonstrate a correlation between surface area and catalytic activity. This is in good agreement with literature as it is known that the catalytic activity is strongly dependent on the surface

area of the support especially for silica in heterogeneous polyolefin synthesis.[203]

To characterize the melting behavior of the products, DSC measurements were performed. The samples possessed melting points (T_m) in the range of 137-140 °C which are slightly higher than typical values for high density polyethylene (HDPE). These values might be related with the content of PU which generally has a higher T_m and PE. The weight-averaged molecular weights (M_w) were measured after extracting the soluble part in 1,2,4-trichlorobenzene (TCB) at 140 °C. In this way, polyolefins can be selectively extracted as PU is insoluble in TCB. The M_w of the soluble polymer was determined by GPC to be in the range of approximately 6.3 to 10.7 × 10^2 kg·mol^{-1} which are typical values for metallocene catalysts. These samples show the unusually broad polydispersities (PDI) of 6 to 17 for heterogeneous metallocene polymerization. Several possible explanations can be suggested, although further studies on the broad PDI were not followed. In the case of Ziegler-Natta catalysts, due to the formation of the multi-active sites, it results a broad range of PDI.[204-205] As similar to that, the PU particles might have a multi-site catalyst due to the coexistence of polyurethane and polyurea. As M_w increases with the urea content of the different supports (Table 4.5.1), we assume that the urea structural moiety reacts with the cationic metallocene species (after MAO activation) leading to a catalytic site with a different activity than the non-bonded complex. Another explanation is a fragmentation behavior of the PU particles during the ethylene polymerization. Generally, conventional silica particle-supported metallocene fragmentizes by a "layer-by-layer" mode.[170] Due to the almost regular fragmentation of silica particles, it results commonly a PDI in the range of 3 to 5. In case of the PU particles, due to the hard segment of polyurea, mechanical strength is relatively higher than the conventional silica case. This difference might affect the irregular speed

of fragmentation and results in a various polymerization time on the outer layer through the core of the PU particles.

The growth of particles over the olefin polymerization time is typically related to the surface area and particle size of the supports. In order to investigate the influence of the surface area on the activity toward ethylene polymerization, a gas phase reactor equipped with an optical video microscope was applied. For comparison between non-porous PU particles (sample 1, Table 4.5.1) and porous PU particles (sample 3, Table 4.5.1), ethylene polymerizations were performed under same condition. During the ethylene polymerization, MCP/MAO-supported PU particles (non-porous and porous) were photographed every 10s using the optical video microscope. The volume of the PU particles were calculated from the photographs based on the assumption that all particles have isotropic shape and spherical shape. The values of volume were normalized and plotted as a function of polymerization time (Figure 4.5.4).

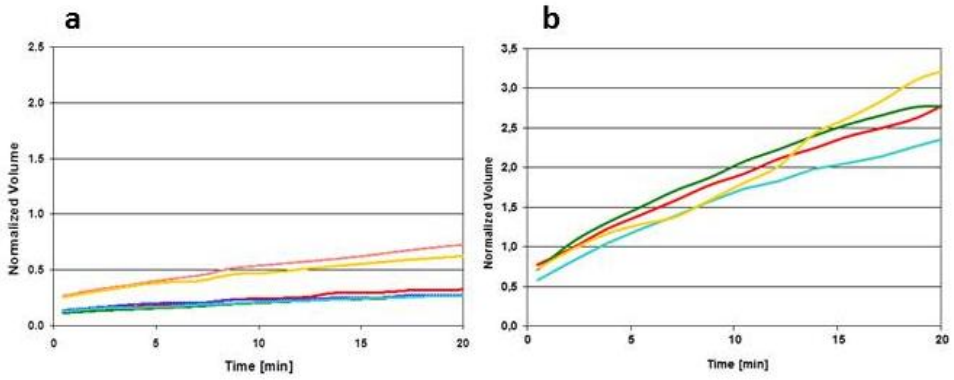

Figure 4.5.4. Graphs of normalized volume of (a) non-porous PU microspheres and (b) porous PU microspheres as a function of ethylene polymerization time from a gas phase reactor equipped with an optical microscope.

The porous PU particles showed significant volume changes of particles over ethylene polymerization (Figure 4.5.4 b), comparing to the non-porous particles (Figure 4.5.4 a). Similar behavior was observed in the literature

when studying aggregates of nanoparticles *vs.* Merrifield resins[206] of similar size corresponding to the studied porous and nonporous supports.[189] In the case of the resins, the catalysts are localized only at the surface of the particle. This results in a highly active catalyst layer where the diffusion is too limited to deliver sufficient monomer. As a result the activity drops, additionally, overheating may occur in this highly active zone forming a very dense molten layer which further limits the diffusion. In the case of a fragmentable support, the catalyst is homogeneously distributed within the whole particle, diffusion problems and overheating effects become negligible, and the activity remains high. Furthermore, due to fragmentation, large cracks are formed facilitating the monomer transport into the interior of the supported catalyst system.[170]

Morphology of the obtained polyolefin/polyurethane particles

Morphology of the final products, especially the spherical shape, is of important for the processing of polyolefins. Morphology studies on the PE particles obtained from a gas phase reactor were conducted via SEM and cryo-TEM. For non-porous PU particles (sample 1, Table 4.5.2), the smooth surface was vanished after 5 min of ethylene polymerization as shown in Figure 4.5.5 a. For elucidating the internal structure of the PE particle they were studied via cryo-TEM. By this method, two phases with different contrasts were detected in the particles (Figure 4.5.5 b). The brighter spherical part in the core of the obtained particle originates from the PU. The darker rim around the spherical particle corresponds to the PE formed by the MCP/MAO complexes. This core-shell structure indicates that the MCP/MAO complexes were immobilized only on the outer surface of the non-porous PU particles, which led to ethylene polymerization exclusively around the PU particles.

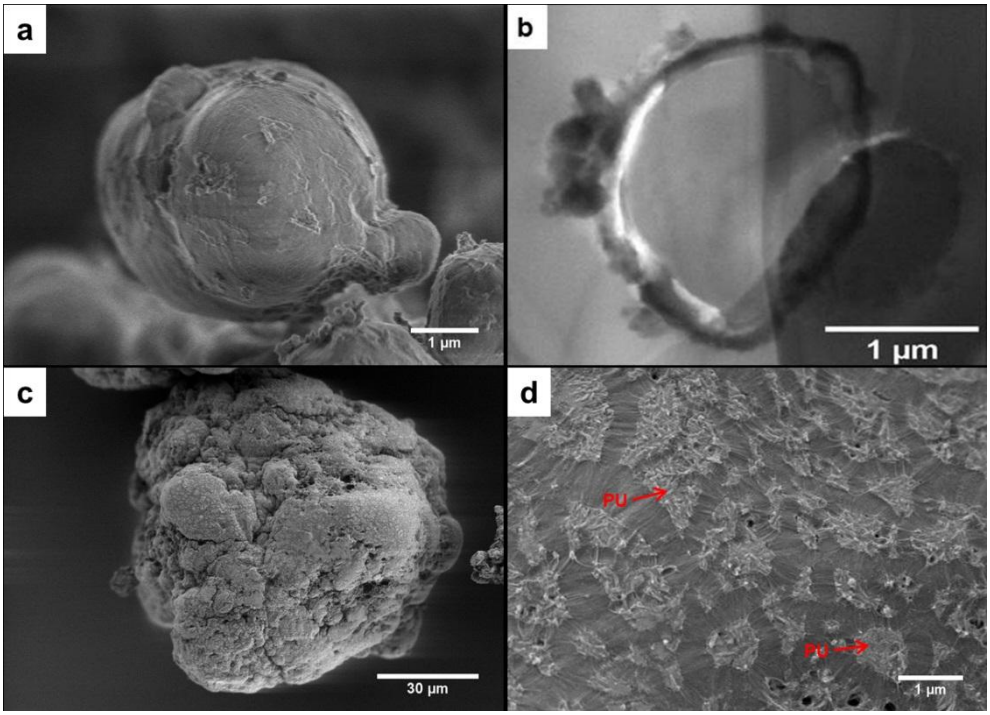

Figure 4.5.5. SEM and cryo-TEM micrographs of non-porous PU particle (a,b). SEM micrographs of most porous PU particle (c,d) after ethylene polymerization.

For the porous PU particles, a significant growth of the diameter of the supporting particle was observed during the ethylene polymerization (sample 3, Table 4.5.2). According to the SEM micrograph shown in Figure 4.5.5 c, the obtained products were approximated 100 micrometer-diameter particles with a spherical shape. With higher resolution, it was observed that the outer layer of the obtained products was composed of PE and fragmented PU as shown in Figure 4.5.5 d. Before ethylene polymerization, the mean pore diameter of the porous PU particles was 89 ± 27 nm, as derived from the SEM micrograph (Figure 4.5.2 c). Remarkably, the distance between the PU fragments becomes much wider after polymerization. It indicates a fragmentation induced by the mechanical stresses of the growing PE chains in the pores. Cryo-TEM shows no distinguishable boundary between PU and PE which also indicates a homogeneous distribution of PE in PU. To further investigate the fragmentation behaviors, laser scanning confocal fluorescence microscopy

(LSCFM) was applied to the PE particles. This technique allows the optical sectioning of an object containing a suitable dye without any physical destruction of the sample itself. [182, 189]

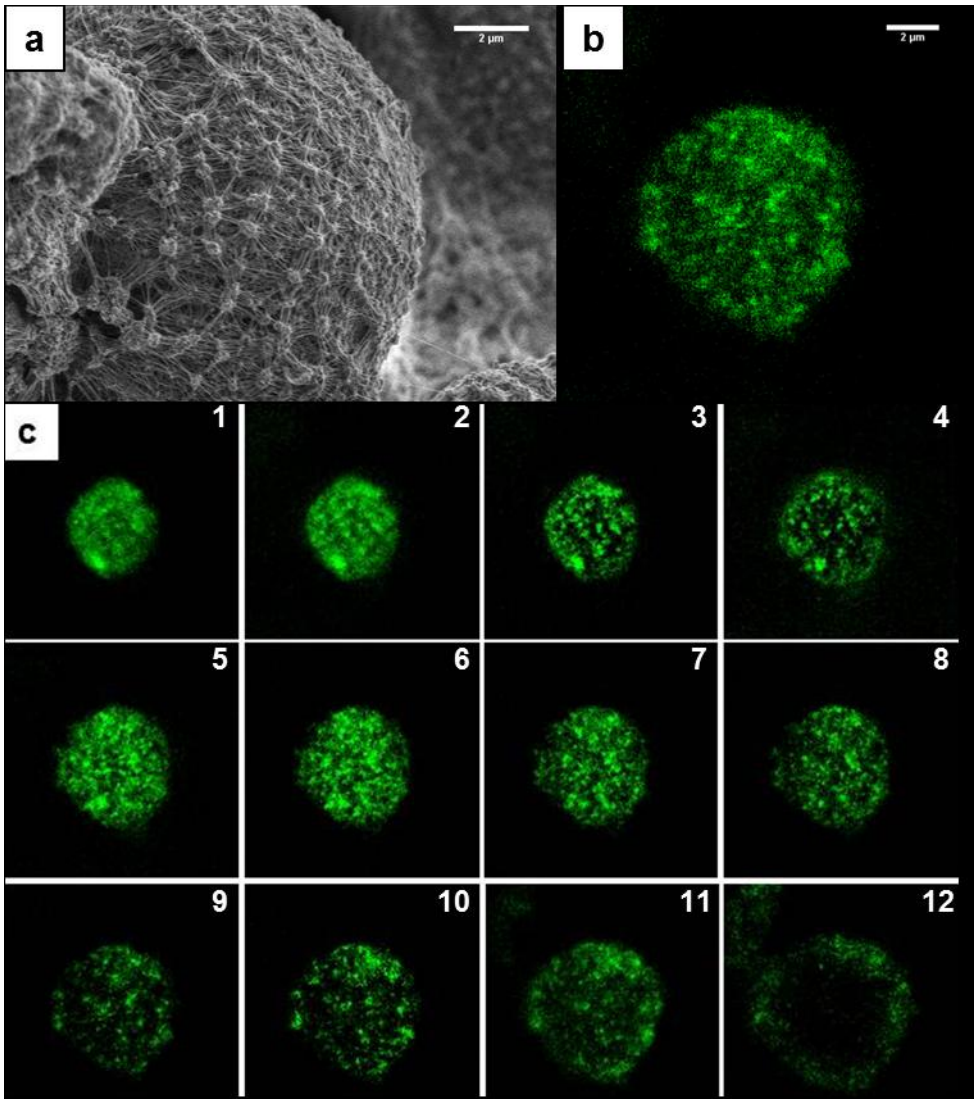

Figure 4.5.6. (a) SEM micrograph of the ethylene polymerized particles obtained from metallocene supported on the dye stained porous PU particle. LSCFM micrographs of (b) a single PE particle and (c) its 12 slices of PE particle by optical sectioning from top of the particle (1) to the middle of the particle (12).

After staining the porous PU particles with RhoB, ethylene polymerization was performed under the same conditions as previously mentioned for non-

stained PU particles. A comparison between the catalytic activities of stained and non-stained particles shows negligible differences, indicating that RhoB has no influence on the polymerization. To compare the morphologies of stained and non-stained particle, SEM was performed. As shown in Figure 4.5.6 a, the outer layer of the ethylene polymerized particle is composed of PE and the fragmented PU, revealing similar fragmentation behavior as the non-stained case. Information on the internal structure of the PE particles was obtained by LSCFM. Figure 4.5.6 b displays the fluorescence image of the PE particle produced with a gas phase reactor after a 30 min polymerization. The PE particles having a diameter of around 10 µm maintain their spherical shape and display multiple fluorescence spots (green colored) that are considered to be PU fragments. The spherical shape of PE particles indicates that the replicated fragmentation of PU particles occurs during ethylene polymerization, and the monomer can continuously diffuse to the active sites within the PU particles. By optical sectioning of LSCFM, the PE particle was further investigated from top of the particle to its middle. Figure 4.5.6 c shows the homogeneous distribution of the dye throughout the PE particle, indicating the porous PU particle is well fragmented and dispersed during the ethylene polymerization. The fragmentation behavior of the PU particles implies that metallocene catalysts have been evenly immobilized over the support materials since otherwise the LSCFM would contain larger inhomogenities.

Conclusion

Metallocene-catalyzed ethylene polymerization has been performed using organic supports based on polyurethanes which possess micrometer-sized diameters with a controlled morphology, size distribution and porosity. While up to now, supports for metallocenes have always needed a two-step procedure, separating the primary and secondary particle formation. We

have demonstrated that similar supports can be created in a simple one-pot reaction. The PU microspheres can be easily adjusted in size and porosity in a nonaqueous emulsion polymerization by adding small amounts of water to form CO_2 as blowing agent. A process based on the agglomeration of nanoparticles as it is the case for silica supports or organic nanoparticles results in secondary particles with a non-spherical shape and a broad size distribution. As a replication of the shape and size is normally occurring when using them as supports in metallocene-catalyzed olefin polymerization also the products are not becoming very uniform. Industry overcomes that by sieving of the supports. Our system here is avoiding the aggregation step as the porosity of the supports is obtained by combining particle formation with a blowing process, creating micrometer size particles with a microporous structure in a one-pot reaction in a confined geometry. Further separation of the particles is not required, and they can be directly used as uniform carriers in the olefin polymerization. Other essential requirements for metallocene supports are also fulfilled by these particles. Although the porous PU particles-supported metallocene system display relatively lower activity as compared to the conventional silica support. They are fragmentable and the catalyst can be loaded within the whole particle due to the open pore structure. Although not all necessary properties to consider the microporous PU particles as a new support were fulfilled, we can address that the PU particles are advantageous in terms of tunable porosity, open pore, and isotropic shape as well as one-step procedure of support particle preparation.

Experimental

General methods and materials

All air and water sensitive reactions were performed using standard Schlenk techniques or a glovebox system under inert atmosphere. 4,4′-

Methylenebis(phenyl isocyanate) (MDI) 98 % purity, 1,4-diazabicyclo[2.2.2]octane (DABCO), 1,4-bis(hydroxymethyl)cyclohexane (BHC) and bis(2-dimethylaminoethyl)ether (BDMAEE) were purchased from Sigma-Aldrich and used as received. *N*,*N*′-Dimethylformamide (DMF) and cyclohexane were obtained from Acros organics and dried over CaH_2, and stored over molecular sieves (4 Å) after distillation. Polyisoprene-*block*-polymethyl methacrylate (PI-*b*-PMMA) copolymer was prepared using a sequential anionic polymerization technique.[207] Bis(methylcyclopentadienyl)zirconium(IV) dichloride (Aldirich, 97 %) was purchased and used as received. The cocatalyst, methylaluminoxane (MAO), was purchased from Aldrich as a 10 wt% solution in toluene and used to activate the metallocene complex. For the immobilization procedure, dried toluene (Acros) was purchased and used after further purification via distillation over Na/K and benzophenone. For ethylene polymerizations in a gas phase reactor, ethylene (Linde AG, grade 5.0) was purified by passing through sequential columns of activated 4 Å molecular sieves, BASF R3-15 deoxygenation catalyst, a $NaAlEt_4$ and an activated 4 Å molecular sieve.

Preparation of the porous polyurethane particles

The porous PU particles were synthesized by self-expansion in nonaqueous emulsion. PI-*b*-PMMA copolymer (0.210 g) was magnetically stirred in cyclohexane (15.60 g, 185 mmol) at room temperature. BHC (0.216 g, 1.50 mmol), DABCO (0.012 g, 0.10 mmol) and BDMAEE (0.050 g, 0.31 mmol) were dissolved in DMF (1.430 g, 19.5 mmol) and then added dropwise to the cyclohexane/PI-*b*-PMMA dispersion. The emulsion was treated with sonication for 15 min by a Bandelin Sonorex RK255H ultrasonic bath operating at 640 W. During sonication, a defined amount of water was added. MDI (0.400 g, 1.60 mmol) was dissolved in DMF (0.480 g, 6.50 mmol) and added dropwise to the emulsion under inert atmosphere. The

emulsion was stirred for 15 min at room temperature in order to generate polyurethane particles with a water-dependent porosity. A sample was taken out of the emulsion in order to analyze the particle size and morphology via dynamic light scattering (DLS) and scanning electron microscopy (SEM). The particles of the remaining emulsion were precipitated in methanol and separated by centrifugation to form 0.60 g of a white solid. The degree of polymerization (DP) and the polydispersities (PDI) were determined via GPC after drying the solid under vacuum.

Structural characterization of porous polyurethane particles

To determine the molecular weight and the PDI of the polyurethane gel permeation chromatography (GPC) was carried out at 30 °C using MZ-Gel SDplus 10E6, 10E4 and 500 columns in tetrahydrofuran (THF) as the eluent *vs.* PMMA standards. The detector was an ERC RI-101 differential refractometer. The composition of the block copolymers was determined by ^{1}H-NMR spectroscopy (Bruker Avance spectrometer, 300 MHz) in dichloromethane (DCM) *via* peak analysis. SEM (Zeiss Gemini 912) was performed on samples prepared via drop-casting of the particle dispersion on a silica wafer. DLS was used to determine the size of generated polyurethane particles. The measurements were performed on a Malvern Zetasizer 3000 with a fixed scattering angle of 90° and on an ALV/LSE-5004-correlator using a He/Ne-laser operating at 632.8 nm. Fourier transform infrared (FTIR) measurements were performed on a Nicolet 730 FTIR spectrometer using a thermo electron endurance attenuated total reflection (ATR) single-reflection ATR crystal. The specific BET surface area of the porous PU particles was examined by nitrogen adsorption and desorption isotherms at 77 K with a Micromeritcs Tristar II 3020 analyzer (USA).

Staining the polyurethane particles with Rhodamine B

The PU particles (100 mg) were placed in a 50 mL round-bottomed flask with 10 mL of methanol. The solution of Rhodamine B (4.7 mg, 0.01 mmol) in methanol (10 mL) was separately prepared and added to the flask. The flask was mounted on a shaker with 100 rpm at ambient temperature overnight. The solution was removed by a syringe and 20 mL of fresh methanol was added again to wash the particles. This procedure was repeated several times until there was no leaching of the dye from the particles. The Rhodamine B stained PU particles were filtered and dried under reduced pressure.

Immobilization of the metallocene catalyst on the polyurethane particles

The immobilization of the catalyst on the PU particles was carried out under inert atmosphere. The PU particles were dried overnight at elevated temperature under reduced pressure and delivered into a glovebox. The particles (0.5 g) were placed in a 50 mL Schlenk flask with 20 mL of dry toluene. In order to extract the residual water in the PU particles, the flask was mounted on a shaker at 100 rpm. After 3 h, the toluene was removed by a syringe, and 20 mL of fresh toluene was added again. This procedure was repeated 3 times. After removal of toluene from the flask, a mixture of toluene (4.0 mL) and a 1.0 M MAO solution (1.0 mL) was added into the flask and shaken for additional 3 h to make sure there was no residual water in the PU particles. The particles were washed with toluene (3 × 5 mL) prior to addition of the catalytic solution. Separately, bis(methylcyclopentadienyl)zirconium(IV) dichloride (MCP) (10 mg, 0.03 mmol) was dissolved in toluene (5 mL) and stirred for 5 min to preactivate with the addition of MAO solution. To the flask containing the PU particles, the solution of MCP/MAO complex was added at room temperature, and the flask was shaken at 100 rpm overnight. The resulting particles were washed

with toluene (3 × 5 mL) and dried under reduced pressure. The calculated support loading was estimated to be 33 µmol of Zr·(g of PU particles)$^{-1}$. The aluminum to zirconium ratio was estimated as 100:1.

Polymerization procedure in a gas phase reactor

All ethylene polymerizations were performed in a customized 100 mL volume autoclave (Premex reactor gmbh) equipped with an external heating controller and a connection line to ethylene supply. Prior to the polymerization, the autocalve (gas phase reactor) was evacuated at 80 °C at 5.0×10^{-4} mbar overnight to remove moisture and oxygen. Subsequently, the reactor was delivered to a glove box, and the PU particle-supported MCP/MAO was placed in the gas phase reactor under inert condition. After removal from the glove box, the reactor was connected with a vacuum line which had an internal ethylene supply valve. The line was heated overnight at 150 °C under reduced pressure. The reactor was heated to the desired temperature by an external heating controller. After the temperature had stabilized, ethylene polymerization was initiated by charging with a desired pressure of ethylene. The polymerizations were terminated by releasing the monomer, and subsequently, the products were exposed to air to quench the catalysts.

Characterization of polyethylene/polyurethane composites

Melting points (T_m) of products were determined by differential scanning calorimeter (DSC) using a heating rate of 10 °C/min in the temperature range of 20-200 °C. For gel permeation chromatography (GPC) measurements, the obtained polymer from the PU particles was dissolved in 1,2,4-trichlorobenzene (2.0 g/L concentration). After filtration by a glass syringe equipped with a membrane (Milipore, Miltex^{TM} membrane, 5.0 µm

LS), GPC was performed on a Waters 150-C gel permeation chromatograph at 145 °C using three TSKgel columns (two sets of TSKgelGMH$_{HR}$-H(S)HT and TSKgelGMH$_6$-HTL) with refractive index detection and calibration versus narrow polystyrene standards. For morphological observations, scanning electron microscopy (SEM) was carried out at low-voltage using a LEO 1530 Gemini, Zeiss. For stained PU particles, laser scanning confocal fluorescence microscopy (LSCFM) was performed using a Zeiss Axiovert 200M equipped with a LSM 510 ConfoCor 2. For cryo-sectioning, the particles were embedded in a mold using an epoxy resin and sectioned by a Leica ultracut UCT with a various thickness under liquid nitrogen stream. For cryo-transmission electron micrographs (TEM), the sectioned samples with 60 nm thickness were placed on a 300 mesh carbon-coated copper grid and measured with a Zeiss EM912 operating at 80 kV. The analysis of the particle diameters from SEM and TEM micrographs was carried out using the ImageJ program.

5 Annotations / Unpublished Results

5.1 Reproducible Synthesis of Poly(L-Lactide) Nanoparticles

The described methods in chapters 4.1, 4.2, and 4.3 likewise involve the ring-opening polymerization of L-lactide with 1,3-bis(2,4,6-trimethylphenyl)-2-imidazolidinylidene (SIMes) as a catalyst. Also, they describe to use a poly(isoprene)-*block*-poly(ethylene glycol) (PI-*b*-PEG) copolymer to emulsify the resulting particles in nonaqueous emulsion. The fundamental work of how to synthesize poly(L-lactide) nanoparticles in a single step, where those methods are based on, is described in my diploma thesis[12]: it comprises the challenges of finding a suitable catalyst for the ring-opening of lactide at room temperature and the synthesis of emulsifiers that stabilize a nonaqueous emulsion, while being inert to this sensitive catalyst.

5.2 Reproducible Synthesis of Poly(Urethane) Particles

In chapter 4.5, the synthesis of PU particles having different porosity and their use as a support material for ethylene polymerizations has just been described. This chapter 5.2 describes the pathway toward the reproducible generation of porous PU structures, where only the water content determines the porosity of particles.

Former group members Kevin Müller and Yi Gerkmann studied the synthesis of porous PU particles as well. Kevin Müller used BHC as the diol component, MDI as the isocyanate component, and dibutyltin diacetate (DBTDA) as catalyst[33]. As described in his dissertation[33], he succeeded in generating porous structures. Attempts to reproduce such porous structures in order to use them as a support, however, failed: particle porosity could not be achieved. The tin catalyst was strongly suggested to be the reason for the missing porosity. DBTDA strongly catalyzes the reaction of isocyanates and diols (gelation reaction) owing to the electron-withdrawing acetate groups and the resulting high Lewis acidity of the tin species[208]. To generate pores, the reaction between the isocyanate and water molecules must be promoted (blowing reaction). In general, the effectivity of water chelation by the catalyst determines its blowing selectivity: an increase in both a) the number of hydrogen-bonding sites and b) the ratio of ligands per water molecule favors the blowing reaction[208].

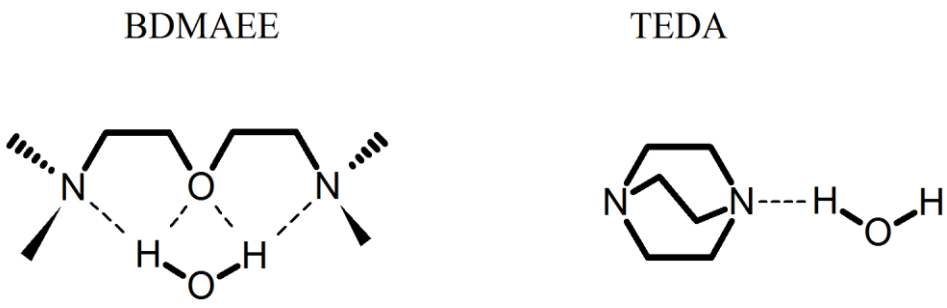

Figure 5.2.1. Scheme of water chelation by either BDMAEE or TEDA.

For example, bis(2-dimethylaminoethyl)ether (BDMAEE) has a higher blowing selectivity than triethylene diamine (TEDA)[208] - while BDMAEE possesses three binding sites and allows multidentate chelation of water[208], TEDA has two binding sites and chelates a water molecule with only one site, due to the molecule's rigidity[208] (Figure 5.2.1).

To start with, TEDA was used as a catalyst. Due to aforementioned reasons, it is a catalyst with a rather low blowing selectivity[208]. Based on Kevin Müller's work[33], BHC and MDI were reacted in a nonaqueous emulsion for 8 h at 40°C (Figure 5.2.2).

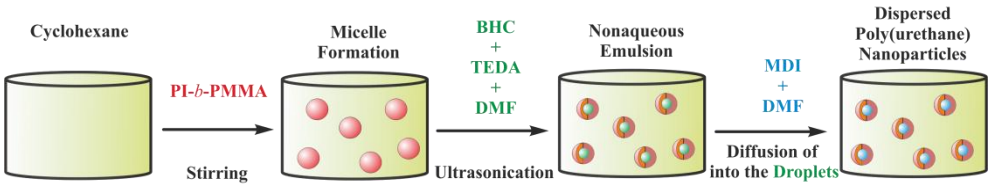

Figure 5.2.2. Scheme for the preparation of PU particles in nonaqueous emulsion.

After micelle formation, BHC and TEDA were dissolved in DMF and subsequently dispersed. The addition of MDI and its diffusion into the droplets started the polymerization. In the absence of water, the polymerization led to stably dispersed PU particles having a smooth surface (Figure 5.2.3).

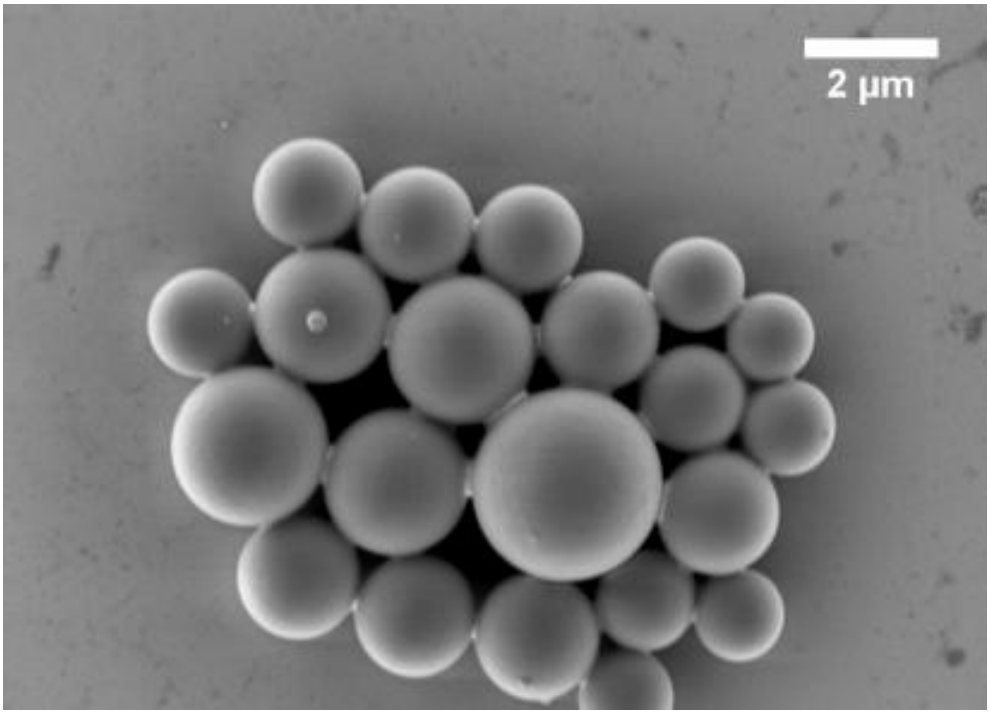

Figure 5.2.3. SEM micrograph of PU particles, synthesized in nonaqueous emulsion.

The particles were completely soluble in THF, proving the absence of hard poly(urea-urethane) segments that are caused by the blowing reaction[209]. In order to generate porous structures, the polymerization was repeated, but this time, equimolar amounts of water were added to the emulsion before polymerization. However, the resulting particles were not porous. Therefore, they were spherical and possessed a wrinkled surface (Figure 5.2.4).

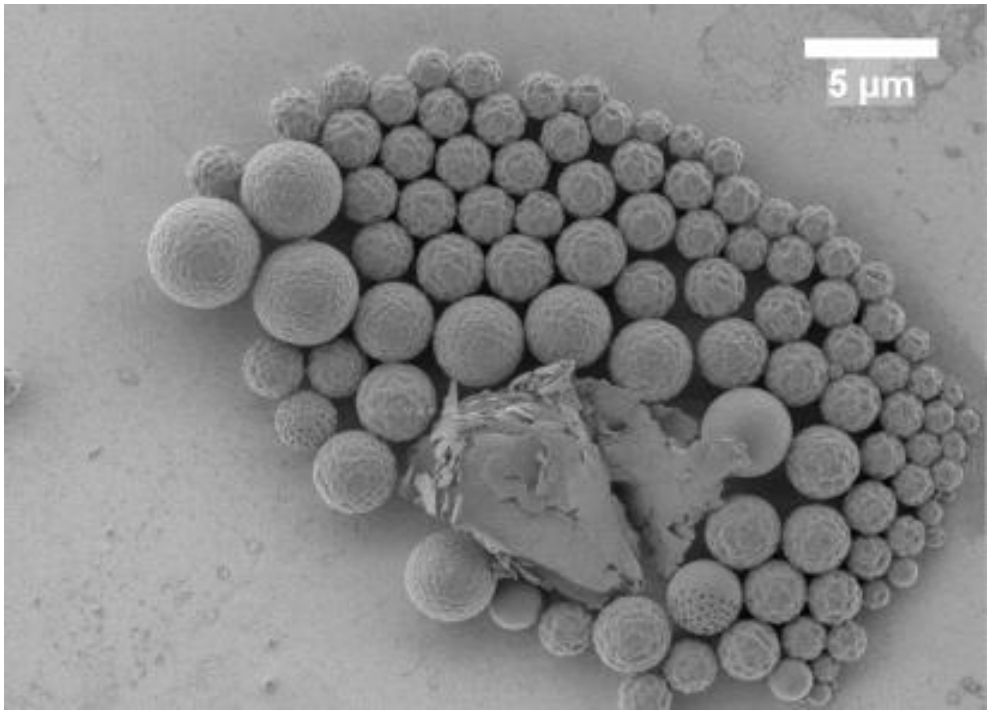

Figure 5.2.4. SEM micrograph of PU particles that were synthesized in nonaqueous emulsion, wherein equimolar amounts of water were present.

The surface topology indicated a blowing reaction at some point of the reaction. In order to elucidate whether a soluble *polymer skin* is being formed on top of porous particles, the particles were washed with THF.

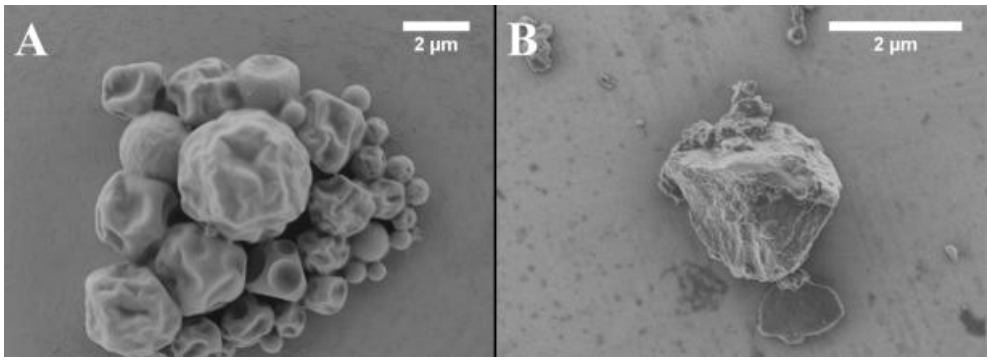

Figure 5.2.5. SEM micrograph of PU particles before (A) and after (B) THF washing.

Figure 5.2.5 shows that treatment with THF did not lead to porous structures in this case. The particle in Figure 5.2.5 B possesses an irregular and

nonporous morphology. From this observation, it was assumed that soluble PU was likely being formed on top of THF-insoluble hard poly(urea-urethane) segments[209], what indicates that the blowing reaction must have occurred rather in the beginning of the polymerization. Nonetheless, this *washing approach* was not pursued due to lack of control.

To postpone the release of CO_2 to the end of the polymerization, experiments were performed where water was added either stepwise or at the end of the experiment. However, the results did not vary from those before: particles with wrinkled surfaces were obtained. Also, changing the BHC/MDI ratio in favor of the isocyanate component to promote the blowing reaction didn't lead to porous structures. The low blowing selectivity of TEDA was suggested to be the reason for that.

Therefore, a second catalyst was introduced to the procedure: BDMAEE is a catalyst that promotes the reaction of isocyanate and water[208]. Different catalyst ratios (BDMAEE : TEDA) were studied. A polymerization with a catalyst ratio of roughly 3:1 in favor of BDMAEE turned out to finally lead to porous particles, however with a pore diameter of 1.17 ± 1.07 µm (Figure 5.2.6).

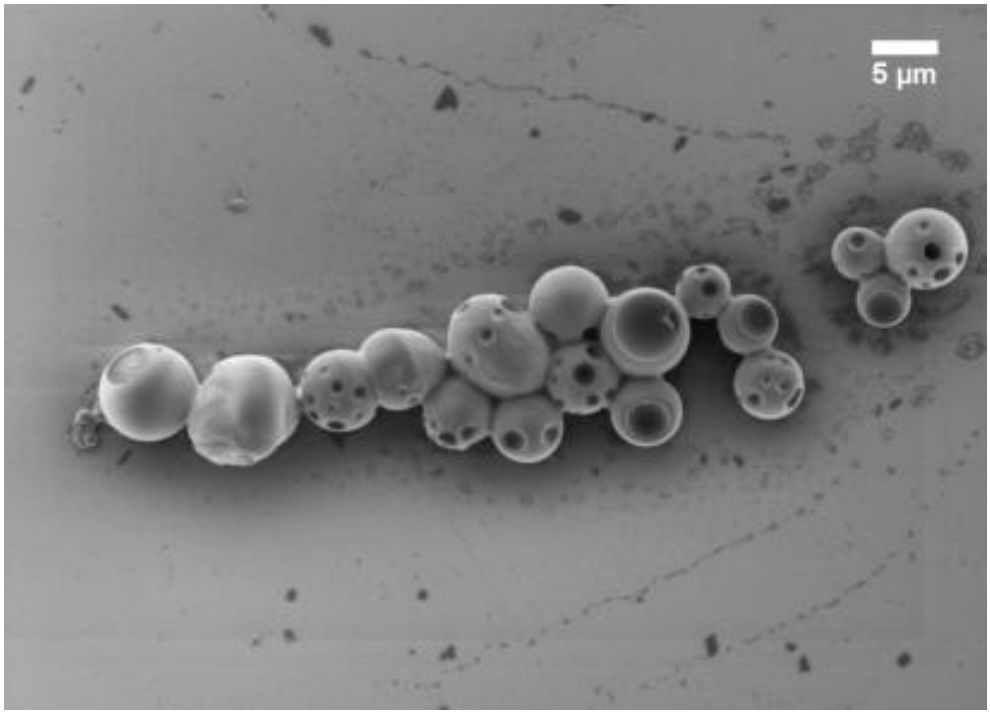

Figure 5.2.6. SEM micrograph of PU particles having craters on the particle surface (reaction time = 4 h).

The large pore size is evidence of a strong blowing reaction throughout the polymerization. However, to obtain a large surface area for catalyst immobilization, the pore size had to be decreased. Therefore, the reaction temperature was lowered from 40 °C to room temperature, since low temperatures slow down the reaction between the isocyanate and water[210]. In this way, the blowing reaction most likely occurs gradually and less intense. Furthermore, different reaction times were chosen (t = 8 h and t = 30 min) to investigate its dependence on potential pore formation.

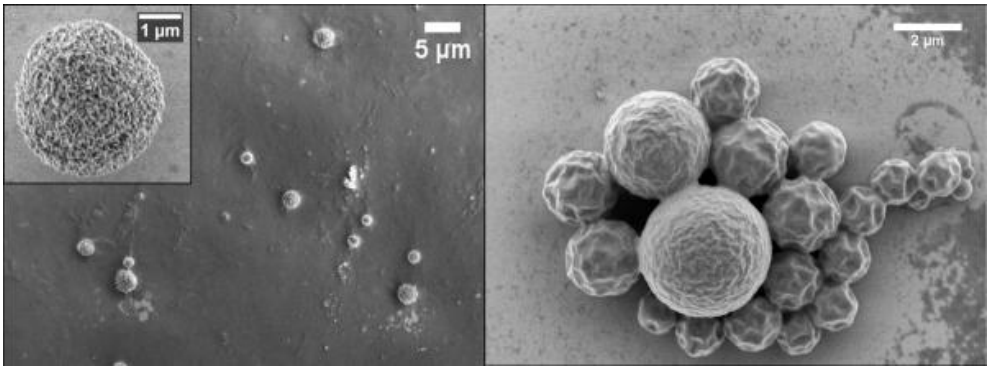

Figure 5.2.7. SEM micrographs of PU particles. Left: porous particles after a reaction time of 30 min. Right: particles after a reaction time of 8 h.

Figure 5.2.7 demonstrates that the reaction time strongly influences the particle porosity. While the reaction after 30 min gave highly porous structures (Figure 5.2.7 left), the particles after 8 h of polymerization were obviously not porous. Despite the comparatively shorter polymerization time, the molecular weight of the highly porous particles was 8700 $g \cdot mol^{-1}$, implying a conversion of > 0.99 according to Carothers equation[198]. Hence, the reaction time frame (t = 30 min) suffices for complete polymerization. The fact that the PU particles after a polymerization time of 8 h are nonporous, indicates that either the pores collapsed at some point due to energy input (strong stirring) or the polymer chains in the dispersed phase reorganized. Potential driving force for reorganization is the intermolecular formation of hydrogen bonds: poly(urea) is known to form strong hydrogen bonds[192].

The reactions were repeated three times to demonstrate reproducibility. Furthermore, reactions with different water contents demonstrated adjustable porosity (see chapter 4.5).

In conclusion, reproducible porous PU particles having tunable porosity were obtained. A combination of two catalysts (TEDA and BDMAEE) was used to ensure both a) polymers with high molecular weights and b) CO_2 formation during polymerization and a resulting porous structure. The

reaction time was demonstrated to highly influence the porosity of the particles. This reproducible synthesis of porous PU particles was further used as starting point for the production of poly(ethylene) particles, described in chapter 4.5.

6 Summary and Outlook

The nonaqueous emulsion was proven to be a highly versatile system for the generation of particles that are distinctively functionalized for the desired application.

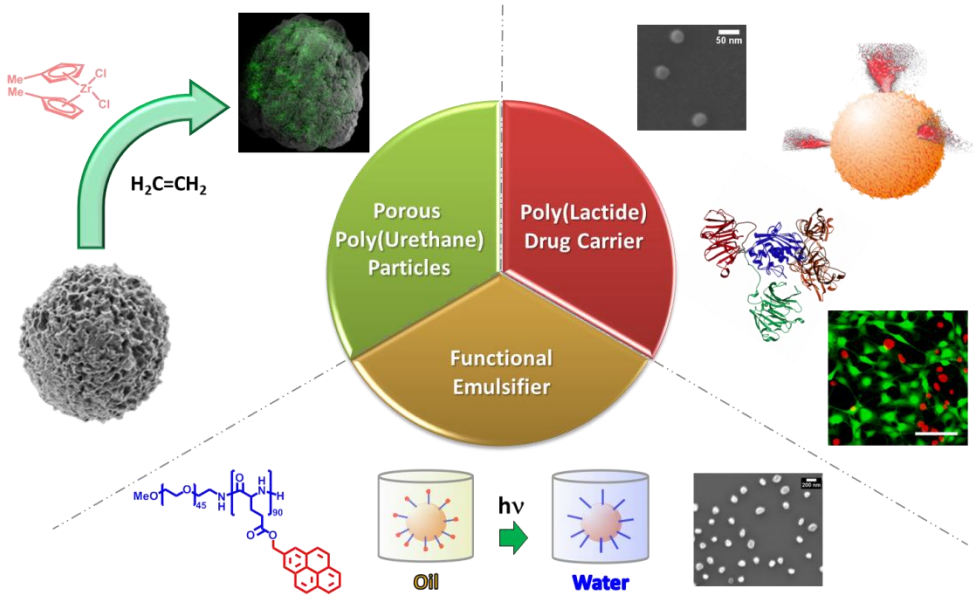

Figure 5.2.1. Overview of the achieved particle dispersions with their most striking features for a desired application.

Within this system, drug-carrying nanoparticles were accessible that showed selective drug release in tumor tissue. The approach in nonaqueous emulsion allowed for a successful moisture-sensitive polymerization of L-lactide in a single step. The resulting well-defined PLLA nanoparticles were readily transferred into aqueous medium, retaining their initial size of roughly 100 nm, which is in the ideal size range of a drug delivery system ($50 \leq d \leq 250$ nm)[104-106]. To use such particles for drug delivery, bioresponsivity had to be imparted to selectively release encapsulated drug molecules. Therefore, a peptide was designed that on the one hand contained a sequence, which is selectively cleaved by tumor-associated enzymes, and on the other hand possessed two hydroxyl groups on each side of the peptide to initiate the lactide polymerization. Owing to the

bifunctionality of the peptide, the resulting PLLA-*b*-peptide-*b*-PLLA copolymers in the particle had a predetermined breaking point in the middle of the polymer. When incubated with cancer cells, those particles showed drug release and corresponding cytotoxicity. On the contrary, particles having a scrambled peptide that is not enzymatically recognized showed no cytotoxicity, demonstrating the polymer constitution to be the only trigger for drug release.

Instead of a cleavable peptide, the use of a drug-binding peptide within the peptide sequence is conceivable: they not only stably bind drugs such as doxorubicin[211], but they also lower multi-drug resistance, which has remained a major obstacle in cancer chemotherapy[211]. Furthermore, this system might be applicable to diseases besides cancer as well, such as inflammatory diseases, which would make this design more universal. By interchanging the peptide, atherosclerosis e.g. could be addressed: various peptides were proven to target cysteine proteases (cathepsins)[212], which are overexpressed in atherosclerotic lesions[213].

In a further project, defined porous PU particles were successfully synthesized in nonaqueous emulsion and were subsequently applied as support material for ethylene polymerization. Porosity was achieved by adding water to the nonaqueous emulsion before polymerizing isocyanates and diols. The reaction of isocyanates and water causes release of gaseous carbon dioxide. The fact that the amount of water could be precisely adjusted in nonaqueous emulsion gave control over the porosity, the corresponding surface area and the amount of immobilized catalyst on the PU support. They, in turn, strongly correlated with the PE product after ethylene polymerization: while the polymerization on nonporous PU support showed low monomer consumption and resulted in comparatively small particles, ethylene polymerization on porous PU supports led to significantly larger PE particles. A microscopic fragmentation study of

dye-labeled particles before and after ethylene polymerization demonstrated full fragmentation only in the case of porous PU supports.

Despite the advantages of tunable porosity, the isotropic shape and the one-step procedure of support synthesis, the PU particle cannot be considered as profitable substitute for conventional silica supports in a large-scale production due to its significantly lower reactivity.

Within this dissertation, the synthesis and application of a PEG-*b*-PGlu(Pyr) copolymer as efficient emulsifier for the PLLA particle formation in a nonpolar solvent was demonstrated. Upon UV irradiation and subsequent removal of hydrophobic pyrenyl methyl units from hydrophilic PGlu, the particle's surface polarity was reversed from hydrophobic to hydrophilic. As a result, the PLLA particles were effectively dispersed in water without aggregation and further surfactants. The biocompatibility of the emulsifier's constituents (PEG and PGlu) was assessed and proven by cell viability studies.

This new emulsifier is likely applied to other particle dispersions that require transfer into aqueous medium. Within Chapter 4.4 it was strongly suggested that entanglement of polymer chains (PLLA) with PEG-*b*-PGlu(Pyr) copolymers must occur, in order to achieve particle stabilization by the entirely hydrophilic PEG-*b*-PGlu copolymer in water (after UV irradiation). Such entanglement is likely occurring in other polymerizations as well. But, what about bead structures which can't entangle, such as inorganic nanoparticles? Therefore, a functional group is conceivable at the terminal position of the PEG block to achieve covalent bonding of the emulsifier to the particle surface. In case of gold nanoparticles, a thiol group in this position might afford this kind of attachment. This allows for particle stabilization in organic solvent, wherein gold nanoparticles are synthesized, and light-induced particle transfer into water without the conventional addition of a further surfactant[149].

So far, the aggregation issue while transferring the particles from nonaqueous into aqueous medium dominated the benefits of a nonaqueous approach, such as the broad portfolio of techniques and applicable components. Therefore, multi-step approaches including final immersion of dissolved polymer into an aqueous surfactant solution remain predominant in the literature. The new biocompatible emulsifier design, however, proved to be applicable for the generation of particles in nonaqueous medium and their stabilization in aqueous medium, without aggregation. So now the benefits of the nonaqueous approach overweigh. As a result, this method will potentially become a common tool for future custom-designed particle dispersions that are borne in organic solvent and are applied as aqueous dispersion.

7 Supporting Information

Contents:

4.2: Biocompatible Polylactide-*block*-Polypeptide-*block*-Polylactide Nanocarrier

4.3: Polylactide-*block*-Polypeptide-*block*-Polylactide Copolymer Nanoparticles with Tunable Cleavage and Controlled Drug Release

4.4: Polarity Reversal of Nanoparticle Surfaces by the Use of UV-Sensitive Emulsifiers

7.1 To 4.2: Biocompatible Polylactide-block-Polypeptide-block-Polylactide Nanocarrier

General Remarks

All solvents and reagents were purchased from Sigma Aldrich if not stated otherwise. The poly(isoprene)-*block*-poly(ethylene oxide) (PI-*b*-PEO) copolymer was prepared using a sequential anionic polymerization technique.[82] L-lactide and 1,3-bis(2,4,6-trimethylphenyl)-2-imidazolidinylidene (SIMes) were used as received. SIMes was stored under inert atmosphere at -20 °C. Lutensol AP 20 was obtained from BASF SE in Ludwigshafen. To determine the molecular weight and the molecular weight distribution (MWD) of the polylactide peptide conjugate a gel permeation chromatography (GPC) was carried out at 30 °C using MZ-Gel SDplus 10E6, 10E4 and 500 columns in tetrahydrofuran (THF) as eluent vs. polystyrene standards. The detector was an ERC RI-101 differential refractometer. The composition of the block copolymers was determined by ^{1}HNMR spectroscopy in deuterated dichloromethane (DCM-d2) via peak analysis, using a Bruker Avance III spectrometer operating at 700 MHz. The structure of the polylactide peptide conjugate was investigated via ^{1}HNMR spectroscopy and diffusion ordered spectroscopy (DOSY) in deuterated dimethylsulfoxide (DMSO-d6). For a ^{1}HNMR spectrum 128 transients were used with an 13,8 µs long 90° pulse and a 12600 Hz spectral width together with a recycling delay of 5 s. The temperature was kept at 298.3 K and regulated by a standard ^{1}H methanol NMR sample using the Topspin 3.1 software (Bruker). The DOSY (Diffusion Ordered Spectroscopy) experiments were done with a 5 mm BBI ^{1}H/X z-gradient probe and a gradient strength of 5.516 [G/mm] on the 700 MHz spectrometer. In this work, the gradient strength was 32 steps from 2 % to 100 %. The diffusion time d20 was optimized to 80 ms and the gradient length p30 was kept at 1.4 ms. Scanning electron microscopy

(SEM) images were taken using a Zeiss Gemini 912 microscope. The SEM sample preparation proceeded the following way: the nanoparticles were dispersed in cyclohexane and drop casted on a silica wafer. The average diameters of the particles visualized in SEM images were determined by diameter measurements of 100 randomly chosen particles. Dynamic light scattering (DLS) was used to determine the droplet size of the investigated emulsions and the size of generated polylactide-peptide nanoparticles. The measurements were performed on a Malvern Zetasizer 3000 with a fixed scattering angle of 90° and on an ALV/LSE-5004-correlator using a He/Ne-laser operating at 632.8 nm.

Typical preparation of labeled Poly(L-lactide)-b-Peptide-b-Poly(L-lactide) Nanoparticles

PI-*b*-PEO copolymer (0.050 g) was magnetically stirred in cyclohexane (14.4 g, 171 mmol) at room temperature. L-lactide (76.0 mg, 0.53 mmol) and 9-bromo-*N*-(2,5,8,11,15,18,21,24-octaoxapentacosan-13-yl)perylene-3,4-dicarboxy monoimide (PMI) (0.30 mg, 0.39 µmol) were dissolved in acetonitrile (0.230 g, 5.59 mmol) and then added dropwise to the cyclohexane/PI-*b*-PEO dispersion. The emulsion was formed by treatment with sonication for 15 min using a Bandelin Sonorex RK255H ultrasonic bath operating at 640 W. SIMes (9.36 mg, 30.6 µmol) and the peptide (15.3 µmol) were dissolved in acetonitrile (0.176 g, 4.29 mmol) and added dropwise to the emulsion under inert atmosphere. The emulsion was stirred for 15 min at room temperature to produce poly(L-lactide)-*block*-peptide-*block*-poly(L-lactide) (PLLA-*b*-peptide-*b*-PLLA) nanoparticles. A sample was taken out of the emulsion in order to analyze the particle size and morphology via DLS and SEM. 5 ml of the emulsion were precipitated in methanol, separated by centrifugation and dried *in vacuo*. The methanol

solution was investigated through UV/Vis spectroscopy in order to determine the amount of non-encapsulated dye. The orange colored polymer was investigated via NMR spectroscopy and via GPC. Furthermore, this solid was investigated by HPLC analysis in order to determine the encapsulation efficiency.

The remaining emulsion was mixed with a 0.05 wt-% Lutensol AP 20 solution in order to disperse the obtained particles in aqueous medium. The organic solvents were evaporated and the aqueous dispersion was dialyzed against deionized water for 3 days in order to remove unreacted components and organic solvents. Two samples were taken out of the emulsion: One sample was diluted with water and investigated via DLS and SEM to study the morphology. The other sample was dried *in vacuo* and the resulting solid was analyzed via GPC and NMR spectroscopy. The remaining aqueous dispersion was used for cell uptake experiments.

Synthesis and Characterization of 9-Bromo-N-(2,5,8,11,15,18,21,24-octaoxapentacosan-13-yl)perylene-3,4-dicarboxy monoimide (PMI)

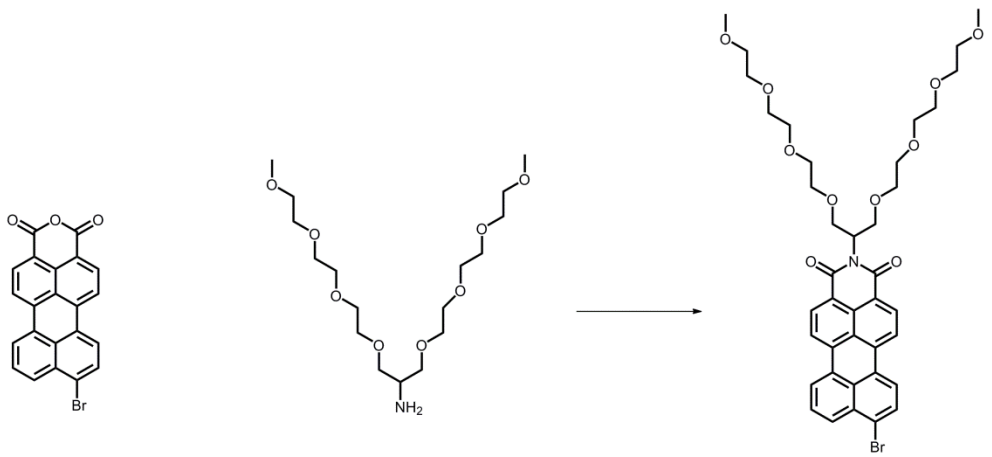

2 **3** **1**

Scheme 7.1.1. PMI **1** was synthesized according to the literature[214] by reaction of 9-bromo-3,4-perylenedicarboxylic anhydride **2** with the TEG swallow-tailed amine **3** in

molten imidazol. The TEG swallow-tailed amine 3 was synthesized according to the literature.[214]

9-Bromo-perylenedicarboxymonoimide (**2**) (0.400 g, 1.00 mmol), 2,5,8,11,15,18,21,24-octaoxapentacosane-13-amine (**3**) (0.573 g, 1.53 mmol) and zinc acetate (0.182 mg, 1.00 mmol) were mixed in a flask containing 3 g of imidazole and 0.5 mL of propionic acid. The reaction mixture was heated up to 130°C for 12 hours. After cooling to room temperature, the mixture was triturated with 200 mL hydrochloric acid (1.0 M) and then filtered. The solid was dissolved in dichloromethane and the precipitate was removed by filtration. After evaporating the solvent, the material is purified via column chromatography (silica gel, CH_2Cl_2/acetone/MeOH 30/5/1) and obtained as a dark red solid (0.200 g, 0.26 mmol) in 26% yield.

PMI (1)

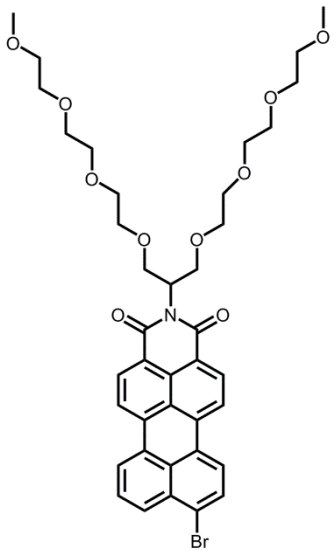

1

^{1}H-NMR (300 MHz, CD_2Cl_2, 293 K)

d[ppm]: 8.37 (br, 2H), 8.22 (d, 1H), 8.15 (m, 2H), 8.07 (d, 1H), 7.97 (d, 1H), 7.77 (d, 1H), 7.61 (t, 1H), 5.64 (m, 1H), 4.18 (m, 2H), 3.96 (m, 2H), 3.74 – 3.56 (m, 8H), 3.54 – 3.39 (m, 16H), 3.26 (s, 6H).

^{13}C-NMR (300 MHz, CD_2Cl_2, 293 K)

d[ppm]: 164.65, 136.51, 136.34, 133.09, 131.61, 130.18, 130.02, 129.81, 129.28, 128.54, 126.39, 126.32, 124.72, 124.04, 121.93, 121.03, 120.76, 72.40, 71.07, 71.01, 70.98, 70.88, 70.02, 59.12, 52.69.

FD-MS

m/z (%): 765.0 (100), calculated for $C_{39}H_{44}BrNO_{10}$: 765.2

Synthesis and Characterization of the peptides

(L)-peptide Ac-SWWWWWS-NH_2 was prepared via microwave-assisted solid-phase peptide synthesis (SPPS) with an automated synthesizer (Liberty, CEM) on rink amide resins using standard Fmoc (Fluorenylmethoxycarbonyl)-amino acids. The peptides were purified by reversed phase solid-phase extraction (Sep-Pak C18, Waters) and characterized by ^{1}H-NMR (nuclear magnetic resonance), MALDI-ToF (matrix assisted laser desorption ionization-time of flight) and RP-HPLC (reversed phase-high performance liquid chromatography).

Ac-SWWWWWS-NH_2

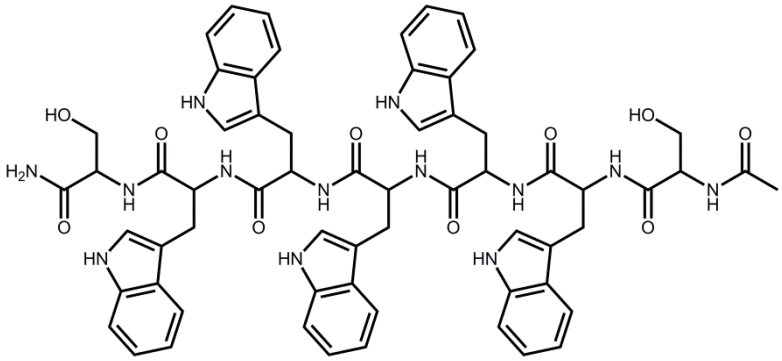

^{1}H-NMR (300 MHz, DMSO-d6, 293 K)

d[ppm]: 10.74 (br, 5H), 8.10 – 7.83 (m, 7H), 7.53 (m, 5H), 7.30 (m, 5H), 7.17 - 6.87 (m, 18H), 5.10 (t, 1H), 4.85 (t, 1H), 4.59 – 4.45 (m, 5H), 4.28 (q, 1H), 4.20 (dt, 1H), 3.64 – 3.61 (m, 2H), 3.54 – 3.48 (m, 2H), 3.18 – 2.82 (m, 10H), 1.81 (s, 3H).

MALDI-ToF

m/z (%):1187.0 (100), calculated for $C_{63}H_{65}N_{13}NaO_{10}$: 1187.3

Characterization of PLLA-b-(Ac)SWWWWWS(NH_2)-b-PLLA structure by NMR

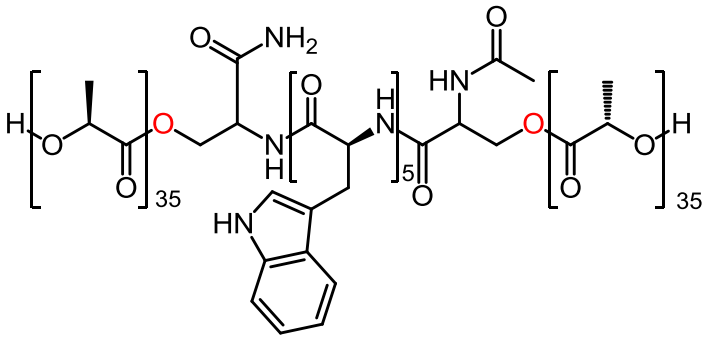

[1]H-NMR Study(700 MHz, DMSO-d6, 293 K)

d[ppm]: 10.72 (br, 5H), 8.35 – 7.85 (m, 7H), 7.53 (m, 5H), 7.30 – 7.14 (m, 10H), 7.02 (m, 10H), 6.92 (m, 5H), 5.20 (q, 79H), 4.59 – 4.45 (m, 5H), 4.25 (m, 2H), 3.82 – 3.75 (m, 3H), 3.67 – 3.64 (m, 1H), 3.18 – 2.82 (m, 10H), 2.01 (s, 3H), 1.47 (d, 237H).

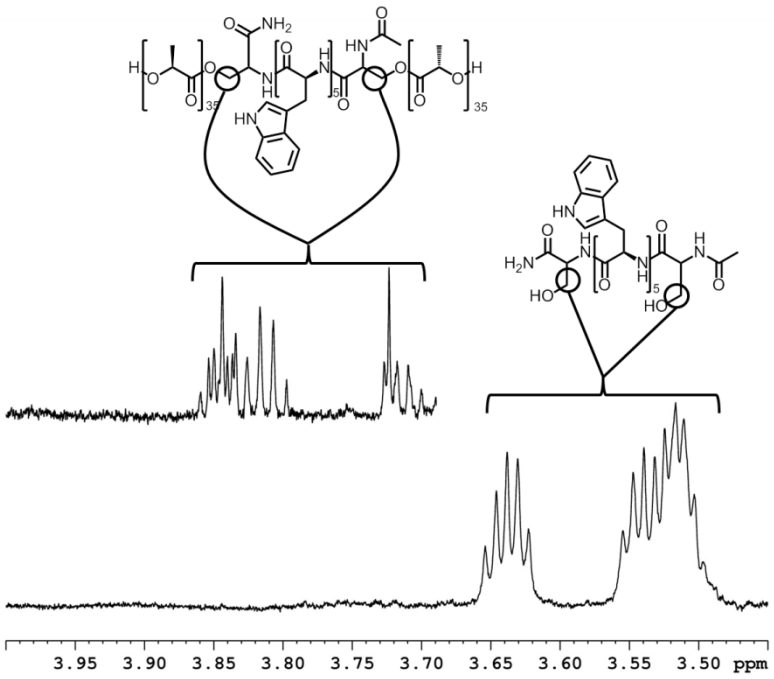

Figure 7.1.1. ^{1}H-NMR spectra of PLLA-b-(Ac)SWWWWWS(NH_2)-b-PLLA (top left) and Ac-SWWWWWS-NH_2 (bottom right) in DMSO-d6; Chemical shift area of the signals corresponding to the methylene protons in both serine groups.

A significant downfield shift of the signals, displayed in Figure 7.1.1, corresponds to the methylene protons in both serine groups of the initiating peptide Ac-SWWWWWS-NH_2 after polymerization. This proves the successful initiation of the lactide polymerization by both serine units.

Diffusion Ordered Spectroscopy (DOSY) Study (700 MHz, DMSO-d6, 293 K)

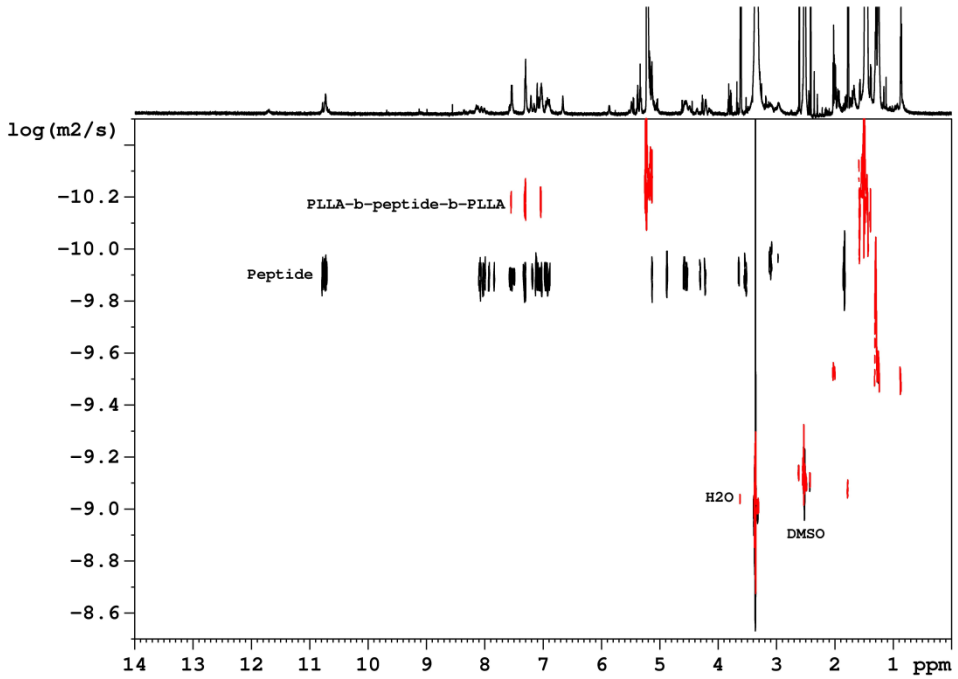

Figure 7.1.2. DOSY spectra of PLLA-b-(Ac)SWWWWWS(NH_2)-b-PLLA (top, red) and Ac-SWWWWWS-NH_2 (bottom, black) in DMSO-d6.

The superimposed DOSY spectra of PLLA-*b*-peptide-*b*-PLLA and Ac-SWWWWWS-NH_2 in Figure 7.1.2 prove a covalent attachment of the Ac-SWWWWWS-NH_2 peptide to the polylactide chain after polymerization, since the polylactide signals and the peptide signals in the polymer possessed the same diffusion coefficient. In addition the polymer composite retains a lower diffusion than the non-attached peptide.

Encapsulation Efficiency through High-Pressure-Liquid-Chromatography (HPLC)

The HPLC analysis was carried out with a reversed phase HD C8 column (Macherey-Nagel) using a series 1100 pump (Hewlett Packard). The components, containing in the particles, were detected by a UV-Vis detector S-3702 (Soma). The encapsulation efficiency was calculated by

determination of the PMI concentration in the solid and its comparison to the applied amount of PMI before the polymerization.

Cellular Uptake Assays

HeLa cells (below passage 6) were used for cellular uptake assays. Cells were cultured in standard media, DMEM with low glucose (1 mg/mL) (GIbco: Paisley, UK) and 10% fetal bovine serum (Gibco: Paisley, UK) without antibiotics. Cells were grown to near confluence in tissue culture T125 flasks before trypsinization and plating at a density of 2000 cells/cm^2 on sterilized 22 x 22 mm glass coverslips. After a 24-hour incubation period, cells were incubated with a 1:30 dilution (vol/vol) of nanoparticle solution for 12 hours. This was independently determined to be the maximal concentration of particles without substantial cytotoxicity. Following incubation, cells were washed 3X in PBS, fixed in 4% paraformaldehyde in PBS for 30 minutes, and washed in 3X PBS. Samples were imaged after fixation with no further preparation by mounting the coverslip against a glass slide with two pieces of double-sided tape (Tesa: Amsterdam, The Netherlands) under hydrated conditions.

Cellular Uptake Imaging

All cellular uptake microscopy was performed on a Leica SP 5 II TCS CARS (Leica Microsystems GmbH, Wetzlar, Germany) microscope equipped with transmitted and reflected light photomultiplier tubes (PMT). Nanoparticles were detected using laser-based, multiphoton fluorescence in the reflected (epi) PMT while the transmitted PMT was used for forward, label-free coherent anti-Stokes Raman scattering (CARS) microscopy. The excitation for CARS was a picosecond 1064 nm and 817 nm laser while multiphoton fluorescence used the 817 nm laser alone. Both detection paths

utilized the standard Leica filter sets. Briefly, CARS is a multi-photon coherent Raman microscopy technique that derives contrast from the chemical nature of the sample itself without labels. Using this imaging system, we targeted the CH-stretching vibration in CARS to image the cell borders and intracellular membranes while imaging the multiphoton fluorescence in the epi PMT. Care was taken to make sure that both PMT gains were below 900 to avoid detector nonlinearity. All images were acquired with a Nikon 60X 1.49 NA TIRF objective and subsequently analyzed with ImageJ.

Nanoparticle Fluorescence Imaging

Nanoparticle suspensions (1:1300 in Ethanol) were dried on glass coverslips and imaged in the epi direction using multiphoton fluorescence with the Leica SP 5 II TCS CARS instrument as described above. These images were acquired with the Nikon 1.49 NA TIRF objective. To study the fluorescent properties of the labeled PLLA-*b*-peptide-*b*-PLLA nanoparticles, the particles were physisorbed onto glass coverslips and investigated using two-photon fluorescence (TPEF) microscopy (Methods). A picosecond 817 nm laser was used to excite the PMI encapsulated within the particles, which has a single photon absorbance maximum near 500 nm. The fluorescence response was collected in the spectral range from 545-755 nm, taking care to block the excitation beam.

7.2 To 4.3: Polylactide-*block*-Polypeptide-*block*-Polylactide Copolymer Nanoparticles with Tunable Cleavage and Controlled Drug Release

Supplemental Figures:

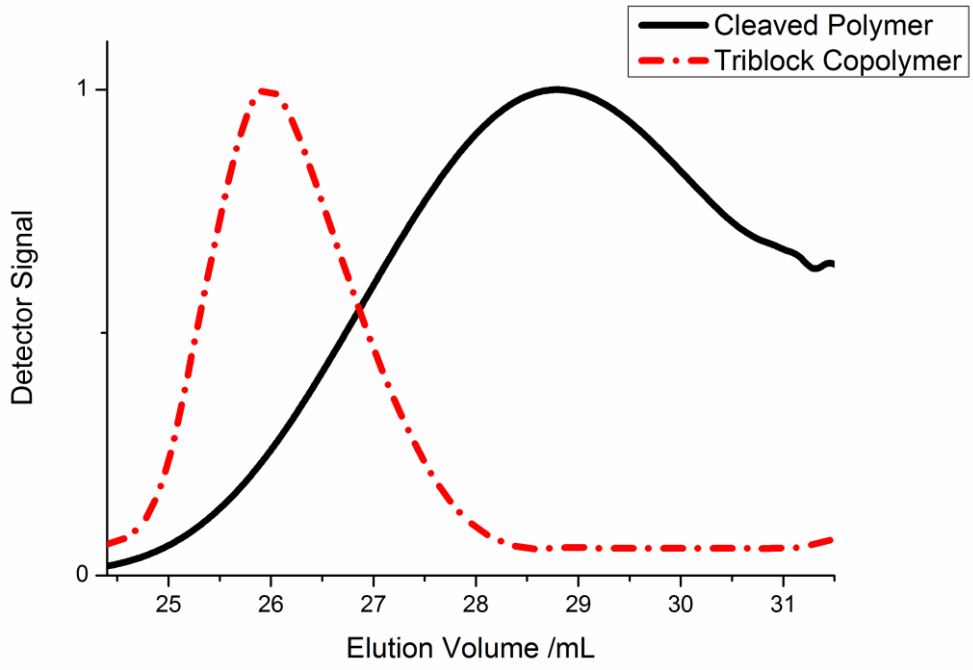

Figure 7.2.1. Normalized GP chromatograms of PLGLAG nanoparticles before (red) and after MMP-2 incubation (blue).

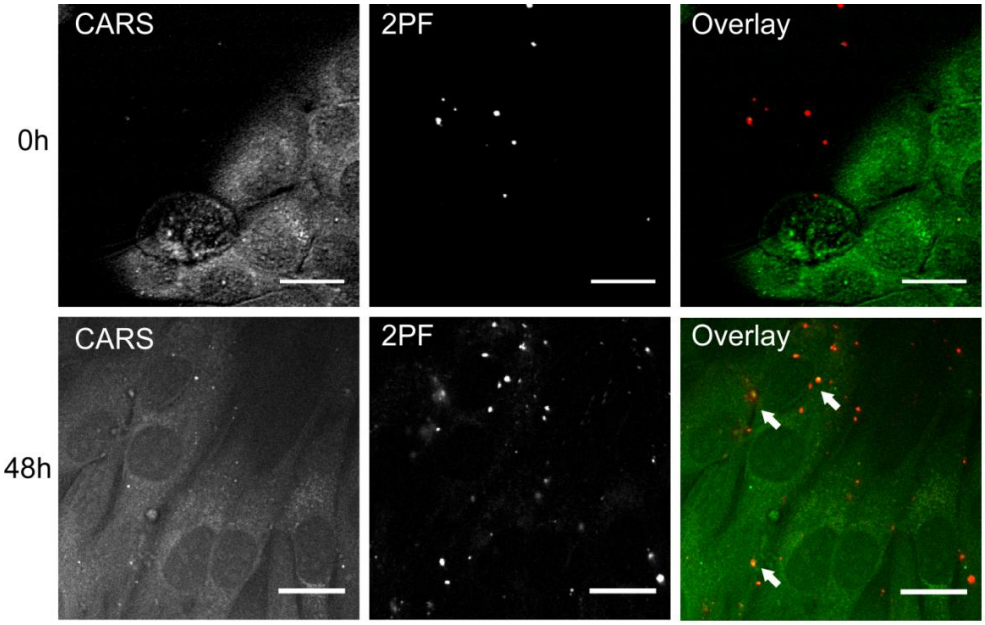

Figure 7.2.2. CARS and two-photon fluorescence images of cultured C2C12 myoblasts directly after addition of PLGLAG (upper panel) and after 48h of culture (lower panel). CARS signal is derived exclusively from symmetric vibrations of CH_2 modes of acyl chains, thus highlighting membranes and lipid deposits. Multiphoton excitation allows detection of fluorescent PMI dye loaded into the PLGLAG particles. Over time, PMI was seen to associate with cells, and predominantly in the vicinity lipid deposits, highlighted by the yellow appearance (arrows). Scale bar = 20 µm.

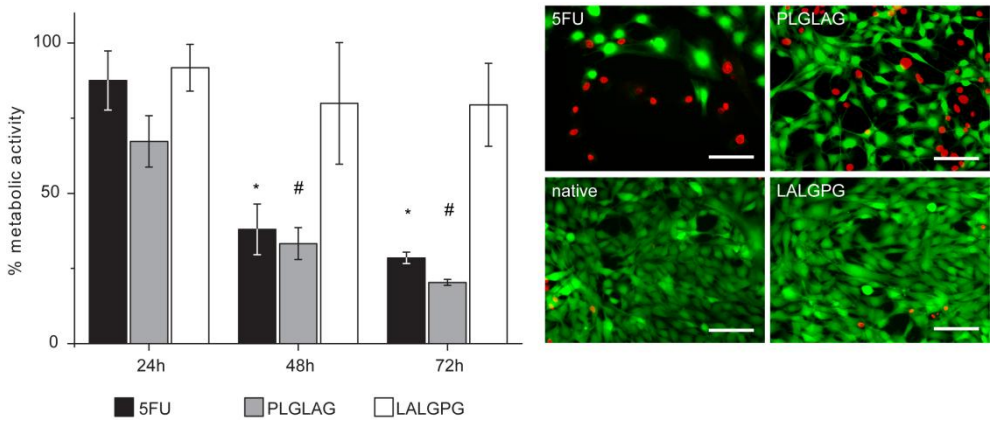

Figure 7.2.3. Time dependence of cytotoxicity with 5-FU loaded nanocarriers. 5-FU samples were administered 10 µg/mL drug directly in the media. * and # mark statistically significant differences ($p < 0.05$) relative to the corresponding sample at 24 h. Error bars are standard deviation from three experiments. Pictures show live (green) and dead (red) cells after 72 h incubation. Scale bar = 100 µm.

7.3 To 4.4: Polarity Reversal of Nanoparticle Surfaces by the Use of UV-Sensitive Emulsifiers

General Remarks

All solvents and reagents were purchased from Sigma Aldrich if not stated otherwise. α-methoxy-ω-amino-poly(ethylene glycol) (PEG-NH_2) (M_n ~ 2000 g·mol^{-1}) was purchased from Rapp Polymere. L-lactide and 1,3-bis(2,4,6-trimethylphenyl)-2-ididazolidinylidene (SIMes) were used as received. SIMes was stored under inert atmosphere at -20 °C. To determine the polydispersity index (PDI) of block copolymers and poly(L-lactide) a gel permeation chromatography (GPC) was carried out at 30 °C using MZ-Gel SDplus 10E6, 10E4 and 500 columns in tetrahydrofuran (THF) as eluent vs. polystyrene standards. The detector was an ERC RI-101 differential refractometer. The molecular weight of the block copolymers and poly(L-lactide) was determined by ^{1}H NMR spectroscopy in deuterated dichloromethane (DCM-d2) via end-group analysis, using a Bruker Avance III spectrometer operating at 700 MHz. The structure of the block copolymers was investigated via diffusion ordered spectroscopy (DOSY) in deuterated dimethylsulfoxide (DMSO-d6). For a ^{1}H NMR spectrum 128 transients were used with an 13.8 µs long 90° pulse and a 12600 Hz spectral width together with a recycling delay of 5 s. The temperature was kept at 298.3 K and regulated by a standard ^{1}H methanol NMR sample using the

Topspin 3.1 software (Bruker). The DOSY experiments were done with a 5 mm BBI ^{1}H/X z-gradient probe and a gradient strength of 5.516 [G/mm] on the 700 MHz spectrometer. In this work, the gradient strength was 32 steps from 2 % to 100 %. The diffusion time d20 was optimized to 80 ms and the gradient length p30 was kept at 1.4 ms. Scanning electron microscopy (SEM) images were taken using a Zeiss Gemini 912 microscope. The SEM sample preparation proceeded the following way: the nanoparticles were dispersed in cyclohexane and drop casted on a silica wafer. The average diameters of the particles visualized in SEM images were determined by diameter measurements of 100 randomly chosen particles. Dynamic light scattering (DLS) was used to determine the mean size of generated self-assemblies and nanoparticles (number distribution). The DLS measurements were performed on a Malvern Zetasizer 3000 with a fixed scattering angle of 90° and on an ALV/LSE-5004-correlator using a He/Ne-laser operating at 632.8 nm.

Supplemental Table:

Table 7.3.1. Hydrodynamic diameters of block copolymer aggregates in cyclohexane and copolymer stabilized PLLA nanoparticles in cyclohexane, respectively, water.

	D_h (Number) /nm	D_h (Volume) /nm	D_h (Intensity) /nm
PEG-*b*-PGlu(Pyr) in Cyclohexane	99 ± 38	105 ± 31	106 ± 34
PEG-*b*-PGlu(Pyr) PLLA Particles in Cyclohexane	130 ± 19	148 ± 34	140 ± 8
PEG-*b*-PGlu PLLA Particles in Water	199 ± 6	203 ± 9	202 ± 10

Supplemental Figures:

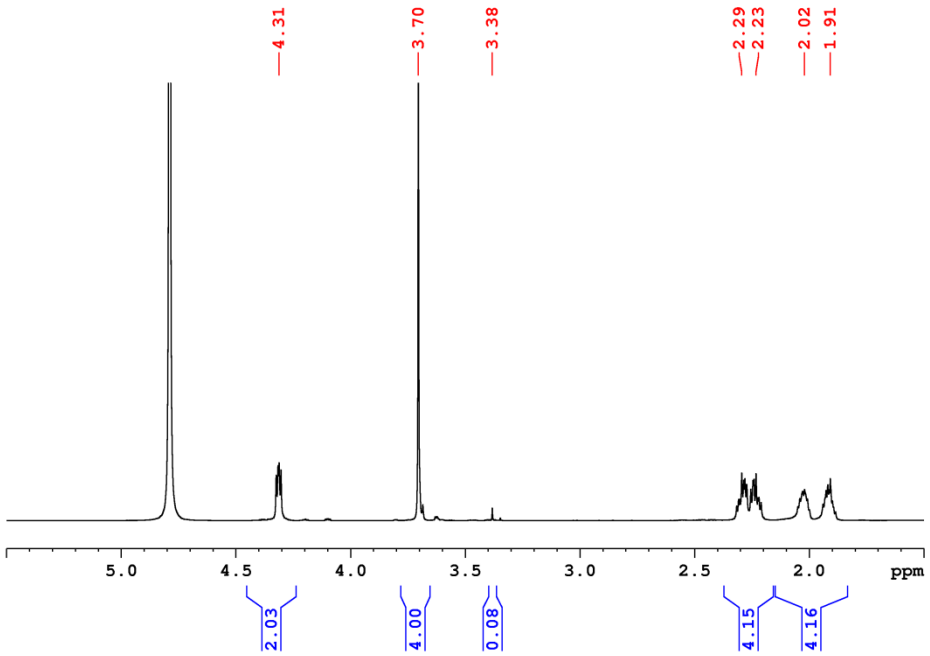

Figure 7.3.1. ^{1}H NMR spectrum of PEG-b-PGlu copolymer (4) in D_2O.

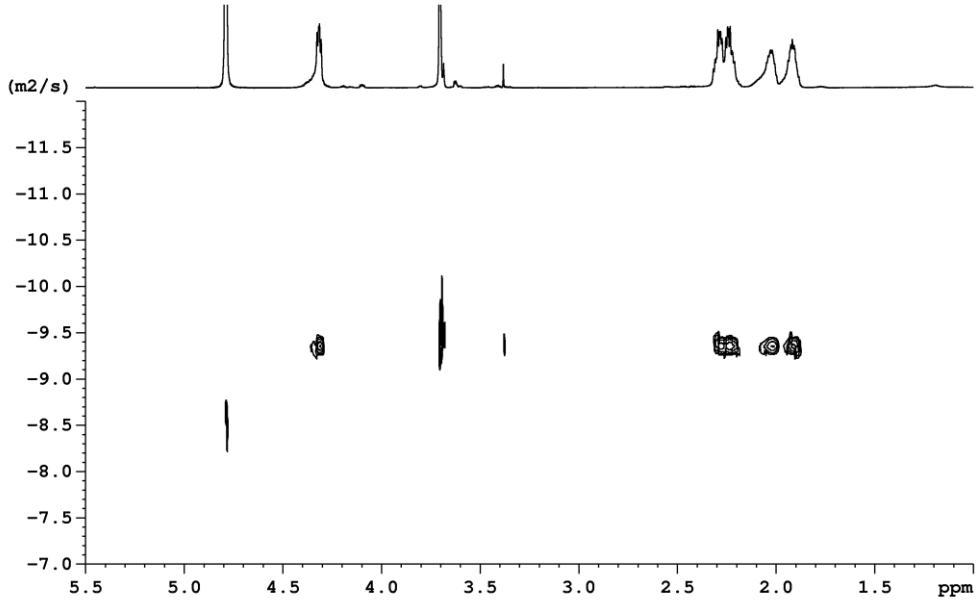

Figure 7.3.2. Diffusion ordered spectrum of PEG-b-PGlu copolymer (4) in D_2O.

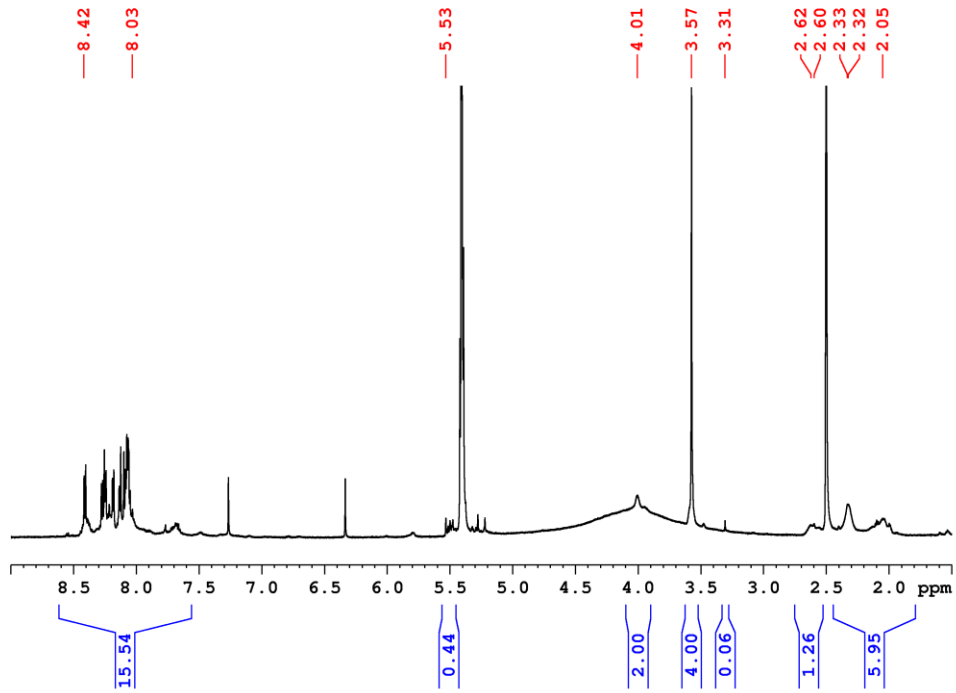

Figure 7.3.3. ^{1}H NMR spectrum of PEG-b-PGlu(Pyr) copolymer before deprotection in D_2O.

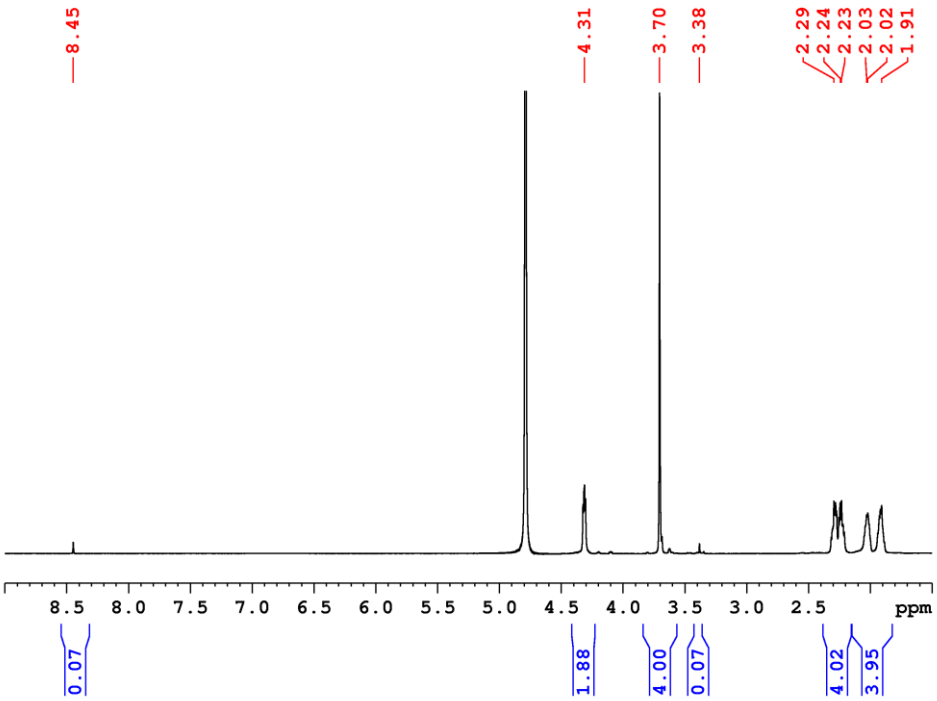

Figure 7.3.4. ^{1}H NMR spectrum of PEG-b-PGlu(Pyr) copolymer after deprotection in D_2O.

8 References

[1] D. J. Siegwart, A. Srinivasan, S. A. Bencherif, A. Karunanidhi, J. K. Oh, S. Vaidya, R. Jin, J. O. Hollinger, K. Matyjaszewski, *Biomacromolecules* **2009**, *10*, 2300-2309.

[2] J. Andrieu, N. Kotman, M. Maier, V. Mailänder, W. S. L. Strauss, C. K. Weiss, K. Landfester, *Macromol. Rapid Commun.* **2012**, *33*, 248-253.

[3] K. Müller, M. Klapper, K. Müllen, *Colloid Polym. Sci.* **2007**, *285*, 1157-1161.

[4] S. Kawaguchi, K. Ito, **2005**, *175*, 299-328.

[5] E. S. Daniels, E. D. Sudol, M. S. El-Aasser, *Vol. 801*, ACS Publications, **2001**, pp. 1-12.

[6] A. Nel, T. Xia, L. Madler, N. Li, *Science* **2006**, *311*, 622-627.

[7] L. Zhang, F. X. Gu, J. M. Chan, A. Z. Wang, R. S. Langer, O. C. Farokhzad, *Clin. Pharmacol. Ther.* **2008**, *83*, 761-769.

[8] P. A. Lovell, M. S. El-Aasser, P. Lovell, *Emulsion polymerization and emulsion polymers*, Wiley Chichester, UK, **1997**.

[9] C.-S. Chern, *Principles and applications of emulsion polymerization*, John Wiley & Sons, **2008**.

[10] B. Tieke, *Makromolekulare Chemie*, Wiley-VCH, **2005**.

[11] D. Distler, *Wäßrige polymerdispersionen: synthese, eigenschaften, anwendungen*, Wiley-VCH Weinheim, **1999**.

[12] R. Dorresteijn, Johannes Gutenberg-Universität (Mainz), **2011**.

[13] R. Haschick, Johannes Gutenberg-Universität (Mainz), **2011**.

[14] M. I. Volz.

[15] V. Holzapfel, Universität Ulm, Fakultät für Naturwissenschaften **2006**.

[16] H. D. Dörfler, *Grenzflächen und kolloid-disperse Systeme: Physik und Chemie*, Springer, **2002**.

[17] K. Landfester, *Nachrichten aus der Chemie* **2008**, *56*, 649-652.

[18] J. Periard, A. Banderet, G. Riess, *J. Polym. Sci. B Polym. Lett.* **1970**, *8*, 109-114.

[19] J. Periard, G. Riess, *Colloid Polym. Sci.* **1973**, *251*, 97-102.

[20] J. Periard, G. Riess, *Colloid Polym. Sci.* **1975**, *253*, 362-372.

[21] G. Riess, J. Nervo, D. Rogez, *Polym. Eng. Sci.* **1977**, *17*, 634-638.

[22] V. G. Riess, J. Kohler, C. Tournut, A. Banderet, *Die Makromolekulare Chemie* **1967**, *101*, 58-73.

[23] N. R. Cameron, D. C. Sherrington, *J. Chem. Soc., Faraday Trans.* **1996**, *92*, 1543-1547.

[24] A. Imhof, D. Pine, *J. Colloid Interface Sci.* **1997**, *192*, 368-374.

[25] N. Bechthold, F. Tiarks, M. Willert, K. Landfester, M. Antonietti, *Vol. 151*, Wiley Online Library, **2000**, pp. 549-555.

[26] K. Mueller, *Johannes-Gutenberg Universität Mainz* **2008**.

[27] K. Muller, M. Klapper, K. Mullen, *Macromol. Rapid Commun.* **2006**, *27*, 586-593.
[28] G. Riess, C. Labbe, *Macromol. Rapid Commun.* **2004**, *25*, 401-435.
[29] T. Nicolai, O. Colombani, C. Chassenieux, *Soft Matter* **2010**, *6*, 3111-3118.
[30] K. Müller, M. Klapper, K. Müllen, *J. Polym. Sci. A Polym. Chem.* **2007**, *45*, 1101-1108.
[31] K. Müller, M. K. Park, M. Klapper, W. Knoll, K. Müllen, *Macromol. Chem. Phys.* **2007**, *208*, 1394-1401.
[32] C. M. Hansen, *Hansen solubility parameters*, CRC Press, **1999**.
[33] K. Müller, Johannes Gutenberg-Universität Mainz, Fachbereich 09: Chemie, Pharmazie und Geowissenschaft **2008**.
[34] R. Haschick, M. Klapper, K. B. Wagener, K. Müllen, *Macromol. Chem. Phys.* **2010**, *211*, 2547-2554.
[35] M. Klapper, S. Nenov, R. Haschick, K. Muller, K. Mullen, *Acc. Chem. Res.* **2008**, *41*, 1190-1201.
[36] N. Bechthold, Universitätsbibliothek **2000**.
[37] E. J. Anglin, L. Cheng, W. R. Freeman, M. J. Sailor, *Adv Drug Deliv Rev* **2008**, *60*, 1266-1277.
[38] R. Langer, *Nature* **1998**, *392*, 5-10.
[39] A. Krais, L. Wortmann, L. Hermanns, N. Feliu, M. Vahter, S. Stucky, S. Mathur, B. Fadeel, *Nanomedicine: Nanotechnology, Biology and Medicine* **2014**, *10*, 1421-1431.
[40] H. Wang, J. Wu, J. Li, Y. Ding, G. Shen, R. Yu, *Biosens. Bioelectron.* **2005**, *20*, 2210-2217.
[41] A. G. Wu, P. Ou, L. Y. Zeng, *NANO* **2010**, *5*, 245-270.
[42] Y. I. Chung, J. C. Kim, Y. H. Kim, G. Tae, S. Y. Lee, K. Kim, I. C. Kwon, *J. Controlled Release* **2010**, *143*, 374-382.
[43] R. Tong, L. Tang, Q. Yin, J. Cheng, in *Engineering in Medicine and Biology Society, EMBC, 2011 Annual International Conference of the IEEE*, IEEE, **2011**, pp. 8337-8339.
[44] *BCC Research Global Markets and Technologies for Advanced Drug Delivery Systems; Report Code: PHM006J;* **Published: January 2014**, *http://www.bccresearch.com/market-research/pharmaceuticals/advanced-drug-delivery-markets-phm006j.html [Accessed: January 2015]*.
[45] B. Gupta, T. S. Levchenko, V. P. Torchilin, *Adv Drug Deliv Rev* **2005**, *57*, 637-651.
[46] C. H. Heldin, K. Rubin, K. Pietras, A. Ostman, *Nat. Rev. Cancer* **2004**, *4*, 806-813.
[47] A. E. Nel, L. Mädler, D. Velegol, T. Xia, E. M. Hoek, P. Somasundaran, F. Klaessig, V. Castranova, M. Thompson, *Nat. Mater.* **2009**, *8*, 543-557.
[48] J. Zupanc, J. Valant, A. Dobnikar, V. Kralj-Iglic, A. Iglic, D. Drobne, in *Engineering in Medicine and Biology Society, 2009.*

EMBC 2009. Annual International Conference of the IEEE, IEEE, **2009**, pp. 1400-1403.
[49] J. Park, W. Lu, *Phys. Rev. E Stat. Nonlin. Soft Matter Phys.* **2009**, *80*, 021607.
[50] L. J. McCawley, L. M. Matrisian, *Mol. Med. Today* **2000**, *6*, 149-156.
[51] G. Chen, T. G. Gharib, C. C. Huang, D. G. Thomas, K. A. Shedden, J. M. Taylor, S. L. Kardia, D. E. Misek, T. J. Giordano, M. D. Iannettoni, M. B. Orringer, S. M. Hanash, D. G. Beer, *Clin. Cancer Res.* **2002**, *8*, 2298-2305.
[52] H. Ishiguro, N. Nakaigawa, Y. Miyoshi, K. Fujinami, Y. Kubota, H. Uemura, *Prostate* **2005**, *64*, 92-100.
[53] A. Sehgal, C. Keener, A. L. Boynton, J. Warrick, G. P. Murphy, *J. Surg. Oncol.* **1998**, *69*, 99-104.
[54] V. Papa, B. Gliozzo, G. M. Clark, W. L. McGuire, D. Moore, Y. Fujita-Yamaguchi, R. Vigneri, I. D. Goldfine, V. Pezzino, *Cancer Res.* **1993**, *53*, 3736-3740.
[55] C. Grüttner, K. Müller, J. Teller, F. Westphal, A. Foreman, R. Ivkov, *J. Magn. Magn. Mater.* **2007**, *311*, 181-186.
[56] S. Y. Chae, S. Son, M. Lee, M. K. Jang, J. W. Nah, *J. Control. Release* **2005**, *109*, 330-344.
[57] L. Brannon-Peppas, J. O. Blanchette, *Adv. Drug Delivery Rev.* **2012**, *64*, 206-212.
[58] R. Duncan, *Nat. Rev. Drug Discovery* **2003**, *2*, 347-360.
[59] R. Haag, *Angew. Chem., Int. Ed.* **2004**, *43*, 278-282.
[60] D. F. Hayes, A. D. Thor, L. G. Dressler, D. Weaver, S. Edgerton, D. Cowan, G. Broadwater, L. J. Goldstein, S. Martino, J. N. Ingle, I. C. Henderson, L. Norton, E. P. Winer, C. A. Hudis, M. J. Ellis, D. A. Berry, Cancer, B. I. Leukemia Group, *N. Engl. J. Med.* **2007**, *357*, 1496-1506.
[61] K. Müller, M. Klapper, K. Müllen, *Macromol. Rapid Commun.* **2006**, *27*, 586-593.
[62] G. Dvorakova, R. Haschick, K. Chiad, M. Klapper, K. Müllen, A. Biffis, *Macromol. Rapid Commun.* **2010**, *31*, 2035-2040.
[63] R. Haschick, K. Mueller, M. Klapper, K. Muellen, *Macromolecules* **2008**, *41*, 5077-5081.
[64] A. Finne-Wistrand, A.-C. Albertsson, *Annu. Rev. Mater. Res.* **2006**, *36*, 369-395.
[65] S. Karlsson, A.-c. Albertsson, *Polym. Eng. Sci.* **1998**, *38*, 1251-1253.
[66] G. M. Kim, Y. H. Bae, W. H. Jo, *Macromol. Biosci.* **2005**, *5*, 1118-1124.
[67] F. Chécot, S. Lecommandoux, Y. Gnanou, H.-A. Klok, *Angewandte Chemie International Edition* **2002**, *41*, 1339-1343.
[68] F. Checot, S. Lecommandoux, H. A. Klok, Y. Gnanou, *The European physical journal. E, Soft matter* **2003**, *10*, 25-35.

[69] T. Jiang, E. S. Olson, Q. T. Nguyen, M. Roy, P. A. Jennings, R. Y. Tsien, *Proc. Natl. Acad. Sci. U. S. A.* **2004**, *101*, 17867-17872.
[70] M. Vert, S. Li, G. Spenlehauer, P. Guerin, *J. Mater. Sci.: Mater. Med.* **1992**, *3*, 432-446.
[71] J. Sarasua, A. L. Arraiza, P. Balerdi, I. Maiza, *Polym. Eng. Sci.* **2005**, *45*, 745-753.
[72] A. Sodergard, *Vol. 627*, ACS Publications, **1996**, pp. 103-117.
[73] O. Dechy-Cabaret, B. Martin-Vaca, D. Bourissou, *Chem. Rev.* **2004**, *104*, 6147-6176.
[74] N. E. Kamber, W. Jeong, R. M. Waymouth, R. C. Pratt, B. G. G. Lohmeijer, J. L. Hedrick, *Chem. Rev.* **2007**, *107*, 5813-5840.
[75] E. F. Connor, G. W. Nyce, M. Myers, A. Möck, J. L. Hedrick, *J. Am. Chem. Soc.* **2002**, *124*, 914-915.
[76] J. Kadota, D. Pavlovic , J. P. Desvergne, B. Bibal, F. Peruch, A. Deffieux, *Macromolecules* **2010**, *43*, 5010-5030.
[77] P. Legrand, S. Lesieur, A. Bochot, R. Gref, W. Raatjes, G. Barratt, C. Vauthier, *Int. J. Pharm.* **2007**, *344*, 33-43.
[78] R. Tong, J. Cheng, *J. Am. Chem. Soc.* **2009**, *131*, 4744-4754.
[79] M. Ueda, J. Kreuter, *J. Microencapsulation* **1997**, *14*, 593-605.
[80] J. Vandervoort, A. Ludwig, *Int. J. Pharm.* **2002**, *238*, 77-92.
[81] R. Haschick, M. Klapper, K. B. Wagener, K. Mullen, *Macromol. Chem. Phys.* **2010**, *211*, 2547-2554.
[82] O. Tcherkasskaya, S. Ni, M. A. Winnik, *Macromolecules* **1996**, *29*, 610-616.
[83] O. Coulembier, B. G. G. Lohmeijer, A. P. Dove, R. C. Pratt, L. Mespouille, D. A. Culkin, S. J. Benight, P. Dubois, R. M. Waymouth, J. L. Hedrick, *Macromolecules* **2006**, *39*, 5617-5628.
[84] A. P. Dove, R. C. Pratt, B. G. Lohmeijer, R. M. Waymouth, J. L. Hedrick, *J. Am. Chem. Soc.* **2005**, *127*, 13798-13799.
[85] D. A. Culkin, W. Jeong, S. Csihony, E. D. Gomez, N. P. Balsara, J. L. Hedrick, R. M. Waymouth, *Angew. Chem.* **2007**, *119*, 2681-2684.
[86] G. W. Nyce, T. Glauser, E. F. Connor, A. Möck, R. M. Waymouth, J. L. Hedrick, *J. Am. Chem. Soc.* **2003**, *125*, 3046-3056.
[87] M. Save, M. Schappacher, A. Soum, *Macromol. Chem. Phys.* **2002**, *203*, 889-899.
[88] J. R. Dorgan, J. Janzen, D. M. Knauss, S. B. Hait, B. R. Limoges, M. H. Hutchinson, *J. Polym. Sci., Part B: Polym. Phys.* **2005**, *43*, 3100-3111.
[89] D. Garlotta, *J. Polym. Environ.* **2001**, *9*, 63-84.
[90] A. Kowalski, A. Duda, S. Penczek, *Macromolecules* **1998**, *31*, 2114-2122.
[91] S. Csihony, D. A. Culkin, A. C. Sentman, A. P. Dove, R. M. Waymouth, J. L. Hedrick, *J. Am. Chem. Soc.* **2005**, *127*, 9079-9084.
[92] C. Geidel, S. Schmachtel, A. Riedinger, C. Pfeiffer, K. Müllen, M. Klapper, W. Parak, *Small* **2011**.
[93] S. Wang, W. Cui, J. Bei, *Anal. Bioanal. Chem.* **2005**, *381*, 547-556.

[94] K. Zhu, L. Xiangzhou, Y. Shilin, *J. Appl. Polym. Sci.* **1990**, *39*, 1-9.
[95] K. Kataoka, A. Harada, Y. Nagasaki, *Adv. Drug Delivery Rev.* **2001**, *47*, 113-131.
[96] N. Nasongkla, E. Bey, J. Ren, H. Ai, C. Khemtong, J. S. Guthi, S.-F. Chin, A. D. Sherry, D. A. Boothman, J. Gao, *Nano Lett.* **2006**, *6*, 2427-2430.
[97] H. Bader, H. Ringsdorf, B. Schmidt, *Ang. Makromol. Chem.* **1984**, *123*, 457-485.
[98] E. S. Gil, S. M. Hudson, *Prog. Polym. Sci.* **2004**, *29*, 1173-1222.
[99] Y. Zhang, M. K. So, J. Rao, *Nano Lett.* **2006**, *6*, 1988-1992.
[100] E. S. Olson, T. Jiang, T. A. Aguilera, Q. T. Nguyen, L. G. Ellies, M. Scadeng, R. Y. Tsien, *Proc. Natl. Acad. Sci. U. S. A.* **2010**, *107*, 4311-4316.
[101] T. J. Harris, G. von Maltzahn, M. E. Lord, J.-H. Park, A. Agrawal, D.-H. Min, M. J. Sailor, S. N. Bhatia, *Small* **2008**, *4*, 1307-1312.
[102] C. Bremer, C.-H. Tung, R. Weissleder, *Nat. Med.* **2001**, *7*, 743-478.
[103] H. Chen, C. Khemtong, X. Yang, X. Chang, J. Gao, *Drug Discov. Today* **2011**, *16*, 354-360.
[104] W. E. Bawarski, E. Chidlowsky, D. J. Bharali, S. A. Mousa, *Nanomed.* **2008**, *4*, 273-282.
[105] K. Cho, X. Wang, S. Nie, D. M. Shin, *Clin. Cancer Res.* **2008**, *14*, 1310-1316.
[106] D. F. Emerich, C. G. Thanos, *Biomol. Eng.* **2006**, *23*, 171-184.
[107] S. Matsumura, I. Aoki, T. Saga, K. Shiba, *Mol. Pharm.* **2011**, *8*, 1970-1974.
[108] R. Dorresteijn, R. Haschick, M. Klapper, K. Müllen, *Macromol. Chem. Phys.* **2012**, *213*, 1996-2002.
[109] H. Lee, J. B. Park, J. Y. Chang, *J. Polym. Sci., Part A: Polym. Chem.* **2011**, *49*, 2859-2865.
[110] S. Koeller, J. Kadota, A. Deffieux, F. d. r. Peruch, S. p. Massip, J.-M. Léger, J.-P. Desvergne, B. Bibal, *J. Am. Chem. Soc.* **2009**, *131*, 15088-15089.
[111] G. Li, M. Lamberti, M. Mazzeo, D. Pappalardo, G. Roviello, C. Pellecchia, *Organometallics* **2012**, *31*, 1180-1188.
[112] G. R. J. Müller, C. Meiners, V. Enkelmann, Y. Geerts, K. Müllen, *J. Mater. Chem.* **1998**, *8*, 61-64.
[113] Y. Zagranyarski, L. Chen, Y. Zhao, H. Wonneberger, C. Li, K. Müllen, *Org. Lett.* **2012**, *14*, 5444-5447.
[114] P. Xu, E. Gullotti, L. Tong, C. B. Highley, D. R. Errabelli, T. Hasan, J.-X. Cheng, D. S. Kohane, Y. Yeo, *Mol. Pharmaceutics* **2008**, *6*, 190-201.
[115] Y. J. Lee, D. Moon, K. B. Migler, M. T. Cicerone, *Anal. Chem.* **2011**, *83*, 2733-2739.
[116] J.-X. Cheng, Y. K. Jia, G. Zheng, X. S. Xie, *Biophys. J.* **2002**, *83*, 502-509.
[117] J.-X. Cheng, X. S. Xie, *J. Phys. Chem. B* **2003**, *108*, 827-840.

[118] C. L. Evans, E. O. Potma, M. Puoris'haag, D. Côté, C. P. Lin, X. S. Xie, *Proc. Natl. Acad. Sci. U. S. A.* **2005**, *102*, 16807-16812.
[119] G. Rago, C. M. Langer, C. Brackman, J. P. R. Day, K. F. Domke, N. Raschzok, C. Schmidt, I. M. Sauer, A. Enejder, M. T. Mogl, M. Bonn, *Biomed. Opt. Express* **2011**, *2*, 2470-2483.
[120] G. Rago, B. Bauer, F. Svedberg, L. Gunnarsson, M. B. Ericson, M. Bonn, A. Enejder, *J. Phys. Chem. B* **2011**, *115*, 5008-5016.
[121] Y. Takakura, M. Hashida, *Crit. Rev. Oncol. Hematol.* **1995**, *18*, 207-231.
[122] F. Yuan, M. Dellian, D. Fukumura, M. Leunig, D. A. Berk, V. P. Torchilin, R. K. Jain, *Cancer Res.* **1995**, *55*, 3752-3756.
[123] M. Maier, N. Kotman, C. Friedrichs, J. Andrieu, M. Wagner, R. Graf, W. S. L. Strauss, V. Maila□nder, C. K. Weiss, K. Landfester, *Macromolecules* **2011**.
[124] E. S. Olson, T. A. Aguilera, T. Jiang, L. G. Ellies, Q. T. Nguyen, E. H. Wong, L. A. Gross, R. Y. Tsien, *Integr. Biol.* **2009**, *1*, 382-393.
[125] G. W. M. Vandermeulen, H.-A. Klok, *Macromol. Biosci.* **2004**, *4*, 383-398.
[126] M. L. Becker, J. Liu, K. L. Wooley, *Biomacromolecules* **2004**, *6*, 220-228.
[127] R. M. Broyer, G. N. Grover, H. D. Maynard, *Chem. Commun.* **2011**, *47*, 2212-2226.
[128] M. L. Becker, J. Liu, K. L. Wooley, *Chem. Commun.* **2003**, 180-181.
[129] P. Rivera-Gil, S. De Koker, B. G. De Geest, W. J. Parak, *Nano Lett.* **2009**, *9*, 4398-4402.
[130] M. Chanana, P. Rivera_Gil, M. A. Correa-Duarte, L. M. Liz-Marzán, W. J. Parak, *Angew. Chem., Int. Ed.* **2013**, *52*, 4179-4183.
[131] M. Maier, N. Kotman, C. Friedrichs, J. Andrieu, M. Wagner, R. Graf, W. S. L. Strauss, V. Maila□nder, C. K. Weiss, K. Landfester, *Macromolecules* **2011**, *44*, 6258-6267.
[132] Y. Huang, Y. Jiang, H. Wang, J. Wang, M. C. Shin, Y. Byun, H. He, Y. Liang, V. C. Yang, *Adv. Drug Delivery Rev.* **2013**, *65*, 1299-1315.
[133] R. Dorresteijn, R. Ragg, G. Rago, N. Billecke, M. Bonn, S. H. Parekh, G. Battagliarin, K. Peneva, M. Wagner, M. Klapper, K. Müllen, *Biomacromolecules* **2013**, *14*, 1572-1577.
[134] K. Kazunori, K. Glenn S, Y. Masayuki, O. Teruo, S. Yasuhisa, *J. Controlled Release* **1993**, *24*, 119-132.
[135] S. Kherif, C. Lafuma, M. Dehaupas, S. Lachkar, J.-G. Fournier, M. Verdière-Sahuqué, M. Fardeau, H. S. Alameddine, *Dev. Biol.* **1999**, *205*, 158-170.
[136] J. Fried, A. G. Perez, J. M. Doblin, B. D. Clarkson, *Cancer Res.* **1981**, *41*, 2627-2632.
[137] P. A. McCarron, A. D. Woolfson, D. F. McCafferty, J. H. Price, H. Sidhu, G. I. Hickey, *Int. J. Pharm.* **1997**, *151*, 69-74.

[138] S. Yamamoto, H. Tanaka, T. Kanamori, M. Nobuhara, M. Namba, *Cancer Lett.* **1983**, *20*, 131-138.
[139] J. W. Krumpfer, T. Schuster, M. Klapper, K. Müllen, *Nano Today* **2013**, *8*, 417-438.
[140] D. Hühn, K. Kantner, C. Geidel, S. Brandholt, I. De Cock, S. J. H. Soenen, P. Rivera_Gil, J.-M. Montenegro, K. Braeckmans, K. Müllen, G. U. Nienhaus, M. Klapper, W. J. Parak, *ACS Nano* **2013**, *7*, 3253-3263.
[141] J. F. Kukowska-Latallo, K. A. Candido, Z. Cao, S. S. Nigavekar, I. J. Majoros, T. P. Thomas, L. P. Balogh, M. K. Khan, J. R. Baker, *Cancer Res.* **2005**, *65*, 5317-5324.
[142] W. H. De Jong, P. J. Borm, *Int. J. Nanomed.* **2008**, *3*, 133-149.
[143] Q. A. Pankhurst, J. Connolly, S. K. Jones, J. Dobson, *J Phys D Appl Phys* **2003**, *36*, R167-R181.
[144] F. Debuigne, L. Jeunieau, M. Wiame, J. B.Nagy, *Langmuir* **2000**, *16*, 7605-7611.
[145] D. Horn, J. Rieger, *Angewandte Chemie International Edition* **2001**, *40*, 4330-4361.
[146] K. Margulis-Goshen, S. Magdassi, *Curr. Opin. Colloid Interface Sci.* **2012**, *17*, 290-296.
[147] M. Antonietti, K. Landfester, *Prog. Polym. Sci.* **2002**, *27*, 689-757.
[148] R. Dorresteijn, N. Billecke, M. Schwendy, S. Pütz, M. Bonn, S. H. Parekh, M. Klapper, K. Müllen, *Adv. Funct. Mater.* **2014**, *24*, 4026-4033.
[149] C. Geidel, S. Schmachtel, A. Riedinger, C. Pfeiffer, K. Müllen, M. Klapper, W. J. Parak, *Small* **2011**, *7*, 2929-2934.
[150] J. Jiang, X. Tong, Y. Zhao, *J. Am. Chem. Soc.* **2005**, *127*, 8290-8291.
[151] N. Chowdhury, S. Dutta, S. Dasgupta, N. D. Singh, M. Baidya, S. K. Ghosh, *Photochem. Photobiol. Sci.* **2012**, *11*, 1239-1250.
[152] J. W. Meyer, G. S. Hammond, *J. Am. Chem. Soc.* **1972**, *94*, 2219-2228.
[153] W. H. Daly, D. Poche, *Tetrahedron Lett.* **1988**, *29*, 5859-5862.
[154] R. Obeid, C. Scholz, *Biomacromolecules* **2011**, *12*, 3797-3804.
[155] L. Kaufner, R. Cartier, R. Wustneck, I. Fichtner, S. Pietschmann, H. Bruhn, D. Schutt, A. F. Thunemann, U. Pison, *Nanotechnology* **2007**, *18*, 115710.
[156] U. Paiphansiri, J. Dausend, A. Musyanovych, V. Mailander, K. Landfester, *Macromol. Biosci.* **2009**, *9*, 575-584.
[157] F. Eeckman, A. J. Moës, K. Amighi, *J. Controlled Release* **2003**, *88*, 105-116.
[158] D. Yang, Y. Dai, P. Ma, X. Kang, Z. Cheng, C. Li, J. Lin, *Chemistry* **2013**, *19*, 2685-2694.
[159] D. Stefanakis, D. F. Ghanotakis, *Journal of Nanoparticle Research* **2010**, *12*, 1285-1297.

[160] C. Moyuan, J. Haixia, Y. Weijuan, L. Peng, W. Liqun, J. Hongliang, *J. Appl. Polym. Sci.* **2012**, *123*, 3137-3144.
[161] B.-J. Kim, S.-G. Oh, M.-G. Han, S.-S. Im, *Synth. Met.* **2001**, *122*, 297-304.
[162] M. Mori, N. Kawakubo, M. Wakabayashi, *Fish. Sci.* **2002**, *68*, 1124-1128.
[163] H. Sinn, W. Kaminsky, in *Adv. Organomet. Chem., Vol. Volume 18* (Eds.: F. G. A. Stone, W. Robert), Academic Press, **1980**, pp. 99-149.
[164] W. Kaminsky, *Macromolecular Chemistry and Physics* **1996**, *197*, 3907-3945.
[165] P. C. Möhring, N. J. Coville, *Journal of Organometallic Chemistry* **1994**, *479*, 1-29.
[166] H. H. Brintzinger, D. Fischer, R. Mülhaupt, B. Rieger, R. M. Waymouth, *Angewandte Chemie International Edition in English* **1995**, *34*, 1143-1170.
[167] F. Langhauser, J. Kerth, M. Kersting, P. Kölle, D. Lilge, P. Müller, *Die Angewandte Makromolekulare Chemie* **1994**, *223*, 155-164.
[168] J. R. Severn, J. C. Chadwick, R. Duchateau, N. Friederichs, *Chemical Reviews* **2005**, *105*, 4073-4147.
[169] B. Heurtefeu, C. Bouilhac, É. Cloutet, D. Taton, A. Deffieux, H. Cramail, *Progress in Polymer Science* **2011**, *36*, 89-126.
[170] G. Fink, B. Steinmetz, J. Zechlin, C. Przybyla, B. Tesche, *Chemical Reviews* **2000**, *100*, 1377-1390.
[171] M. Koch, A. Falcou, N. Nenov, M. Klapper, K. Müllen, *Macromolecular Rapid Communications* **2001**, *22*, 1455-1462.
[172] V. F. Tisse, F. Prades, R. Briquel, C. Boisson, T. F. L. McKenna, *Macromolecular Chemistry and Physics* **2010**, *211*, 91-102.
[173] R. Quijada, R. Rojas, L. Alzamora, J. Retuert, F. M. Rabagliati, *Catalysis Letters* **1997**, *46*, 107-112.
[174] J. C. W. Chien, D. He, *Journal of Polymer Science Part A: Polymer Chemistry* **1991**, *29*, 1603-1607.
[175] J.-H. Yim, K.-J. Chu, K.-W. Choi, S.-K. Ihm, *European Polymer Journal* **1996**, *32*, 1381-1385.
[176] T. Uozumi, T. Toneri, K. Soga, T. Shiono, *Macromolecular Rapid Communications* **1997**, *18*, 9-15.
[177] S. S. Sarma, S. Sivaram, *Macromolecular Chemistry and Physics* **1997**, *198*, 495-503.
[178] K. Soga, T. Uozumi, M. Saito, T. Shiono, *Macromolecular Chemistry and Physics* **1994**, *195*, 1503-1515.
[179] K. Soga, T. Arai, B. T. Hoang, T. Uozumi, *Macromolecular Rapid Communications* **1995**, *16*, 905-911.
[180] S. C. Hong, H. T. Ban, N. Kishi, J. Jin, T. Uozumi, K. Soga, *Macromolecular Chemistry and Physics* **1998**, *199*, 1393-1397.
[181] S. C. Hong, U. Rief, M. O. Kristen, *Macromolecular Rapid Communications* **2001**, *22*, 1447-1454.

[182] Y. J. Jang, K. Bieber, C. Naundorf, N. Nenov, M. Kapper, K. Mullen, D. Ferrari, S. Knoke, G. Fink, *E-Polymers* **2005**.
[183] Y. Yamauchi, P. Gupta, K. Sato, N. Fukata, S.-i. Todoroki, S. Inoue, S. Kishimoto, *Journal of the Ceramic Society of Japan* **2009**, *117*, 198-202.
[184] C. Naundorf, D. Ferrari, G. Rojas, G. Fink, M. Klapper, K. Müllen, *Macromol React Eng* **2009**, *3*, 456-466.
[185] S. B. Roscoe, C. Gong, J. M. J. Fréchet, J. F. Walzer, *Journal of Polymer Science Part A: Polymer Chemistry* **2000**, *38*, 2979-2992.
[186] M. Stork, M. Koch, M. Klapper, K. Müllen, H. Gregorius, U. Rief, *Macromolecular Rapid Communications* **1999**, *20*, 210-213.
[187] S. C. Hong, T. Teranishi, K. Soga, *Polymer* **1998**, *39*, 7153-7157.
[188] N. Nenov, M. Koch, M. Klapper, K. Mullen, *Polymer Bulletin* **2002**, *47*, 391-398.
[189] Y. J. Jang, C. Naundorf, M. Klapper, K. Mullen, *Macromolecular Chemistry and Physics* **2005**, *206*, 2027-2037.
[190] C. Naundorf, D. Ferrari, G. Rojas, G. Fink, M. Klapper, K. Mullen, *Macromol React Eng* **2009**, *3*, 456-466.
[191] T. E. L. M. E. Rogers, J. Wiley, *"Frontmatter", in Synthetic Methods in Step-Growth Polymers, John Wiley & Sons, Inc* **2003**, p. 197.
[192] J. P. Armistead, G. L. Wilkes, R. B. Turner, *J. Appl. Polym. Sci.* **1988**, *35*, 601-629.
[193] V. R. H. Haugen, M. Brunner, J. Will, E. Wintermantel, *Journal of Materials Science: Materials in Medicine* **2004**, *15*, 343-346.
[194] A. S. S. Guelcher, A. Hafeman, K. Gallagher, J. Doctor, S. Khetan, S. McBride, J. Hollinger, *Tissue engineering* **2007**, *13*, 2321-2333.
[195] K. Müller, M. Klapper, K. Müllen, *Colloid and Polymer Science* **2007**, *285*, 1157-1161.
[196] K. Müller, M. Klapper, K. Müllen, *Journal of Polymer Science Part A: Polymer Chemistry* **2007**, *45*, 1101-1108.
[197] K. Müller, M. Klapper, K. Müllen, *Macromolecular Rapid Communications* **2006**, *27*, 586-593.
[198] P. J. Flory, *"Principles of polymer chemistry", Cornell University Press, Ithaca* **1953**.
[199] H. K. G. Rossmy, W. Lidy, H. Schator, M. Wiemann, *Journal of Cellular Plastics* **1981**, *17*, 319.
[200] G. L. W. J. P. Armistead, R. B. Turner, *Journal of applied polymer science* **1988**, *35*, 601.
[201] R. A. G. T. H. Mourey, T. G. Bryan, R. F. Thornbury, R. Blevins, R. J. Perry, S. R. Turner, *Journal of Applied Polymer Science* **1992**, *45*, 1983.
[202] A. Chow, W. Branagh, J. Chance, *Talanta* **1990**, *37*, 407-412.
[203] F. Silveira, G. P. Pires, C. F. Petry, D. Pozebon, F. C. Stedile, J. H. Z. d. Santos, A. Rigacci, *Journal of Molecular Catalysis A: Chemical* **2007**, *265*, 167-176.

[204] U. Zucchini, G. Cecchin, *Advances in Polymer Science* **1983**, *51*, 101-153.
[205] J. B. P. Soares, A. E. Hamielec, *Polymer Reaction Engineering* **1995**, *3*, 261-324.
[206] S. B. Roscoe, J. M. J. Fréchet, J. F. Walzer, A. J. Dias, *Science* **1998**, *280*, 270-273.
[207] O. Tcherkasskaya, S. Ni, M. A. Winnik, *Macromolecules* **1996**, *29*, 610-616.
[208] M. E. Rogers, T. E. Long, J. Wiley, in *Synthetic Methods in Step-Growth Polymers*, John Wiley & Sons, Inc., **2003**, pp. 197-263.
[209] L. Ning, W. De-Ning, Y. Sheng-Kang, *Polymer* **1996**, *37*, 3577-3583.
[210] G. A. Howarth, *Surface Coatings International Part B: Coatings Transactions* **2003**, *86*, 111-118.
[211] Z. Zheng, H. Aojula, D. Clarke, *J. Drug Target.* **2010**, *18*, 477-487.
[212] D. Kato, K. M. Boatright, A. B. Berger, T. Nazif, G. Blum, C. Ryan, K. A. H. Chehade, G. S. Salvesen, M. Bogyo, *Nat. Chem. Biol.* **2005**, *1*, 33-38.
[213] J. Liu, G. K. Sukhova, J. S. Sun, W. H. Xu, P. Libby, G. P. Shi, *Arterioscler. Thromb. Vasc. Biol.* **2004**, *24*, 1359-1366.
[214] M. R. Hansen, T. Schnitzler, W. Pisula, R. Graf, K. Müllen, H. W. Spiess, *Angew. Chem., Int. Ed.* **2009**, *48*, 4621-4624.

9 List of Figures

Figure 2.1.1. Scheme of biphasic emulsion. 5

Figure 2.1.2. Scheme of a surfactant-stabilized O/W-emulsion. 6

Figure 2.1.3. Schematic representation of coalescence and Ostwald ripening. 7

Figure 2.2.1. Schematic representation of a nonaqueous emulsion with an amphiphilic block copolymer as emulsifier. 9

Figure 2.2.2. Hansen solubility parameters of certain organic solvents and polymers. 10

Figure 2.2.3. Schematic representation of a nonaqueous emulsion polymerization. 11

Figure 2.2.4. Schematic representation of homogenization by ultrasonication[24] 12

Figure 2.3.1. Schematic illustration of the use of a nonaqeous emulsion as starting point for the design of functional particles for specific applications. 16

Figure 4.1.1. DLS measurement of 0.406 g acetonitrile dispersed in 14.4 g cyclohexane using a PI-b-PEO copolymer (left to right: 0.010 g, 0.020 g, 0.030 g, 0.040 g, 0.050 g, 0.100 g, 0.200 g) as emulsifier. Stirring and ultrasonification of the mixture led to emulsion. 28

Figure 4.1.2. Preparation of poly(L-lactide) nanoparticles in non-aqueous emulsion. 29

Figure 4.1.3. SEM micrograph of poly(L-lactide) nanoparticles synthesized in non-aqueous emulsion stabilized by a PI-b-PS copolymer; the mean particle size determined by SEM (based on 100 randomly chosen particles) was 100 nm (± 8 nm). 31

Figure 4.1.4. SEM micrographs of poly(L-lactide) nanoparticles synthesized in non-aqueous emulsion stabilized by a PI-b-PEO copolymer; **a**: SEM micrograph of poly(L-lactide) nanoparticles before washing with a mean particle size of 65 nm (± 5 nm) determined by SEM (based on 100 randomly chosen particles); **b**: SEM micrograph of poly(L-lactide) nanoparticles after washing with a mean particle size of 44 nm (± 6 nm) determined by SEM (based on 100 randomly chosen particles). 33

Figure 4.2.1. Typical SEM micrographs of PLLA-b-peptide-b-PLLA nanoparticles prepared in non-aqueous emulsion (a-b) and after transfer into aqueous media (c-d). 44

Figure 4.2.2. TPEF image of a single nanoparticle (left); chemical structure of the encapsulated PMI dye (right). 46

Figure 4.2.3. (a) and (b): Lateral and axial projections of overlayed CARS (red) and TPEF (green) of HeLa cells incubated for 12h with PLLA-*b*-peptide-*b*-PLLA nanoparticle-containing medium. Axial projections (right and below each lateral image) show the YZ and XZ localization of nanoparticle (circled in yellow) within the depth of the cell. In both cases, the fluorescent response of the particles is entirely found within the cell boundaries, demonstrating successful internalization. These projections were reconstructed from a three-dimensional stack with dimensions of 72 x72 μm^2 and slice spacing of 210 nm. 48

Figure 4.3.1. MALDI ToF MS spectra: PLLA-b-(Ac)SGFG-PLGLAG-GFGS(NH_2)-b-PLLA copolymer sample before (top, green) and after 4 days of incubation with MMP-2 (top, blue); PLLA-b-(Ac)SGFG-LALGPG-GFGS(NH_2)-b-PLLA copolymer sample before (bottom, green) and after 4 days of incubation with MMP-2 (bottom, blue). 58

Figure 4.3.2. Exemplary PLLA-b-(Ac)SGFG-PLG-OH (left) and LAG-GGFGS(NH_2)-b-PLLA copolymer fragments (right) before (green) and after 4 days of incubation with MMP-2 (blue). 59

Figure 4.3.3. Scheme for preparation of nanoparticles bearing the triblock structure and a typical SEM image of the nanoparticles. 61

Figure 4.3.4. Dye release from nanocarriers bearing either the cleavable sequence (PLGLAG) or the scrambled sequence (LALGPG) in the polymer chain after 4 day incubation time. Each measurement is presented as % released relative to control specimens not incubated with MMP-2. Error bars are standard deviation from three experiments and * marks statistically significant differences between samples with $P < 0.05$. 62

Figure 4.3.5. a) Glass transition temperatures of PLGLAG triblock copolymers before (red) and after peptide cleavage (blue) by MMP-2; b) DLS graph of PLGLAG nanoparticles before (non-degraded) and after (degraded) MMP-2 incubation (sample 3). 63

Figure 4.3.6. Cytotoxicity by 5-FU-encaspulated nanocarriers bearing the PLGLAG sequence or the LALGPG sequence. Quantitative analysis reveals cytotoxicity for cleavable particles is comparable to soluble 5-FU (10 μg/mL) whereas LALGPG-5-FU and PLGLAG without 5-FU particles show similarly limited toxicity as untreated cells. Images show more living cells retaining calcein-AM (green) and fewer dead cells containing ethidium homodimer (red) in the LALGPG-5FU particles. Error bars are standard deviation from three experiments, * marks statistically significant differences between samples and untreated with $P < 0.05$. 64

Figure 4.4.1. SEM micrographs of a PEG b PGlu(Pyr) copolymer/cyclohexane dispersion before (a,b) and after UV irradiation (λ = 366 nm, P = 4 W, t = 3h). 79

Figure 4.4.2. SEM micrographs of PLLA nanoparticles before (a, b) and after photo induced cleavage of pyrenyl methylene units from the PEG b PGlu(Pyr) copolymer (c, d) (λ = 366 nm, P = 4 W, t = 3h). 81

Figure 4.4.3. Live/dead staining of hMSC cells after 24-hour incubation of PEG-b-PGlu(Pyr) emulsified PLLA nanoparticles at various dilutions. Live cells stained positive for calcein (green) whereas dead cells stained positive for ethidium homodimer (red). Scale bar = 100 μm. 83

Figure 4.5.1. Reaction scheme for the formation of polyurethane and polyurea..... 94

Figure 4.5.2. SEM micrographs of (a, e) non-porous and (b-d, f) porous PU particles. The amount of water during the polymerization was varied (a-d: 0, 0.78, 1.67, and 3.27 mmol of water). 97

Figure 4.5.3. LSCFM image of the porous particles stained with Rhodamine B. 99

Figure 4.5.4. Graphs of normalized volume of (a) non-porous PU microspheres and (b) porous PU microspheres as a function of ethylene polymerization time from a gas phase reactor equipped with an optical microscope. 103

Figure 4.5.5. SEM and cryo-TEM micrographs of non-porous PU particle (a,b). SEM micrographs of most porous PU particle (c,d) after ethylene polymerization. 105

Figure 4.5.6. (a) SEM micrograph of the ethylene polymerized particles obtained from metallocene supported on the dye stained porous PU particle. LSCFM micrographs of (b) a single PE particle and (c) its 12 slices of PE particle by optical sectioning from top of the particle (1) to the middle of the particle (12). 106

Figure 5.2.1. Scheme of water chelation by either BDMAEE or TEDA... 115

Figure 5.2.2. Scheme for the preparation of PU particles in nonaqueous emulsion. 116

Figure 5.2.3. SEM micrograph of PU particles, synthesized in nonaqueous emulsion. 117

Figure 5.2.4. SEM micrograph of PU particles that were synthesized in nonaqueous emulsion, wherein equimolar amounts of water were present. 118

Figure 5.2.5. SEM micrograph of PU particles before (A) and after (B) THF washing.....118

Figure 5.2.6. SEM micrograph of PU particles having craters on the particle surface (reaction time = 4 h). 120

Figure 5.2.7. SEM micrographs of PU particles. Left: porous particles after a reaction time of 30 min. Right: particles after a reaction time of 8 h.....121

Figure 5.2.1. Overview of the achieved particle dispersions with their most striking features for a desired application. 123

Figure 7.1.1. ^{1}H-NMR spectra of PLLA-b-(Ac)SWWWWWS(NH_2)-b-PLLA (top left) and Ac-SWWWWWS-NH_2 (bottom right) in DMSO-d6; Chemical shift area of the signals corresponding to the methylene protons in both serine groups. 135

Figure 7.1.2. DOSY spectra of PLLA-b-(Ac)SWWWWWS(NH_2)-b-PLLA (top, red) and Ac-SWWWWWS-NH_2 (bottom, black) in DMSO-d6.....136

Figure 7.2.1. Normalized GP chromatograms of PLGLAG nanoparticles before (red) and after MMP-2 incubation (blue).....139

Figure 7.2.2. CARS and two-photon fluorescence images of cultured C2C12 myoblasts directly after addition of PLGLAG (upper panel) and after 48h of culture (lower panel). CARS signal is derived exclusively from symmetric vibrations of CH_2 modes of acyl chains, thus highlighting membranes and lipid deposits. Multiphoton excitation allows detection of fluorescent PMI

dye loaded into the PLGLAG particles. Over time, PMI was seen to associate with cells, and predominantly in the vicinity lipid deposits, highlighted by the yellow appearance (arrows). Scale bar = 20 µm..... 140

Figure 7.2.3. Time dependence of cytotoxicity with 5-FU loaded nanocarriers. 5-FU samples were administered 10 µg/mL drug directly in the media. * and # mark statistically significant differences ($p < 0.05$) relative to the corresponding sample at 24 h. Error bars are standard deviation from three experiments. Pictures show live (green) and dead (red) cells after 72 h incubation. Scale bar = 100 µm..... 141

Figure 7.3.1. ^{1}H NMR spectrum of PEG-b-PGlu copolymer (4) in D_2O. . 145

Figure 7.3.2. Diffusion ordered spectrum of PEG-b-PGlu copolymer (4) in D_2O. 145

Figure 7.3.3. ^{1}H NMR spectrum of PEG-b-PGlu(Pyr) copolymer before deprotection in D_2O. 146

Figure 7.3.4. ^{1}H NMR spectrum of PEG-b-PGlu(Pyr) copolymer after deprotection in D_2O. 147

10 List of Tables

Table 4.1.1. Experimental conditions and results of the preparation of poly(L-lactide) in non-aqueous emulsion. 29

Table 4.2.1. Experimental conditions and results of the preparation of PLLA-b-peptide-b-PLLA copolymers in solution (1-2) and in non-aqueous emulsion (3-4). 40

Table 4.3.1. Experimental conditions and results of the preparation of PLLA-b-polypeptide-b-PLLA copolymers in solution and nonaqueous emulsion. 57

Table 4.5.1. Experimental conditions and results of the preparation of PU microspheres in nonaqueous emulsion polymerization. 96

Table 4.5.2. Ethylene polymerization results of the PU particles in a gas phase reactor.....101

Table 7.3.1. Hydrodynamic diameters of block copolymer aggregates in cyclohexane and copolymer stabilized PLLA nanoparticles in cyclohexane, respectively, water.....144

11 List of Publications

R. Dorresteijn, R. Haschick, M. Klapper, K. Müllen: Poly(L-lactide) Nanoparticles via Ring-Opening Polymerization in Non-aqueous Emulsion. *Macromol. Chem. Phys.* **2012**, *213*, 1996-2002.

R. Dorresteijn, R. Ragg, G. Rago, N. Billecke, M. Bonn, S. H. Parekh, G. Battagliarin, K. Peneva, M. Wagner, M. Klapper, K. Müllen: Biocompatible Polylactide-*block*-Polypeptide-*block*-Polylactide Nanocarrier. *Biomacromolecules* **2013**, *14*, 1572-1577.

R. Dorresteijn, R. Haschick, K. Müller, M. Klapper, K. Müllen: Synthesis of Nanosized Polymer Particles in Nonaqueous Emulsion. *MRS Online Proceedings Library* **2013**, *1546, doi:10.1557/opl.2013.696*.

R. Dorresteijn, S. Nietzel, D. Joe, Y. Gerkmann, G. Fink, M. Klapper, K. Müllen: Metallocene supported on porous and nonporous polyurethane particles for ethylene polymerization. *J. Polym. Sci. A Polym. Chem.* **2014**, *52*, 450-459.

R. Dorresteijn, N. Billecke, M. Schwendy, S. Pütz, M. Bonn, S. H. Parekh, M. Klapper, K. Müllen: Polylactide-*block*-Polypeptide-*block*-Polylactide Copolymer Nanoparticles with Tunable Cleavage and Controlled Drug Release. *Adv. Funct. Mat.* **2014**, *24*, 4026-4033.

R. Dorresteijn, N. Billecke, S. H. Parekh, M. Klapper, K. Müllen: Polarity Reversal of Nanoparticle Surfaces by the Use of UV-Sensitive Emulsifiers. *J. Polym. Sci. A Polym. Chem.* **2014**, *53*, 200-205.

12 Acknowledgments

Ich möchte mich zuallererst bei meinen Eltern und bei meiner Frau [redacted] für die großartige Unterstützung und die vielen motivierenden Zusprüche sehr herzlich bedanken. [redacted] danke ich für die Möglichkeit in seiner Forschungsgruppe tätig sein zu dürfen und für die gezielten, aber auch kritischen Diskussionen und die damit verbundene Einflussnahme auf meine persönliche Entwicklung. Meinem Projektleiter [redacted] gehört ein großes Dankeschön für die vielen fachlichen, aber auch persönlichen Gespräche in entspannter Atmosphäre. Seine sehr guten Ratschläge waren mir stets eine große Hilfe auf meinem Promotionsweg. Ich bedanke mich bei allen Kolleginnen, Kollegen und Freunden des AK [redacted] für die schönen privaten Momente und für die fachliche Unterstützung meiner Forschungsarbeit. Speziell möchte ich folgenden lieben Freunden danken:

- [redacted] für das tolle Mentoring zu Beginn meiner Diplomarbeit am MPI und die stetige Unterstützung auf meinem weiteren Werdegang
- Dem [redacted] für das geniale Büroklima und die tollen persönlichen Momente
- [redacted] gilt ein Extra-Dankeschön für die unzähligen wissenschaftlichen Diskussionen, die mich signifikant weitergebracht haben
- [redacted] für ihr Wohltuen, ihre Unterstützung und die vielen lustigen Momente
- [redacted] für die bedingungslose Unterstützung seit Studienbeginn und die vielen privaten Erlebnisse

Mein Dank gilt zudem den vielen Kooperationspartnern und Kollegen:

- [redacted] für die Hilfestellungen im Labor
- [redacted] für die vielen fruchtvollen Kooperationen
- [redacted] für die Synthese der PE-Partikel
- [redacted] für die wissenschaftlichen Hilfestellungen bzgl. NMR-Auswertungen und vor allem für die schönen Momente auf dem Fußballplatz
- [redacted] für die zahlreichen NMR-Messungen
- [redacted] für die vielen DSC- und TGA-Messungen
- [redacted] für die synthetische Hilfe und die lustige Atmosphäre
- [redacted] für die zahlreichen GPC-, HPLC- und DLS-Messungen

Ein herzliches Dankeschön auch an alle, die ich versehentlich nicht erwähnt habe. Bitte seht es mir nach.